

**CHEMOMETRICS -ASSISTED LASER INDUCED BREAKDOWN
SPECTROSCOPY OF HIGH BACKGROUND RADIATION AREA (HBRA)
GEOHERMAL FIELD MATRICES**

By

MUKHONO PAULINE

B. Ed (Hons)

**Thesis submitted in partial fulfillment for the award of Master of Science degree in Physics,
University of Nairobi.**

November, 2012

Declaration

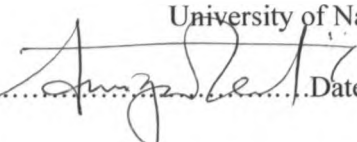
This thesis is my own original work and has not been submitted for the award of a degree at any other University.

Mukhono Pauline
I56/78343/2009
Department of Physics
University of Nairobi


Signature  Date..... 15/11/2012

This thesis has been submitted for examination with our approval as University supervisors,

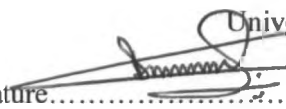
Dr. Kaduki A. Kenneth
Department of Physics
University of Nairobi

Signature  Date 15/11/2012

Dr. Angeyo H. Kalambuka
Department of Physics
University of Nairobi

Signature  Date..... 15/11/2012

Dr. Dehayem A. Massop
Department of Physics
University of Nairobi

Signature  Date..... 15/11/2012

Dedication

This work is dedicated to my parents (Agnes and Peter Mukhono) and to my beloved son Mishael Simiyu who have been my greatest motivation in the research.

Acknowledgements

I wish to acknowledge and appreciate my supervisors; Dr. Kaduki Kenneth, Dr. Angeyo. H. Kalambuka and Dr. Dehayem. A. Massop, for the supervision, constructive comments, encouragement and guidance they offered me throughout my research.

I am grateful to the International Science Programme for giving me a chance to study through the award of scholarship and the University of Nairobi for the provision of conducive environment for research. I also acknowledge my colleagues and all the members of the Department of Physics for their ideas, comments and moral support. Further appreciation goes to Institute of Nuclear Science and Technology for their assistance during sample preparation and research in their laboratory. This work would not have been a success without the kind support, love and prayers from my beloved family and friends. I owe a lot to them. Finally, I thank the Lord Almighty, for His love and grace to carry on, good health and provision of all I needed to carry out this research.

Abstract

In this study, the utility of LIBS with chemometrics techniques namely PCA, PLS, ANNs and SIMCA has been investigated and demonstrated in performing trace quantitative and explorative analysis of High Background Radiation Areas (HBRA) geothermal field matrices (rocks, soils), for the purpose of analyzing atomic and molecular signatures, so as to characterize and evaluate the impact of HBRA geothermal discharges on the surrounding environment. Analytical performance tests based on (multi- signal) standard addition method were done for the elements in the concentration range of 10-150 ppm for the trace elements and 0.1-1.5% for Ti. The classical calibration yielded to predicted concentrations not close (> 10 ppm) to the true/measured concentrations hence the use of chemometrics techniques (PLS and ANNs) for more accurate prediction of the elements' concentration in soils and rocks respectively. PCA and SIMCA were applied on the samples' LIBS spectral signatures. Linear calibration curves from classical univariate approach with $R^2 > 0.84$ were obtained for the lines from which the limit of detection were calculated and found to be: 2.4 ppm, 5.1 ppm, 3.1 ppm, 7.6 ppm, 0.012 % for As, Cr, Cu, Pb and Ti in soils and 8.3 ppm, 6.1 ppm, 9.0 ppm, 3.0 ppm, 0.018 % for As, Cr, Cu, Pb and Ti in rocks respectively. The concentrations of Cr, Cu and Pb in soils were within the range recommended by Environmental Protection Agency. Pearson correlation coefficients showed that HBRA (geothermal) were uniquely characterized by positive correlation of As and Cr concentrations while NBRA had negative correlation of Cu with Pb and Ti. PCA and SIMCA classified samples in the categories of sampling sources i.e. HBRA (geothermal), HBRA (non-geothermal) and NBRA (geothermal) based on full spectrum signatures in the 200 – 980 nm range, hence demonstrating the capability of PCA and SIMCA in identifying similarities and differences between unknown samples based on their LIBS spectra. The results obtained indicate that although univariate multi signal calibration is applicable to a limited degree in LIBS quantitative analysis, chemometrics performs better quantitative calibration and subsequent modeling of spectra in relation to analyte concentrations.

Table of Contents

Declaration.....	i
Dedication.....	ii
Acknowledgements.....	iii
Abstract.....	iv
Table of Contents.....	v
List of Abbreviations and Acronyms.....	viii
List of Figures.....	ix
List of Tables.....	xi
CHAPTER ONE.....	1
INTRODUCTION.....	1
1.1 Background.....	1
1.2 Statement of the problem.....	2
1.3 Objectives.....	3
1.3.1 General Objective.....	3
1.3.2 Specific Objectives.....	3
1.4 Justification and Significance of Study.....	3
CHAPTER TWO.....	5
LITERATURE REVIEW.....	5
2.1 LIBS Application in Various Fields.....	5
2.2. High Background Radiation Areas.....	5
2.3 LIBS Analysis of Environmental Samples.....	7
2.4 Chemometrics and LIBS Analysis of Environmental Samples.....	9
2.5 Chemometric-LIBS in HBRA Geothermics.....	10
CHAPTER THREE.....	12
THEORETICAL BACKGROUND.....	12
3.1 Laser- Induced Breakdown Spectroscopy (LIBS).....	12
3.2 Calibration for Determination of Trace Element Concentrations in Soils and Rocks using LIBS.....	13
3.3 Multivariate Analysis (MVA).....	14

3.3.1 Principal Component Analysis (PCA).....	15
3.3.2 Partial Least Squares (PLS).....	16
3.3.3 Artificial Neural Networks (ANNs).....	17
3.3.4 Soft Independent Modeling of Class Analogy (SIMCA).....	19
CHAPTER FOUR	20
MATERIALS AND METHODS	20
4.1 LIBS Set Up.....	20
4.2 System Optimisation Measurements	21
4.3 Description of Study Sites	22
4.3.1 Lambwe Valley.....	22
4.3.2 Lambwe HBRAs.....	23
4.3.3 Olkaria (Control Site)	23
4.4 Sampling.....	24
4.5 Simulate Sample Preparation and Analysis Procedure.....	24
4.6 LIBS Calibration for Qualitative and Quantitative Analysis.....	26
4.6.1 Limits of Detection (LOD)	27
4.7 Multivariate Data Analysis	28
4.7.1 Spectral Preprocessing	28
CHAPTER FIVE	29
RESULTS AND DISCUSSION.....	29
5.1 Selection of Emission Lines for Quantitative Analysis	29
5.2 Optimization of Laser Parameters for Geothermal Sample Analysis.....	32
5.2.1 Effect of Laser Pulse Energy on LIBS Intensity.....	32
5.2.2 Q-Switch Delay (t_d).....	35
5.2.3 Optical Fiber-to-Sample Distance.....	38
5.2.4. Number of Ablations per Laser Scan.....	39
5.3 Calibration for Quantitative Determination of Trace Element Concentrations	41
5.3.1 PLS Calibration and Prediction of Trace Elements in Soils and Rocks	44
5.3.2 ANNs Calibration for Prediction of Trace Elements in Rocks.....	47
5.3.3 Validation of the PLS and ANNs Models.....	50
5.4 Classification of Rocks and Soil using Chemometric techniques (PCA and SIMCA).....	55
5.4.1 Principal Component Analysis	55

5.4.2 SIMCA Classification of Soil and Rock Samples	62
CHAPTER SIX.....	66
CONCLUSION AND FUTURE PROSPECTS	66
REFERENCES	69
APPENDICES	81
Appendix I: Profiles of emission lines for elements used in generating calibration curves	81
Appendix II: Examples of LIBS spectra for geothermal matrices.....	85
Appendix III: Optimization graphs for different elements in model matrices.....	87
Appendix IV: Classical calibration curves for different elements in the sample matrices	96
Appendix V: Emission lines for elements influencing the clustering of samples in PCA plots.....	100
Appendix VI: Spectra for molecular lines in rocks	100

List of Abbreviations and Acronyms

HBRA - High Background Radiation Areas

NBRA - Normal Background Radiation Areas

LIBS - Laser Induced Breakdown Spectroscopy

EDXRF - Energy Dispersive X-Ray Fluorescence

PCA - Principal Component Analysis

PLS - Partial Least Squares

ANNs - Artificial Neural Networks

SIMCA - Soft Independence Modeling of Class Analogy

NORM - Naturally Occurring Radioactive Materials

LPE - Laser Pulse Energy

SNR - Signal to Noise Ratio

DP – LIBS - Double Pulse LIBS

ICP - AES - Inductively Coupled Plasma- Atomic Emission Spectroscopy

ICP – MS - Inductively Coupled Plasma- Mass Spectrometry

LIBS - LIF - Laser Induced Breakdown Spectroscopy-Laser Induced Fluorescence

RSD - Relative Standard Deviation

AAS - Atomic Absorption Spectroscopy

AES - Atomic Emission Spectroscopy

SEP - Standard Error of Prediction

RMSE - Root Mean Square Error

List of Figures	Page
Fig 3.1 Block diagram illustrating the PCA process	16
Fig 3.2 ANNs network principle and architecture	18
Fig 4.1 Schematic diagram of LIBS	21
Fig 4.2 Geographic map of Homa Mountain and sampling region	25
Fig 5.1 LIBS spectra for soil model showing some of the elements detected and measured	31
Fig 5.2 Profiles of emission lines used for optimization experiments	32
Fig 5.3.1 Optimization graphs for spectral line intensity as a function of LPE in kaolin	33
Fig 5.3.2 Optimization graphs for spectral line intensity as a function of LPE in rock simulate	33
Fig 5.4.1 Optimization graphs for SNR as a function of LPE in kaolin	34
Fig 5.4.2 Optimization graphs for SNR as a function of LPE in a rock simulate	35
Fig 5.5 Optimization graphs for time delay in kaolin and rock simulate	36
Fig 5.6.1 Optimization graphs for intensity and % RSD as a function of delay time (kaolin)	37
Fig 5.6.2 Optimization graphs for intensity, % RSD as a function of delay time (rock simulate)	37
Fig 5.7 Optimization graphs for optical fiber-to-sample distance (rock simulate)	38
Fig 5.8 Optimization graphs for number of ablations per laser scan in kaolin and rock simulate	40
Fig 5.9.1 Univariate calibration curves for As, Pb, Cr, Cu and Ti in soils	42
Fig 5.9.2 Univariate calibration curves for As, Pb, Cr, Cu and Ti in rocks	43
Fig 5.10 PLS calibration curves for As, Pb, Cr, Cu and Ti in kaolin	45
Fig 5.11 Performance plots for elements by ANNs calibration	49
Fig 5.12 ANNs calibration curves for As, Pb, Cr, Cu and Ti in rock simulate	51

Fig 5.13.1 PCA scores and loading plot for soils based on full spectra	56
Fig 5.13.3 PCA scores and loadings plot for soils (partial spectra of elements)	57
Fig 5.13.3 PCA scores plot and loadings for rocks based on full spectra	58
Fig 5.13.4 PCA scores and loadings plots for rocks (feature selection)	59
Fig 5.13.5 PCA scores and loadings plots for soils based on predicted concentrations	60
Fig 5.13.6 PCA scores and loadings plots for rocks based on predicted concentrations	61
Fig 5.14 SIMCA classification of soils and rocks based on full spectra	63
Fig 5.15 SIMCA classification of soils and rocks based on predicted concentrations	64
Fig 5.16 SIMCA prediction of soils and rocks (independent samples)	65

List of Tables	Page
Table 4.1 LIBS 2500 PLUS spectrometer specifications	21
Table 4.2 Emission lines for elements used in optimization	22
Table 4.3 Mercury- Argon light source calibration lines	26
Table 4.4 Spectral emission lines used for calibration	27
Table 5.1 Lines observed in soils and rocks samples	30
Table 5.2 LOD and R^2 values for elements in soils and rocks (univariate calibration)	41
Table 5.3 R^2 and RMSEC values for soils (PLS)	46
Table 5.4(a) Univariate vs. PLS prediction of elements in SRM (soils)	46
Table 5.4(b) Prediction ability of different methods for elements in SRM (rocks)	50
Table 5.5(a) Prediction of elemental concentration in soils and rocks	52
Table 5.6(a) Correlation coefficients for elemental concentrations in soils and rocks	54
Table 5.7 SIMCA classification results for soils and rocks	63

CHAPTER ONE

INTRODUCTION

1.1 Background

Laser Induced Breakdown Spectroscopy (LIBS) is a laser based emission technique for elemental analysis. In LIBS, a laser beam is tightly focused on a sample to ablate the material thus creating micro-plasma. The optical emission from the plasma contains the signatures of the elements present in the sample material (Jean *et al.*, 2008; Dimitra *et al.*, 2000; Rodrigues *et al.*, 2008). LIBS has distinct advantages over other established analytical techniques such as XRF (X-Ray Fluorescence) spectroscopy and PIXE (Particle Induced X-Ray Emission) spectroscopy because LIBS performs relatively rapid analysis, and has ability to detect both low and high atomic number (Z) elements simultaneously with minimal or no sample preparations as samples need only to be optically accessible (Samek *et al.*, 2006; Liang *et al.*, 1997).

Chemometrics techniques may be used to extract useful information from a complex multivariate data by reducing the data complexity while increasing the information gained. Chemometrics techniques include; Principal Component Analysis (PCA), Soft Independent Modeling of Class Analogy (SIMCA) and Partial Least Squares (PLS) among others. These techniques employ multivariate mathematical, statistical and symbolic methods which encompass simultaneous observation and analysis of more than one variable to address problems in a given field (Jorado and Castro, 2003). The advantages of these techniques is that they extract as much information as possible from the data and reduce noise in the data with the information obtained used to model and make accurate predictions about the unknown samples. The techniques are also capable of capturing information about correlated trends in a given dataset which is difficult classically using only analytical spectroscopy (Ashwin *et al.*, 2011).

High background radiation areas (HBRA) are those which have high level of natural radioactivity and background radiation in excess of the International Commission on Radiological Protection recommended radiation dose limit (ICRP, 1991). High levels of ionizing radiation on the surface of the earth are mainly due to naturally occurring radioactive elements (U-238, Th-232, Ra-226 and K-40) in the earth's crust. It can also be due to geothermal activity where the products resulting from the decay of Ra-226 e.g. Rn-222, Pb-214, Bi-210, are brought to the surface by waters of the hot springs. Natural radioactive mineral deposits e.g. feldspar, mica, uraninite and thorite are found in suitable geological environments like surficials (Stanley, 1979). Their occurrence in outcrops/ geothermal surficial systems enhances the

background radiation of an area. High temperature geothermal systems have been found to contain high levels of As, which indicates a high- temperature fluid-rock interaction (Ozgur, 2002).

Geothermal system matrices may hold some trace amounts of heavy metals and toxic chemicals as well as the radionuclides hence understanding of their accumulation in especially HBRA regions is of importance, since some of them are harmful to the environment (Shiwani and Rai, 2008).

The few regions in the world, which are known as high background radiation areas (HBRAs), are due to the local geological and geochemical effects, which cause enhanced levels of terrestrial radiation (UNSCEAR, 2000). Very high background radiation areas are found at Guarapari, coastal region of Esperito Santo and the Morro Do Forro in Brazil; Yangjiang in China (Wei *et al.*, 1993); southwest coast of India (Sunta, 1993); Ramsar in Iran (Sorahbi, 1990); United States and Canada (NCRP, 1987) among others. Examples of HBRA in Kenya are; Homa mountain (Barber, 1974; Bahat, 1979; Clarke and Roberts, 1986; Ohde, 2004), Tinderet hill (Deans and Robert, 1984), Mrima Hill (Mangala, 1987; Patel, 1991; Kebwaro *et al.*, 2011), Ruri hills, Rangwa ring complex, Soklo point and Kuge (Tuige), in Gwasi, Lambwe valley (McCall, 1958, Achola, 2009). Among these sites in Kenya, Homa mountain exhibits an unusual case as it is a HBRA with a volcanic complex making it a HBRA sitting on a geothermal field. Therefore it provides a perfect 'laboratory' for carrying out research on association of the element radioactivity elevated by geothermal activities.

In this work LIBS system has been calibrated and utilized to analyze the atomic signatures of geothermal matrices in a HBRA, in order to determine and characterize elemental and molecular associations present in such region. This is with the view of understanding the impact of HBRA geothermal discharges on the surrounding environment as well as the association between HBRA and geothermal emissions from deep underground. Multivariate calibration approaches (PLS and ANNS) have been developed and used to predict the concentration of heavy trace metals in geothermal field rocks and soils. Pattern recognition techniques (PCA and SIMCA) have been employed for characterization of HBRA and NBRA geothermal areas based on the spectral signatures of heavy trace metals, which contain robust information on elemental and molecular components that are associated with HBRAs and NBRAs. The results obtained indicate the utility of chemometrics - LIBS for trace quantitative and exploratory analysis of HBRA geothermal field matrices.

1.2 Statement of the problem

Conventional analytical techniques for analysis of samples such as soil such as Atomic Absorption Spectroscopy (AAS) and Atomic Emission Spectroscopy (AES) require lengthy sample preparations,

trained operators and long measurement time. This can interfere with the sample in that the sample may be contaminated during preparation, thereby affecting the accuracy of results obtained. In order to realize rapid and reliable analysis, the combination of analytical spectroscopy and chemometrics is of necessity. The complex spatial, temporal multivariate nature of the geothermal matrix composition increases the variance, complexity and amount of data to be analyzed. Thus the uses of classical analytical and statistical methods are limited, leaving chemometrics methods as a better option. The research on the regions chosen above was of significance in utilizing LIBS to analyze the atomic and molecular signatures of geothermal field matrices in a HBRA in order to characterize and understand the association and impact of HBRA geothermal discharges on the surrounding environment

1.3 Objectives

1.3.1 General Objective

The goal of this work was to develop a calibration strategy for, and utilize LIBS to analyze the elemental signatures of geothermal matrices in a HBRA in order to characterize and understand the association and impact of HBRA geothermal discharges on the surrounding environment.

1.3.2 Specific Objectives

- i. To design calibration strategies and utilize the most viable analytical model to perform LIBS analysis of HBRA-derived geothermal matrices.
- ii. To identify and differentiate between the atomic and molecular signatures of HBRA and NBRA geothermal matrices.
- iii. To develop and test the ability of the analytical and multivariate chemometrics models built based on trace element and molecular spectral profiles for exploratory analysis of HBRA geothermal matrices.
- iv. To utilize the data and results obtained above to interpret HBRA geothermal reservoir characteristics and to predict the impact of HBRA geothermal associated heavy metals on the environment.

1.4 Justification and Significance of Study

In HBRA, the soils, rocks and fluids from underground have a higher concentration of radioactive and perhaps altered composition (relative to NBRA) of trace elements. Fluids coming from the earth crust in such areas also carry a mixture of gases such as CO₂, H₂S, CH₄ and NH₃ which further pollute the environment and contribute to global warming. These gases in aqueous form modify the attachment

potential and fractionation of the heavy elements in the surrounding environmental matrices (Tahir *et al.*, 2005; Liang *et al.*, 1997). Dissolved gases and hot water from geothermal sources may hold solutions of trace toxic chemicals like Hg, As and salt which precipitate when water cools thus if released, can cause environmental damage (Shiwani and Rai, 2008). Soils containing heavy metals can be absorbed by crops, posing a threat to living organisms and humans (Nilesh *et al.*, 2008).

Although some work has been done on characterization of HBRA geothermal sources using trace elements as signatures (Barber, 1974; Ohde, 2004), reference to atomic and molecular signatures of geothermal matrices is minimal in literature. Multivariate analysis of the signatures is also important because it can help in the extraction of useful information about the elemental and molecular signatures of the samples; interpretation of sample (chemical) characteristics and properties based on spectral data of the analyte and extraction other information such as underlying patterns (similarities and differences between samples) from the complex data derived from the signatures (Maya *et al.*, 2008).

Some parts of North and West regions of Kenya's Rift Valley e.g. Homa Mountain and Tinderet have been identified as HBRA in a geothermal field (Ohde, 2004; Deans and Robert, 1984) hence they provide study areas for exploration of geothermal resources based on both their combined trace element and radiogenic signatures, since the latter are enhanced (Achola, 2009). The elevated levels of radionuclides and associated trace heavy metals in such environment and their potential for leaching, bioaccumulation, fractionation and translocation within the ecosystem make their study an important exploration and environmental issue (Dipippo, 2005).

As such, there is need to understand the Eco toxicological impact of HBRA geothermal effluents immobilization and HBRA heavy trace metal systematics. LIBS spectra can be interpreted to identify the elemental and molecular signatures present and their quantitative and correlative information can be used to predict the association and impact of the HBRA elements on the environment. The approach may be used to develop novel techniques for HBRA geothermal resource characterization and environmental impact modeling.

CHAPTER TWO

LITERATURE REVIEW

2.1 LIBS Application in Various Fields

So far, LIBS has been used as a technique for analysis of samples in various fields e.g. analyses of particulates in materials (Liang *et al.*, 1997), analysis of soils and marine sediments (Barbini *et al.*, 2000), in military and industry (Adel and Arabi, 2006) but little has been done on its application in geothermics due to limited knowledge of the different processes involved in the laser-matter interaction and analytical figures of merit (accuracy, precision, and detection limits) which have not been satisfactory (Castle *et al.*, 1998). This is because the processes involved in laser-induced plasma formation, ablation, atomization, and excitation are quite complex and difficult to reproduce (Cremers and Radziemski, 1989), hence with respect to geothermics, there is need to employ chemometrics assisted- LIBS technique

LIBS has been successfully applied for the elemental analysis of solids, liquids, gas, and aerosols (Cremers *et al.*, 1984; Eppler *et al.*, 1996; Pichahchy *et al.*, 1997; Martin and Cheng, 2000; Kumar *et al.*, 2003). Sabsabi and Cielo (1995) and Aragón *et al.* (1999) quantitatively analyzed the composition of aluminum alloys and steel by LIBS respectively, and both studies obtained satisfactory analytical results. LIBS was also applied to detect elements in different liquids (Fichet *et al.*, 1999), and the limit of detection (LOD) of Cr was found to be 20 ppm in water and 30 ppm in oil, which made LIBS a tool for the quantitative analysis of liquid samples.

A combination of LIBS and chemometrics has been applied in the processing for material identification (Sabsabi *et al.*, 2009), detection and classification of bio aerosols in soils (Hybl, 2003), extraction of information from spectral data obtained in wood furnish (Maya *et al.*, 2008) and in analysis of molecules in process monitoring of pharmaceuticals (Doucet *et al.*, 2008).

2.2. High Background Radiation Areas

Few regions in the world, which are known as high background radiation areas (HBRAs), are due to the local geological and geochemical effects, which cause enhanced levels of terrestrial radiation (UNSCEAR, 2000). Very high background radiation areas are found at Guarapari, coastal region of Esperito Santo and the Morro Do Forro in Minas Gerais in Brazil Yangjiang in China (Wei *et al.*, 1993); southwest coast of India (Sunta, 1993); Ramsar in Iran (Sorahbi, 1990); in the United States and Canada (NCRP, 1987). The existence of high background radiation areas (HBRAs) is attributed to the availability

of certain radioactive minerals e.g. monazites or elements embedded in the continental rock system of these areas. Carbonatites containing monazite and ironstones are major sources of radioactivity due to high concentrations of thorium and uranium together with their radioactive daughters (McCall, 1958).

Previous studies on HBRA of the world have been carried out. Wei (1980) carried out survey in HBRA in Yangjiang- China. The analysis of soil samples in the area was done by radiometry and field gamma spectrometry and the results showed the estimated annual effective dose of 0.302 mSv/y for ^{238}U , 1.86 mSv/y for ^{232}Th in the high natural radiation area and 0.0101 $\mu\text{Sv/y}$ for ^{238}U and 0.177 $\mu\text{Sv/y}$ for ^{232}Th in the control area (NBRA). Diyun *et al.* (2012) measured the concentrations of the natural radionuclides ^{238}U , ^{226}Ra , ^{232}Th and ^{40}K by γ -ray spectrometry in topsoil samples from the Pearl River Delta Zone (China) and found the mean concentrations to be $140 \pm 37 \text{ Bq kg}^{-1}$, $134 \pm 41 \text{ Bq kg}^{-1}$, $187 \pm 80 \text{ Bq kg}^{-1}$ and $680 \pm 203 \text{ Bq kg}^{-1}$ respectively which were higher than the mean values ($^{238}\text{U}=35 \text{ Bq kg}^{-1}$, $^{232}\text{Th}=30 \text{ Bq kg}^{-1}$ and $^{40}\text{K}=400 \text{ Bq kg}^{-1}$) in soil for China and the world. The corresponding annual outdoor effective dose rate per person was estimated to be between 0.11 and 0.29 mSv y^{-1} , with a mean value of $0.20 \pm 0.06 \text{ mSv/y}$, which was also higher than the world mean value of 0.07 mSv y^{-1} .

Baranwala *et al.* (2006) investigated a HBRA sitting on a geothermal region of Eastern Ghats Mobile Belt (EGMB) of Orissa state in India. Soil and rock samples collected from the high radiation zone were analyzed by γ -ray spectrometry using NaI(Tl) detector. Concentration of Th was reported to be very high compared to their normal abundance in crustal rocks. Concentrations of ^{238}U and ^{40}K were also high compared to normal abundance in crustal rocks but their magnitude was comparatively less than that of Th. The average concentrations of ^{238}U , ^{232}Th and ^{40}K were found to be 33 ppm, 459 ppm and 3%, respectively, in soils and 312 ppm, 1723 ppm and 5%, respectively, in the granitic rocks. Maximum concentrations of ^{238}U , ^{232}Th and ^{40}K were found to be 95 ppm, 1194 ppm and 4%, respectively, in soils and 1434 ppm, 10,590 ppm and 8%, respectively, in the granitic rocks.

Examples of HBRA of Kenya are; Homa mountain (Barber, 1974; Bahat, 1979; Clarke and Roberts, 1986; Ohde, 2004), Tinderet hill (Deans and Robert, 1984), Mrima hill (Mangala, 1987; Patel, 1991; Kebwaro *et al.*, 2011), Ruri hills, Rangwa ring complex, Soklo point and Kuge (Tuige), in Gwasi, Lambwe valley (McCall, 1958, Achola, 2009). Several studies on HBRA of Kenya have been carried out based on radioactive elements (U, Th, Ra). Some of the studies include; Barber (1974) who analyzed carbonatites and carbonitic calcite and magnetites from two carbonatite complexes, Homa and Wasaki in western Kenya to study their trace element geochemistry using spectrometry. Carbonatites contained abundance of carbonatitic trace elements (Sr, Ba, Nb and Rare Earth Elements (REEs)) and generally low concentration of Cr, Co, Ni, Pb, Ge, Sn and Mo. It was concluded that the accumulation of the elements

in the carbonatites was mainly due to fractionation of carbonates from carbonatite magmas which was initially rich in carbonatitic trace elements. Patel (1991), Mangala and Patel (1994), and Mustapha (1999) carried out a study on natural radioactivity and radon concentration measurements on Mrima hill. Mangala and Patel studied elemental analysis of sediments samples in which Th with a mean concentration of 770 ppm was found to be the main source of high environmental radiation. Patel (1991) in research on radiation distribution pattern showed that boreholes in the area had very high radiation anomalies with external radiation in the Mrima hill. Mustapha (1999) tested water samples from the boreholes in the area found out that they contained high level of radon with concentrations ranging from 1 to 410 Bq/m³.

Recent studies on HBRA of Kenya include; Ohde (2004) who analyzed twenty eight (major and trace) elements including eight rare earth elements (REEs) in African carbonatite rock samples from Homa Mountain by instrumental neutron activation analysis. He studied the geochemical behavior of trace elements in relation to the order of carbonatite intrusion. Mn, Fe, Sr, Ba, Th, U and REE was found in the sixteen carbonatites examined. Two sets of carbonatites were found to be extra ordinarily enriched in Mn, Fe and Ba while others had elevated concentration of Na, Sc and Sb with high content of Cr, As, and Th. Achola (2009) found out that the presence of Naturally Occurring Radioactive Materials (NORM) i.e. K-40, Ra-226 and Th-232 in carbonatite rocks was responsible for high background radiation in the area.

2.3 LIBS Analysis of Environmental Samples

Environmental samples are complex and rich in environmetric information but extracting it using other conventional techniques is a challenge. As such several studies have been conducted using LIBS as a fast, non-destructive and in-situ technique for quantitative determination/analysis of these samples. Among this studies are; Liang *et al.* (1997) in analysis of particulate materials by LIBS which resulted to improved limits of detection (LOD) by 1 order of magnitude relative to previous methods applied to the same samples. Chenglie *et al.* (2009) used LIBS in analysis of Pb content in soils; the analyzed spectral line profile was fitted by Lorentzian function for determining the background and the full-width at half-maximum (FWHM) intensity of spectral line. Precision of calibration analysis was achieved by correcting for self-absorption effect resulting to 8 ppm LOD for Pb in soil. In their study, Cremers *et al.* (2001) tested a new analysis method for predicting total soil carbon using LIBS by determining appropriate spectral signatures and calibrating the method using measurements from dry combustion of a Mollisol from a cultivated plot. Their results showed that LIBS method rapidly and efficiently measured soil carbon with fair detection limits (300 ppm), precision (4 - 5%), and accuracy (3 - 14%).

Ferreira *et al.* (2009) evaluated three LIBS instrumental parameters (laser pulse energy, delay time, and integration time gate) regarding their influences on signal-to-noise ratio (SNR) of seven elements (Al, Ca, Fe, K, Mg, Mn, and Ti) in soil samples. To optimize LIBS parameters for each elemental response, multiple response optimization method was used. With only one simple screening design, it was possible to obtain a good combination among the studied parameters in order to simultaneously increase the SNR for all analytes.

Christoph *et al.* (2009) use of a double pulse-laser induced breakdown spectroscopy (DP-LIBS) to determine As concentration in 16 soil samples collected from 5 different mine tailing sites in Korea. The use of double pulse laser led to enhancement of signal intensity (by 13% on average) and SNR of As emission lines (by 16.5% on average) with smaller relative standard deviation (RSD) compared to single pulse laser approach. An internal standardization method using a Fe emission line provided a better correlation and sensitivity between As concentration and the DP-LIBS signal than any other elements used. As concentration determined by DP-LIBS was compared with that obtained by atomic absorption spectrometry (AAS) and found to be correlated with a correlation coefficient of 0.94.

Frank *et al.* (2001) used a hyphenated technique combining laser-induced breakdown spectrometry and laser induced fluorescence (LIBS-LIF) for the analysis of heavy metals in soils. Plasma radiation was detected using a Paschen-Runge spectrometer equipped with photomultipliers for the simultaneous analysis of 22 different elements. Calibration curves were recorded using a set of spiked soil samples. Limits of detection were derived from these curves for As (3.3 ppm), Cd (6 ppm), Cr (2.5 ppm), Cu (3.3 ppm), Hg (84 ppm), Ni (6.8 ppm), Pb (17 ppm), Ti (48 ppm) and Zn (98 ppm) using the LIBS signals. Calibration curves based on the LIF signals showed significantly improved limits of detection of 0.3 and 0.5 ppm for Cd and Ti, respectively.

Mohammed *et al.* (2009) investigated trace elements of environmental significance (Cr, Pb, Mn, Cd, Sr, Ni) present in the volcanic rock samples collected from sites of the Cenozoic era flood basalt flows using a locally developed laser- induced breakdown spectrometer. For spectrochemical analysis of these samples, plasma was generated by pulsed Nd: YAG laser radiation at 1064 nm wavelength on the target rock samples. Concentrations of these elements were found to be 1910 ppm, 1399 ppm, 90.5 ppm, 1241 ppm and 461.5 ppm for Cr, Mn, Pb, Sr and Ni respectively. LIBS results were compared inductively coupled plasma atomic emission spectroscopy (ICP-AES) and found to be in agreement with the accuracy range of 0.02-0.23 %. From these researches, it is apparent that LIBS has been successfully used in analysis of environmental samples but little has been done in analysis of trace elements in environmental samples arising from a HBRA to evaluate influence of trace elements on the environment.

2.4 Chemometrics and LIBS Analysis of Environmental Samples

LIBS and chemometrics have been utilized in the analysis of geo-materials for the purposes of calibration and classification. Among such studies are; Niangfang (2009) who used LIBS and chemometrics to determine Cu and Zn concentrations in soils. In his study, 12 samples with different Cu and Zn concentrations were analyzed by ICP-OES and LIBS, respectively. Univariate and PLS regression were applied to LIBS spectra to develop the calibration models for prediction of Cu and Zn concentrations whose results were compared in both methods. The results demonstrated that PLS regression was powerful in analyzing LIBS spectral data compared to the univariate regression through improved normalized root mean square error of calibration (NRMSEC) of about 15% and the normalized root mean square error of prediction (NRMSEP) of about 10% respectively. PLS regression using the reduced spectral range (300-350 nm) containing Cu and Zn peaks produced the best results, which indicated that use of the suitable spectral range in the PLS regression improved LIBS analytical capability.

Gottfried *et al.* (2009) used LIBS and chemometrics in classification of geological materials to demonstrate how PCA can be used to identify spectral differences between similar sample types. Both single- and double-pulse LIBS spectra were acquired using close-contact bench top and standoff (25 m) LIBS systems. PCA and partial least squares discriminant analysis (PLS-DA) were used to identify the distinguishing characteristics of the geological samples and to classify the materials. Clegg *et al.* (2006) used LIBS to quantitatively analyze 195 rock slab samples with known bulk chemical compositions which were split into training, validation, and test sets. The LIBS spectra and chemical compositions of the training set were analyzed using PLS, multilayer perceptron artificial neural networks (MLP - ANNs) and cascade correlation (CC - ANNs) to predict the chemical compositions of the test set. Both the full LIBS spectrum and the intensity at five pre-selected spectral channels per major element (feature selection) were used as input data for the multivariate calculations. The RMSE for PLS using the igneous rock slab test set was found to be; 3.07 % (SiO_2), 0.87 % (Ti), 2.36 % (Al_2O_3), 2.20. % (Fe_2O_3), 1.74 % (MgO), and 1.14 % (CaO).

Niangfang (2009) demonstrated the feasibility of LIBS as an alternative technique to quantitatively analyze soil samples by using the univariate and PLS techniques to analyze LIBS spectra of 12 soil samples and to build calibration models predicting Cu and Zn concentrations. Results showed that PLS significantly improved the analytical results compared with univariate technique. Normalized root mean square error (NRMSE) and R^2 of the univariate models were found to be 16.60 % and 0.71 in calibration and 18.80 % and 0.62 in prediction for Cu and 18.97 % and 0.62 in calibration and 22.81 % and 0.45 in prediction for Zn. For PLS models using the spectral range 300 - 350 nm, the NRMSE and R^2 were 1.94 % and 0.99 for

both Cu and Zn in calibration and 7.90 % and 0.94 for Cu and 8.14 % and 0.94 % for Zn in prediction respectively. The results indicated that PLS can improve the quantitative analytical ability of LIBS for soil sample analysis.

Marcio *et al.* (2009) classified Brazilian soils based on the use of LIBS and chemometrics techniques. Linear discriminant analysis (LDA) was employed to build a classification model on the basis of a reduced subset of spectral variables. For the purpose of variable selection, three techniques (successive projection algorithm (SPA), the genetic algorithm (GA), and a stepwise formulation (SW)) were considered. The methodology was validated in a case study involving the classification of 149 Brazilian soil samples into three different orders (Argissolo, Latossolo and Nitossolo). For means of comparison, soft independent modeling of class analogy (SIMCA) model was also employed. The best discrimination of soil types was attained by SPA-LDA, which achieved an average classification rate of 90 % in the validation set and 72 % in cross-validation.

Most of the above highlighted studies focused on elements in contaminated soil among others but little attention has been focused on its use in the analyses of atomic and molecular signatures in geothermic applications which is important because they can help in the determination and differentiation of concentrations of the elemental and molecular components present in the samples as well as evaluating the chemical structure of the matrices. Furthermore, most studies on HBRA have been focused mainly on NORM (U, Th, K-40, Ra) yet heavy elements present in these areas could be of importance in characterization and mapping of such areas. Geothermal field matrices (soils and rocks) are chemically complex matrices, and only a few studies coupled MVA and LIBS e.g. soil carbon analysis (Martin *et al.*, 2007).

2.5 Chemometric-LIBS in HBRA Geothermics

In general, previous studies highlighted above (section 2.1 - 2.4) have focused on analysis of NORM in HBRA for determination of activity concentration of radioactive elements such as Th, U, Ra and K with little attention directed to the role of other trace elements in the definition of the characteristics of HBRA and/HBRA impact on the environment. On the other hand, researches on geothermal activities have focused mainly on gaseous compounds e.g. SO₂, H₂S, and CO₂ as responsible for underground geothermal activities. So far (according to our knowledge), very few studies (e.g. Baranwala *et al.*, 2006) have been conducted on a HBRA sitting on geothermal active areas based on analysis of heavy trace elements.

To implement multivariate analysis (MVA) in the analysis of HBRA geothermal field matrices, LIBS spectral data collected from geothermal field samples is of great significance in evaluating the quantitative analytical ability of LIBS in trace heavy metals analysis in geothermal matrices. The combination of LIBS and chemometrics can help to interpret spectral properties of the samples and in calibration for accurate prediction of the trace elements spectral data associated with HBRA geothermal matrices. As such, a new technique of method development through chemometric-LIBS has been developed and applied it in context of Eco toxicological impact of HBRA geothermal effluents immobilization, HBRA heavy trace metal systematics, and utility chemometric - LIBS for geothermal and prospecting in HBRA.

CHAPTER THREE

THEORETICAL BACKGROUND

3.1 Laser- Induced Breakdown Spectroscopy (LIBS)

Laser-Induced Breakdown Spectroscopy (LIBS) is an atomic emission spectroscopic technique capable of obtaining spectra containing analytical line emissions of elements directly from matrices. LIBS operates by focusing a laser onto a small area at the surface of a specimen (a gaseous or solid or liquid sample) in order to produce transient plasma (Cremers and Radziemski, 2002). When the laser is discharged it ablates a very small amount of material of about 10 ng which instantaneously generates a plasma plume with plasma temperatures of about 10,000 – 20,000 K. The ablated material dissociates into excited ionic and atomic species of the constituent atoms that emit characteristic radiation for upwards of 10 μ s per laser pulse (Capitelli *et al.*, 2002).

Meanwhile the plasma expands at supersonic velocities ($\sim 10^6$ cm/s) and cools, allowing for dynamic study of dense plasmas (Rosalba *et al.*, 2010). Because such a small amount of material is consumed during the LIBS process the technique is essentially non-destructive or minimally-destructive and being an optical technique it is non-invasive, non-contact and can even be used as a stand-off analytical technique (Andrez *et al.*, 2006). Due to the nature of this technique sample preparation is typically minimized to homogenization or is often unnecessary where heterogeneity is to be investigated or where a specimen is known to be sufficiently homogenous, this reduces the possibility of chemical contamination during analysis.

LIBS systems are more sensitive, fast and can detect a wide range of elements i.e. both high and low atomic number elements. Atomic and sometimes ionic emission lines excited and detected allow for qualitative identification of the species present in the plasma, while their relative intensities can be used for quantitative determination of the corresponding components (Barbini *et al.*, 2000; Muller and Stege, 2002; Rodrigues *et al.*, 2008).

Once the plasma has reached local thermal equilibrium (LTE), the spectrally integrated line intensity corresponding to a transition between two adjacent levels E_k and E_i of generic atomic species concentration C_α can be expressed as (Cremers and Radziemski, 2002).

$$I_\alpha = \frac{F C_\alpha g_k A_{ik} e^{-\frac{E_k}{K_B T}}}{U_\alpha(T)} \quad (3.1)$$

where I_{α} is the measured integral line intensity of the emitted light, $U_{\alpha}(T)$ is the partition function for the emitting species, T is the plasma temperature, K_B is the Boltzmann's constant, g_k is the statistical weight of the higher energy level, A_{ik} is the oscillator strength and F is a constant depending on the experimental and geometrical conditions (Liwana and Feng, 2008).

The concentrations of elements can be obtained by comparing a given line intensity from an unknown sample to that from a reference sample whose thermal properties are close to the unknown sample (Stavropoulos *et al.*, 2004). The average electron density of the plasma during the spectroscopic detection time window is measured by using the Saha- Boltzmann equation (Barbini *et al.*, 2000).

$$N_e = \frac{N_{\alpha} U_i(T) B (KT)^{\frac{3}{2}} e^{-\frac{E_{\alpha}}{KT}}}{N_i U_{\alpha}(T)} \quad (3.2)$$

where B is the Einstein's coefficient while N_{α} and N_i are the population density of atoms and ions respectively.

3.2 Calibration for Determination of Trace Element Concentrations in Soils and Rocks using LIBS

Univariate calibration is done by generating calibration curves obtained by plotting the intensity of the analyte signals resulting from atomic/ionic lines against the concentrations of known samples. The slope of the calibration curve is termed as the sensitivity, i.e. it is the change in analyte signal intensity for a unit change in concentration. The concentration of an element in any unknown sample may be obtained by recording the LIBS spectrum of an unknown sample and by using the calibration curve equation 3.3 (Boersema *et al.*, 2010).

$$Y = mX + C \quad (3.3)$$

where Y is the analyte signal/ intensity of elements emission line, m is the slope of calibration curve, X is the concentration of element and C is the intercept of calibration curve.

The LIBS spectra for all reference samples are obtained and the intensities of spectral lines corresponding to those elements in all LIBS measurement are calculated. Using the obtained intensity, concentration of the unknown samples is obtained from equation 3.3.

3.3 Multivariate Analysis (MVA)

Multivariate analysis involves statistical analysis of data that arises from more than one variable measurement (e.g. LIBS spectra). MVA takes into account nearly all the variables in the whole spectra, removes the redundant and correlated information, and extracts the most important information from the original LIBS spectra. MVA thus makes LIBS more feasible in the determination of elemental composition and the differentiation of different samples (Labbe *et al.*, 2008). This is because LIBS spectra obtained from e.g. soils and rocks are complex and have an overabundance of emission lines from the various constituent elements. Especially in the 200 nm to 500 nm spectral region, spectral interference is so prominent that conventional data analysis techniques are insufficient in providing spectral correlation with elemental composition. Hence, the use of multivariate analysis to establish correlation between LIBS spectra and the concentration of elements in matrices is of necessity (Doucet *et al.*, 2007). The techniques include, PCA and SIMCA (for pattern recognition), PLS and ANNs (for calibration and spectral modeling).

From equation 3.1, given that other factors are kept constant, ideally, the measured line intensity is proportional to the species concentration in the sample. However, the intensity deviates from the ideal value due to different influencing factors and processes such as self-absorption which is often unavoidable in LIBS quantitative analysis if the concentration of measured species is not low enough. Atoms at the lower energy levels can easily reabsorb the radiation emitted by other atoms of the same species in the plasma leading to a pronounced non-linear relationship between the line intensity and the increasing element concentration i.e. the characteristic line intensity will differ from the ideal straight line as the element concentration increases. Inter-element interference due to line overlap and related matrix effects is also unavoidable, especially for multi-element samples. Spectral interference is prominent when emission lines of other elements are close to an emission line of the analyte. In such situations, the characteristic line intensity might not only result from the transition of one single species, but also be interfered with by other elemental number densities.

Factors such as laser power, lens – to - sample surface distance and delay time of laser pulse, fluctuate from pulse to pulse, leading to the fluctuations of plasma itself. Although the fluctuations can generally be minimized by averaging the measured signal for multi-pulse, deviation of the measured line intensity from expected value is still unavoidable. All these effects shift the line intensity simultaneously, making it very difficult to separate them one by one physically and indicating that the utilization of data processing technology to compensate for these effects can be an effective way to improve the measurement results. Due to these deviations, the intensity of the characteristic lines may not carry enough information to

accurately reflect the measured element concentration, while it still contains the most correlated information (Zhe *et al.*, 2011). Therefore, an ideal way is to extract the major concentration information from these characteristic lines and further correct for deviation by taking the full-range spectrum into account to compensate for the deviations, thus the need to employ multivariate techniques such as PLS, ANNs.

3.3 1 Principal Component Analysis (PCA)

Principal component analysis (PCA) is one of the most extensively used multivariate statistical techniques in chemometrics. PCA is a powerful tool for exploratory data analysis and for building predictive models (Clegg *et al.*, 2009). The linear multivariate PCA models are developed using orthogonal basis vectors (eigenvectors), which are called principal components (PCs), thereby reducing the high dimensional LIBS data onto a lower dimensional space (Ashwin *et al.*, 2011). The application of PCA can remove the redundant and less important information while retaining the most important and original information and differentiate samples by groupings (Mark, 2001; Romanenko and Stromberg, 2007).

In PCA one performs a linear mathematical transformation of the data into a new coordinate space such that the largest variance lies on the first axis and decreases thereafter for each successive axis. The coordinate space of a multidimensional data set is transformed into a coordinate system representing the orthogonal directions of the largest variance within the dataset, thereby reducing large number of variables contributing to total variance to a much smaller set of principal components (Viendra *et al.*, 2011). This is done by approximating a matrix \mathbf{X} defined by variables and small numbers of outer vector products. The matrix \mathbf{X} is approximated by a product of lower dimension $\mathbf{T} \times \mathbf{P}$ (PCs) and a residual matrix \mathbf{E} .

$$\mathbf{X} = \mathbf{T} \mathbf{P} + \mathbf{E} \tag{3.4}$$

where \mathbf{T} is a matrix score that summarizes the x - variables (sample spectra), \mathbf{P} is a matrix of loadings showing the influence of the variables on each score (intensities at different wavelengths or concentrations), \mathbf{E} is a residual matrix containing deviation between original values and the projections (illustrated by Fig 3.1).

The unique scores derived from each data are used to group data in PCs based on coordinate system. On evaluating the score plots, one finds classes of similar multivariate data set. Evaluation of loading plots gives information about the similarities between variables as well as showing which variables strongly

correlate with the estimated components. The view of residuals shows well and badly modeled areas within the spectra (Clegg *et al.*, 2006).

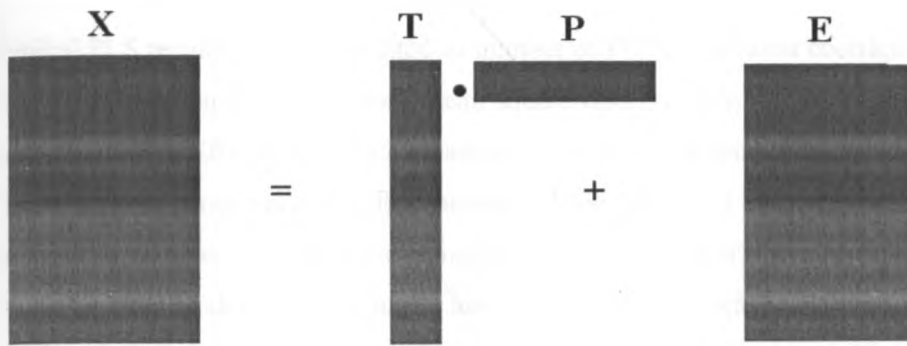


Fig 3.1: Block diagram illustrating the process of data compression by PCA.

3.3.2 Partial Least Squares (PLS)

PLS is a two-block regression method that relates two sets of data by means of regression. The purpose of PLS is to establish a linear model, attempting to derive from each source information that is relevant to a relationship between X and Y, enabling the prediction of properties of interest from a new measured spectrum (Ferrer *et al.*, 2008).

PLS regression linearly relates the variations of dependent variables i.e. known concentrations to the variations of independent variables (spectra of known concentrations), and it works especially well when independent variables are large in number and carry common information such as correlations and collinearity (Wold *et al.*, 2001). PLS regression actively uses dependent variables to help estimate the “latent” variables (PLS components) from the original independent variables, and the first PLS component contains the most relevant information predicting the dependent variables (Clegg *et al.*, 2009). PLS regression simplifies the interpretation of the relationship between independent variables and dependent variables, because this relationship is interpreted with the smallest number of PLS components (Markandey *et al.*, 2009). In conventional LIBS application, PLS generates a regression model that correlates the two matrices, the LIBS spectra (X) and the elemental concentrations (Y) as described by equation 3.5 (Zhe *et al.*, 2011).

$$Y = BX \tag{3.5}$$

where \mathbf{Y} contains the elemental concentrations (the response) in each calibration sample and \mathbf{X} includes the intensity of each wavelength for each calibration sample. \mathbf{B} is the regression coefficient matrix. As a result, PLS analysis obtains a linear combination of values to correlate the spectral intensities with the elemental composition (Sirven *et al.*, 2006).

Typical PLS results can be presented as number of PCs, correlation coefficients (r), the root mean square error of calibration (RMSEC), root mean square error of cross validation, and root mean square error of prediction (RMSEP). RMSEC is a measure of how well the model fits the calibration data; the root mean square error of cross validation is a measure of the predictive ability of the model formed on part of the calibration data set to predict the remaining data; and RMSEP is a measure of the average prediction error. An ideal model will have high r and low RMSEC and RMSEP values (David and Melgaard, 2001). The predictive ability of the regression models can be evaluated by coefficient of multiple determination (R^2) and accuracy determined by standard error of prediction (SEP) given by equation 3.6.

$$SEP = \sum_{i=1}^n \left[\frac{(C_{ij} - \widehat{C}_{ij})^2}{\rho} \right]^{\frac{1}{2}} \quad (3.6)$$

where C_{ij} is the actual concentration, \widehat{C}_{ij} is the estimated concentration of the j^{th} component of the i^{th} sample and ρ is the number of samples used in the validation set (Faber *et al.*, 2003).

3.3.3 Artificial Neural Networks (ANNs)

ANNs are nonlinear computational tools capable of modeling extremely complex functions e.g. LIBS spectra for soils. They operate using a large number of parallel connected simple arithmetic units called neurons. ANNs can be used to build empirical multivariate calibration models of the form

$$y = f(\mathbf{X}) + \varepsilon \quad (3.7)$$

where \mathbf{y} is the vector matrix containing sample response (concentration), f is the network function; \mathbf{X} is the input (sample spectrum) and ε is the error of calibration (Marini *et al.*, 2008).

Each neuron receives a series of inputs that are dynamically weighted; the ANNs compare the weighted sum of its input to a given threshold and finally apply a non-linear function to compute the output. Each input is a continuous variable (LIBS spectra) which becomes weighted by a weight ω that adjusts the influence of the input values in the neurons. All the weighted inputs are summed up to an overall net input of the form

$$Net_j = \sum_{i=1}^q \omega_{ij} x_i + \theta \quad (3.8)$$

where θ is the bias of the neuron, which can be treated as a general weight of the neuron. The weights are initialized randomly and have to be optimized during model development i.e. training of the neurons.

As illustrated in Fig 3.2, an artificial neuron identifies a weighted sum of inputs x_i , compares it to a given threshold (or a bias) b and then transforms the resulting value into a response (output) n using a nonlinear transfer function. The neurons are organized in layers to form a network. Each neuron of the first (input) layer has a single input corresponding to the measured spectrum intensity at one wavelength. The outputs of the last (output) layer constitute ANN results. Each neuron in this output layer is associated with one chemical element contributing to the spectrum. The number of neurons in the second layer (the hidden layer) is a free parameter (Vincent *et al.*, 2008).

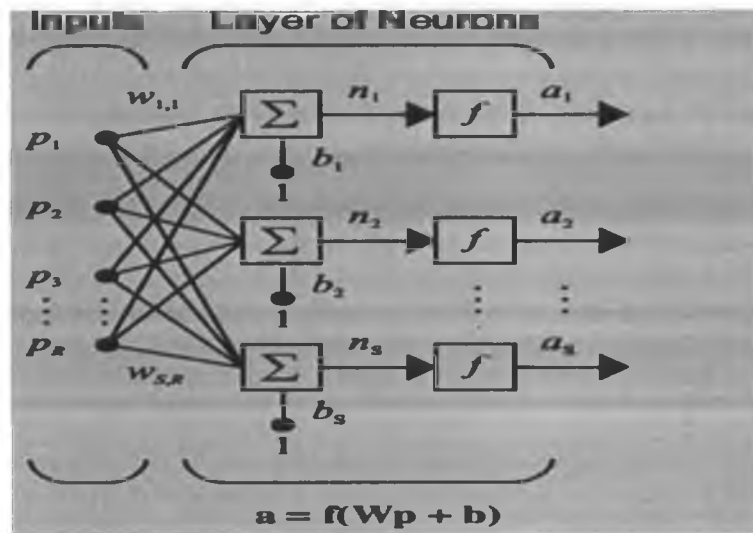


Fig 3.2: ANNs network principle and architecture: R - number of elements in the input vector, s - number of neurons in a layer, a - the output (Howard *et al.*, 2009).

To produce accurate results, the algorithm needs to be trained i.e. calibrated with a set of reference spectra representative of the targets to be analyzed e.g. model samples with known concentrations of elements of interest. The training phase involves finding the best set of weights and bias values that would minimize the network output errors. This is done by using, for example, a back propagation algorithm, which is based on a gradient descent that allows the network to find the best fit to the training set of input-output pairs after a certain number of iterations. Finally, the network prediction ability is evaluated by the validation set (Ying *et al.*, 1993).

3.3.4 Soft Independent Modeling of Class Analogy (SIMCA)

SIMCA is a supervised classification technique which incorporates the application of PCA for dimensionality reduction (Marcio *et al.*, 2009). Because of its supervised nature, it necessitates a training data set consisting of samples (in this case LIBS spectrum) and their class membership (sample type) (Clegg *et al.*, 2009). Soft modeling refers to the fact that the classifier can identify samples as belonging to multiple (overlapping) classes and is not constrained to producing a classification of samples into strictly discrete (non-overlapping) classes (Jose *et al.*, 2003; Snezana and Onjia, 2007). SIMCA enables independent modeling of the classes as opposed to an overall variance modeling as performed in PCA. PCA is performed on each class in the data set and a number of PCs are retained to account for most of the variation within each class. Samples that may be described uniquely by spectra are mapped onto a much lower dimensional subspace for classification (Paul and Laurie, 1989). If a sample is similar to the other samples in the class, it will lie near them in the principal component map defined by the samples representing that class. An unknown is only assigned to the class for which it has a high probability (Chase *et al.*, 2005). SIMCA-based predictive classification is performed by comparing the residual variance of the prospective sample with the mean residual variance of the training samples belonging to the specific class (Ashwin *et al.*, 2011). If the residual variance of a sample exceeds the upper limit for every modeled class in the data set, the sample would not be assigned to any of the classes because it is either an outlier or comes from a class that is not represented in the data set (Richard, 2003).

CHAPTER FOUR

MATERIALS AND METHODS

4.1 LIBS Set Up

A schematic diagram of the LIBS set up used in this work is shown in Fig 4.1. A Q-Switched Nd: YAG (Big Sky Laser) pulsed laser delivering maximum energy of 50 mJ at a fundamental wavelength of 1064 nm, 10ns pulse duration and 10Hz fixed pulse repetition frequency was used. The laser pulse may be varied by a flash lamp Q-Switch delay through the laser controller. The laser beam is focused on the sample placed on manually controlled stage through a quartz lens.

The distance between the focusing lens of focal length 10.16 cm and the sample was kept at 10mm. The emission from the plasma plume was recorded by the LIBS 2500 PLUS (Ocean Optics, Inc) detection system with a fused silica optical fibre (0.22 Numerical Aperture, 101mm focal length) placed at right angle to the direction of plasma expansion. The LIBS 2500 PLUS detection system consists of seven high resolution (0.1 nm) HR 2000 atomic emission spectrometers covering the wavelength range 200 – 980 nm. Each spectrometer has a 2048 pixel linear silicon CCD array with an optical resolution of 0.065nm. The system is connected to a computer via USB port and accessed through the OOILIBS software (LIBS2500 PLUS Operation Manual, 2008).

The spectrometers acquire data simultaneously, and the data are stored on a PC through the OOILIBS software. The OOIBS software automatically identifies the peaks of emission lines, compares the corresponding wavelengths with a data base of atomic and molecular lines and provides the operator with a list of possible elements present in a sample. The data is programmed into a chip of each spectrometer including the wavelength calibration coefficients.

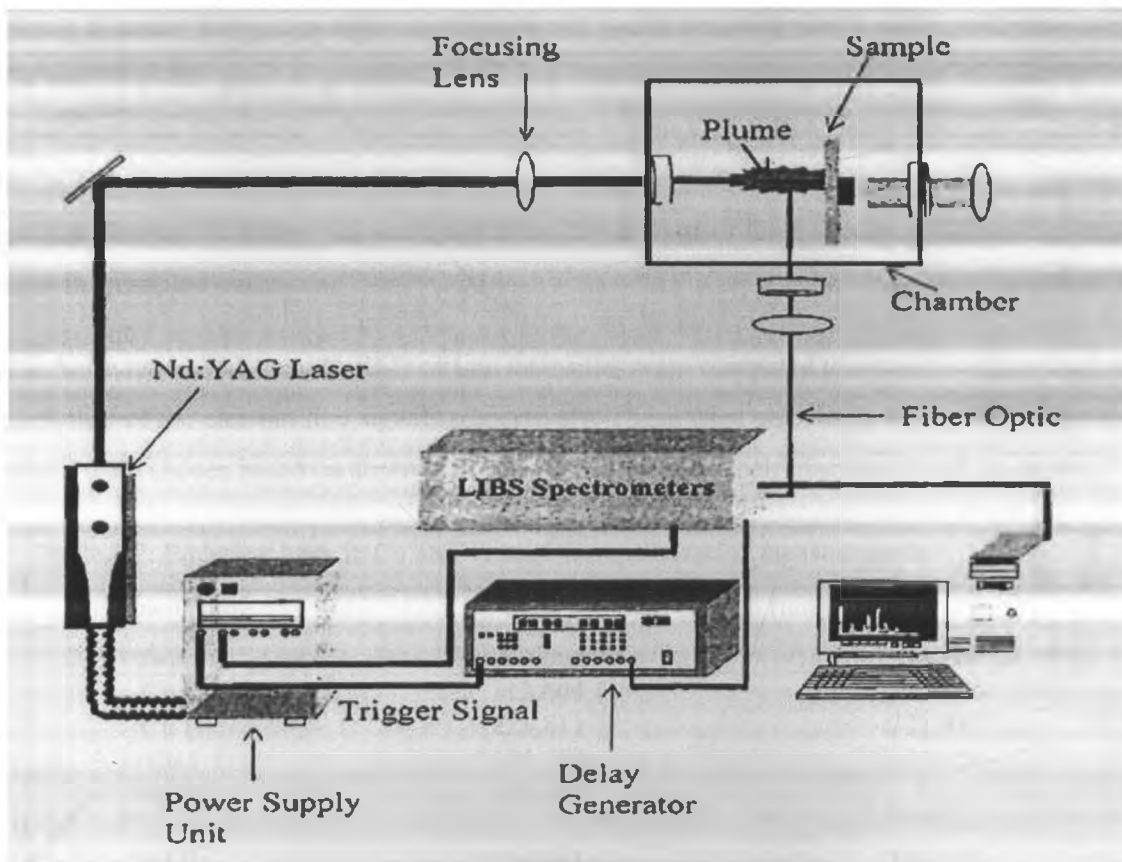


Fig 4.1: A schematic diagram of the LIBS set up.

Specification of each spectrometer is given in Table 4.1.

Table 4.1. LIBS 2500 PLUS spectrometer specifications

Model	Region	Gratings (lines/mm)	λ Range (nm)
HR + C0463	Ultra Violet	2400	200-305
HR + C0464	Ultra Violet	2400	295-400
HR + C0465	Visible	1800	390-525
HR + C0466	Visible	1800	520-635
HR + C0467	Visible-Near Infra-Red	1800	625-735
HR + C0468	Near Infra-Red	1800	725-820
HR + C0469	Near Infra-Red	1800	800-980

4.2 System Optimisation Measurements

Since the analytical performance of LIBS depends strongly on experimental conditions such as ambient purge gas, laser power and wavelength, optimization of laser parameters (laser pulse energy, optical fiber

-to -sample distance, integration time and delay time) was done using kaolin and a rock simulate(doped with Cu and Ti at 200 ppm) as models for soil and rock respectively. Spectra were obtained at different laser pulse energies (15-50mJ) integration times (0.4 – 3 μ s), Q-switch delay time (80 – 250 μ s) and number of ablations per laser scan (1-20). Several measurements were made by holding one parameter constant and varying the others, for each parameter, the average of three spectra at different points on the surface of the samples was taken.

Signal to noise ratio (SNR) and % RSD of line intensities were computed to determine the robustness and reproducibility of the element line signals respectively. These were calculated for the following emission lines which were chosen based on absence of spectral interference, self-absorption and saturation.

Table 4.2. Emission lines in Cu and Ti used for optimization measurements

Element/state	Wavelength (nm)	
	Rock simulate	Kaolin
Cu II	212.604	212.604
Cu II	221.811	221.811
Cu I	324.754	324.754
Cu I	327.396	
Ti II	334.941	336.123
Ti II	336.123	337.280
Ti I	500.721	500.721

4.3 Description of Study Sites

4.3.1 Lambwe Valley

Lambwe valley is located in Homa Bay county of western Kenya within the latitudes 0°30' and 0°45' South and longitudes 34°10' and 34°20' East. It is a south westerly extension of the Kavirondo fault trough lying between Kaniamwia escarpment to the East and the Gwasi massif, which is a dormant volcano, to the West (Allsopp and Baldry, 1972).

Its floor slopes gently at the shore of Winnam gulf. The broader northern end contains Ruri hills with carbonatite complex surrounded by conical volcanic plugs of hard lava. The Gwasi and Kaniamwia support ferruginous tropical and halomorphic soils of rocks rich in ferromagnesian minerals. Also, the escarpment contains mixed soil formations of red-brown, friable clays, gray molted clays and gray compacted loamy sands with high levels of Na, Mg and Ca. The South Ruri hill with cores of calcite supports largely shallow stony soils with relatively high thorium content (Achola, 2009).

4.3.2 Lambwe HBRA

Homa mountain is one of active HBRA in Kenya with part of it being geothermally active. The mountain is located on the southern shore of the Winnam gulf near the north-eastern shore of Lake Victoria in western Kenya, Homa Bay County. Homa mountain is 1754 m high and 600 m above the lake. Homa mountain is one of four alkaline complexes (Fig 4.2) lying within the Winnam Rift which extends westwards from the equatorial portion of the Gregory Rift into Lake Victoria (Clerk and Roberts, 1986). Volcanic development of Homa mountain was revealed and four stages of carbonatite intrusion have been reported. The main igneous and related activity at Homa mountain occurred during Miocene and early Pliocene time and resulted in the emplacement of ijolite at shallow depths and a very well developed series of carbonatites and carbonatitic breccias, mostly as a complex of concentric cone sheets. Melilite bearing rocks are known to exist in the region (Barbe, 1974). Within the melilitite clasts, carbonated ferromagnesian phenocrysts occur in a matrix containing smaller crystals of carbonated perovskite, clinopyroxene, ore and melilite (Bahat, 1979). The carbonatite comprise sovites, alvikites, ferro-carbonatites and late-stage grey carbonatites. The sovites are coarse grained calcitic rocks with accessory apatite and pyrochlore and are characteristically associated with intense feldspathization of country rock and are the earliest carbonatites to be emplaced (Clarke *et al.*, 1979). The alvikites are coarse to medium grained, often well foliated and contain individual grains of magnetite, apatite, pyrochlore and country rock fragments. Alvikites comprise over 90 % of all carbonate intrusions at Homa mountain. The ferro-carbonatites are dense, dark brown to black rocks containing large proportions of iron and manganese oxides. They contain a suite of accessory (including REE) minerals e.g. monazite, fluorite, barite and dahlite (Flegg *et al.*, 1977).

4.3.3 Olkaria (Control Site)

Olkaria geothermal area is located within the greater Olkaria volcanic complex in the south central Kenya rift valley. It consists of a series of lava domes and ashes. The intrusive portions of these magmas are responsible for the high heat flow in the area (Macdonald and Scaillet, 2006). The area is dominated by a peralkaline rhyolite dome contrasting to the meta luminous rocks that more commonly form silicic dome fields. It is bounded to the north by Eburu complex, to the east and south by Longonot and Suswa volcanoes respectively, and to the west by the western rift margin. On the basis of surface outcrops, the main products of volcanism are alkali rhyolite lava and pyroclastic rocks while trachyte and basalt-hawaiite lava has been minor products (Bruno and Ray, 2003). The area has active geothermal features mainly hot springs and fumaroles (Simiyu and Mwakio, 2000).

4.4 Sampling

The geothermal matrices (rocks, soils) were sampled in and near physical features (rivers, fumaroles and hot springs) by digging a few centimeters into the physical features to obtain non-contaminated samples. Carbonatite rocks associated with high radioactivity were selected from the faults in these regions and stored in stopper polythene bags while soil was sampled in places where thermal water was in contact with the surface. Fig 4.2 shows a map of the sampling regions

4.5 Simulate Sample Preparation and Analysis Procedure

For the calibration of the LIBS technique with respect to the analysis of heavy metals (As, Cr, Cu, and Pb) in rocks and soils, a set of samples containing As, Cr, Cu, Pb and Ti over a broad range of concentration (10 ppm - 1.5 %) was made by spiking kaolin and synthetic rocks models with the oxides of these elements. Synthetic rock was prepared by mixing calcium carbonate and silica to the ratio 5:2 equivalent to their occurrence in carbonatite rocks. For spiking, the relative atomic mass the elements' was calculated. The ratio of element to its compound was calculated and used to calculate the amount in grams of the compound that corresponded to the concentration in ppm. The amount of each of the elements was small (approximately tens of micrograms) and as such could not be weighed on an electronic balance. Therefore, the model mass and element mass were multiplied by a factor of 100. A set of three samples per analyte concentration were prepared to span the range of interest. 30 % of binder (starch) was added to each sample and a total mass of the mixture was hand ground in a mortar using a pestle for about 3 minutes. 2 g of the mixture was used to make pellets by pressing the powder under a hydraulic press at 10 tonnes for 2 minutes. The final dimensions of the pellets were 2.5 cm of diameter and about 1mm thickness. The pellets were then stored in petri - dishes

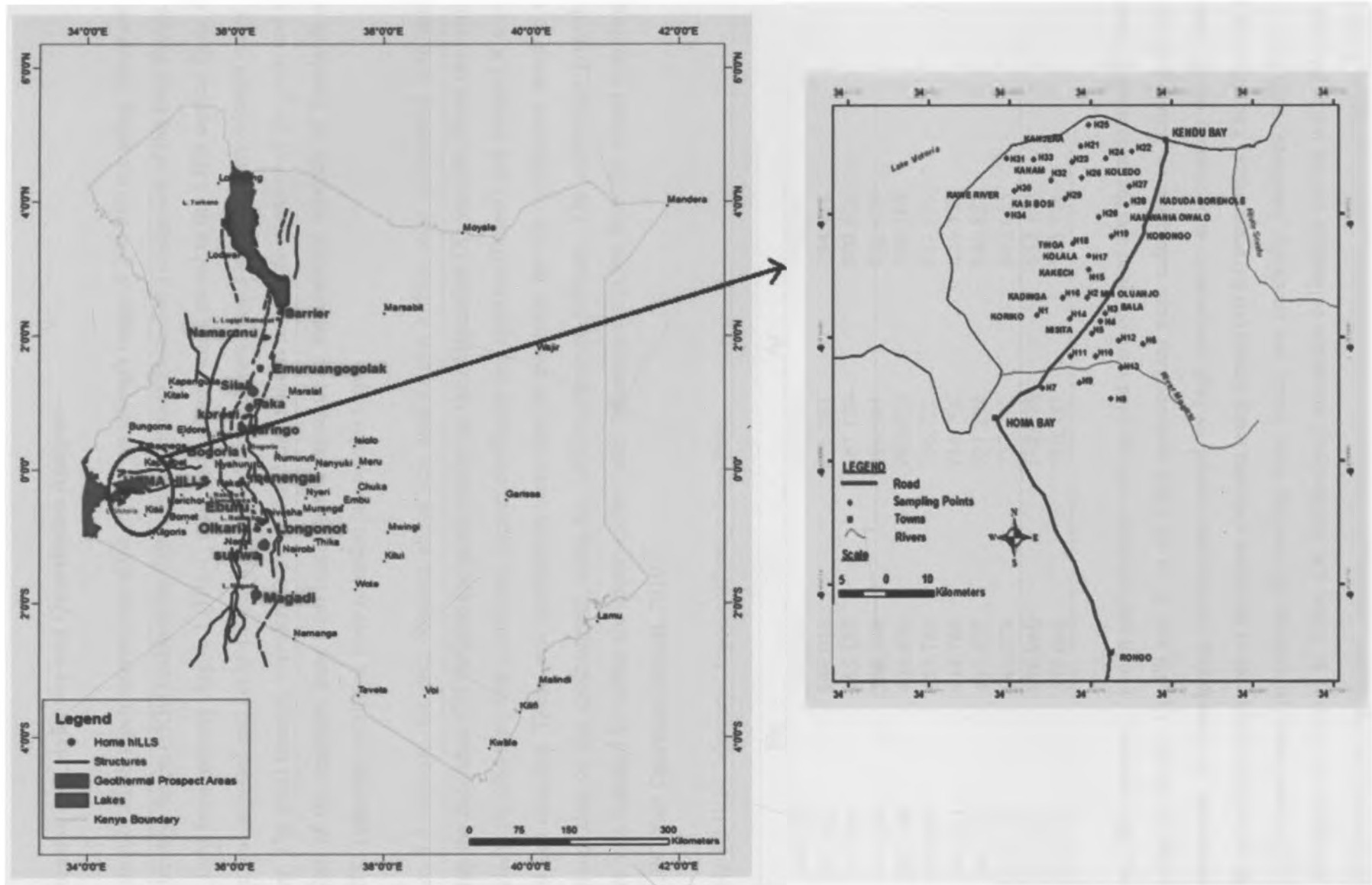


Fig 4.2: Geographic Map of Homa Mountain and other volcanic regions along the Kenya Rift Valley and a section showing regions where rocks and soils were sampled.

4.6 LIBS Calibration for Qualitative and Quantitative Analysis

Spectral calibration of LIBS spectrometers was done for the wavelength range of 200-980 nm using Spectrasuite software and Mercury-Argon (HG-1) calibration light source (Ocean Optics, Inc.) composed of the lines shown in Table 4.3. The light from mercury-Argon 1 (HG-1) calibration source was directed to the LIBS optical fibre, the integration time was adjusted and set to 100ms in order to observe several peaks within the wavelength range of the spectrometer. The pixel number, wavelength indicated at the point of maximum intensity of the peak and the actual wavelength of the emission lines from mercury and argon using the National Institute of Standards and Technology (NIST) elements catalogue were recorded in a tabular form.

Using OriginPro 8.0 software, the data obtained above was used to plot a third order polynomial with actual wavelength being the dependent (Y) variable and pixel number as the independent (X) variable. From the results, the four coefficients (X-intercept, first coefficient, second coefficient and third coefficient) and adjusted R square were calculated and recorded. These new coefficients were used to overwrite the old coefficients saved in the EEPROM memory chip of the spectrometer using the USBProgrammer software. The calibration procedure described above was repeated for other six spectrometers until minimum deviation from the actual wavelength was achieved (HR2000+ Operation Manual, 2010).

Table 4.3 HG-1 Mercury- Argon calibration lines (nm)

Hg		Ar	
248.200	334.148	667.728	772.376
253.652	365.015	675.283	794.818
265.204	365.484	687.129	800.616
275.278	366.328	696.543	801.479
280.346	404.656	703.025	810.369
289.360	407.783	706.722	811.531
292.541	434.749	714.704	826.452
296.728	435.833	727.294	840.821
302.150	546.074	737.212	842.465
312.567	576.960	738.398	852.144
313.155	579.066	750.387	866.794

After calibration, LIBS spectra for kaolin and synthetic rock samples were obtained and the intensities of spectral lines corresponding to As, Cr, Cu, Pb and Ti in all LIBS measurement were calculated by fitting a Gaussian function (to compensate for broadening mechanisms caused by high temperature and pressure during plasma evolution) to the spectral line responses of the above elements using Origin pro 8.0 programme. The lines selected for univariate calibration based on criteria of avoiding lines which are spectrally interfered, saturated, self-absorbed and resonance, are shown in Table 4.4. Multi-signal univariate calibration curves were obtained by plotting the LIBS intensity for the element lines verses their known concentrations in synthetic samples. These are

shown in figures 5.9.2. The concentration of an element in any unknown and/related sample may be obtained by recording the LIBS spectrum of the unknown sample and by using the calibration curve equation.

4.6.1 Limits of Detection (LOD)

Detection limit is the lowest concentration of the analyte that can be detected and determined to be present in a sample using an analytical technique (Cremers and Radziemski, 2002; Marwa *et al.*, 2004). LOD can be estimated using the equation (IUPAC, 1997).

$$LOD = \frac{3\sigma_b}{S} \quad (4.1)$$

where σ_b is the standard deviation of the back ground intensity and S is the sensitivity which is given by the ratio of the intensity to the concentration (Jagdish and Surya, 2007; Sirven *et al.*, 2006).

Table 4.4 Emission lines used for univariate calibration in soils and rocks

Element/ state	λ (nm)	Element/ state	λ (nm)
As I	234.984	Pb I	261.418
As II	278.022	Pb I	280.200
As II	431.566	Pb I	283.305
		Pb I	504.258
Cr II	276.258		
Cr II	276.665	Ti II	334.941
Cr II	284.324	Ti II	336.123
Cr II	425.433	Ti II	337.280
Cr I	425.433	Ti II	338.377
Cr I	427.481	Ti I	365.349
Cr I	428.973	Ti I	398.176
		Ti I	398.976
Cu II	212.604	Ti I	399.864
Cu II	221.811	Ti I	498.173
Cu I	249.215	Ti I	499.951
Cu I	324.754		
Cu I	521.820		

4.7 Multivariate Data Analysis

4.7.1 Spectral Preprocessing

LIBS spectra for the models (kaolin and rock simulate) and field soils and rock samples were pre-processed prior to analysis by chemometrics techniques in order to remove noise and redundant data, to enhance sufficient information within the data as well as to extract information in the data in a form suitable for further analysis. Several methods namely standardization, normalization and mean centering were tested to find the method that gave the optimal results. In mean centering, the average value of the variables is subtracted from each variable to ensure that all results are interpretable in terms of variation around the mean. In normalization, a spectrum is normalized by calculating the area under the curve for the spectrum to correct the spectra for indeterminate path length. Out of these methods; standardization resulted to better calibration and classification models. Standardization is a row oriented transformation which centers and scales individual spectra. It removes scatter effects from spectral data and each spectrum is standardized using only the data from that spectrum. This method was chosen because all variables are put approximately on the same scale thus variables of low concentrations assume equal significance to those of high concentrations (Mark, 2001; Richard, 2003).

CHAPTER FIVE

RESULTS AND DISCUSSION

5.1 Selection of Emission Lines for Quantitative Analysis

The spectral region used (200 -980 nm) to record the emission lines contained most of the strong lines of As, Cr, Cu, Pb and Ti. From the spectra of the samples shown in Fig 5.1, there are many emission lines that are excitable and can be employed for quantitative analysis. Since all of these emission lines cannot be used due to the fact that some have undergone spectral broadening, saturation and spectral overlap, selection of lines for qualitative and quantitative (classical) determination of the elements in the analyzed samples was done to obtain lines that were not spectrally interfered, non- saturated, non -resonance (non -resonance lines undergo self-absorption easily due the presence of atoms having nearly the same wavelength as emitted radiation hence re absorbing the light emitted)and not self-absorbed. By careful comparison and evaluation of emission lines based on intensity and reproducibility (% RSD) of line intensities, four lines of each element were selected. The lines are shown in table 5.1 and they compare well with those reported by other researchers using emission spectroscopy techniques (Christoph *et al.*, 2009; Bousquet *et al.*, 2007; Gondal *et al.*, 2009; Ciucci *et al.*, 1996; Niangfang, 2009). The profiles of some lines are shown in Fig5.2 while others are shown in Appendix I.

The species for each element that are excitable and detectable lines in LIBS for soil and rock matrices are shown in Table 5.1. Most of Ti lines (both ionic and atomic)were detected, As and Pb had few lines that were detected and most of them were atomic, this is due to the fact that these elements have high ionization potential and most of the laser pulse energy absorbed is used to only atomize the elements. Of the molecules excitable, H_α (656.281 nm), CH (844.6 nm) and O (777 nm) bands were observed (Appendix VI). Titanium has low ionization potential (Ti=6.82eV, Pb=7.42 eV, Cu=7.73 eV, As=9.82 eV) and as such, it can easily be excited up to first ionization state using even low laser pulse energy.

From Table 5.1(a) and (b), it can be seen that there are similarities in the lines detected for both rock and soils for As, Pb and Ti while emission lines for Cr and Cu are different in rocks and soils. This is due to difference in the thermo physical and thermochemical properties of samples. The thermo-physical/chemical matrix composition of each sample determines the ease of ablation and detection of embedded trace elements due to factors such as surface reflectivity, conductivity and constituents' melting and boiling points

Table 5.1 Lines detected and observed in soil and rock

Element/ state	λ (nm) (soils)
As I	234.984
As II	278.022
As II	431.565
Cr II	276.258
Cr II	276.665
Cr I	284.324
Cr I	357.868
Cr I	428.973
Cu II	212.604
Cu II	221.811
Cu I	244.164
Cu I	324.754
Cu I	515.324

Element/ state	λ (nm) (rocks)
As I	234.984
As II	278.022
As II	431.565
Cr II	276.258
Cr II	276.665
Cr II	284.324
Cr I	425.433
Cr I	427.481
Cr I	428.973
Cu II	212.604
Cu II	221.811
Cu I	249.215
Cu I	324.754
Cu I	515.324
Cu I	521.820

Element/ state	λ (nm) (soils)
Pb I	261.418
Pb I	280.200
Pb I	283.305
Pb I	504.258
Ti II	334.941
Ti II	336.123
Ti II	337.280
Ti II	338.377
Ti I	365.349
Ti I	398.176
Ti I	398.976
Ti I	399.864
Ti I	498.173
Ti I	499.951

Element/ state	λ (nm) (rocks)
Pb I	261.418
Pb I	280.200
Pb I	283.305
Pb I	504.258
Ti II	334.941
Ti II	336.123
Ti II	337.280
Ti II	338.377
Ti I	365.349
Ti I	398.176
Ti I	398.976
Ti I	399.864
Ti I	498.173
Ti I	499.951

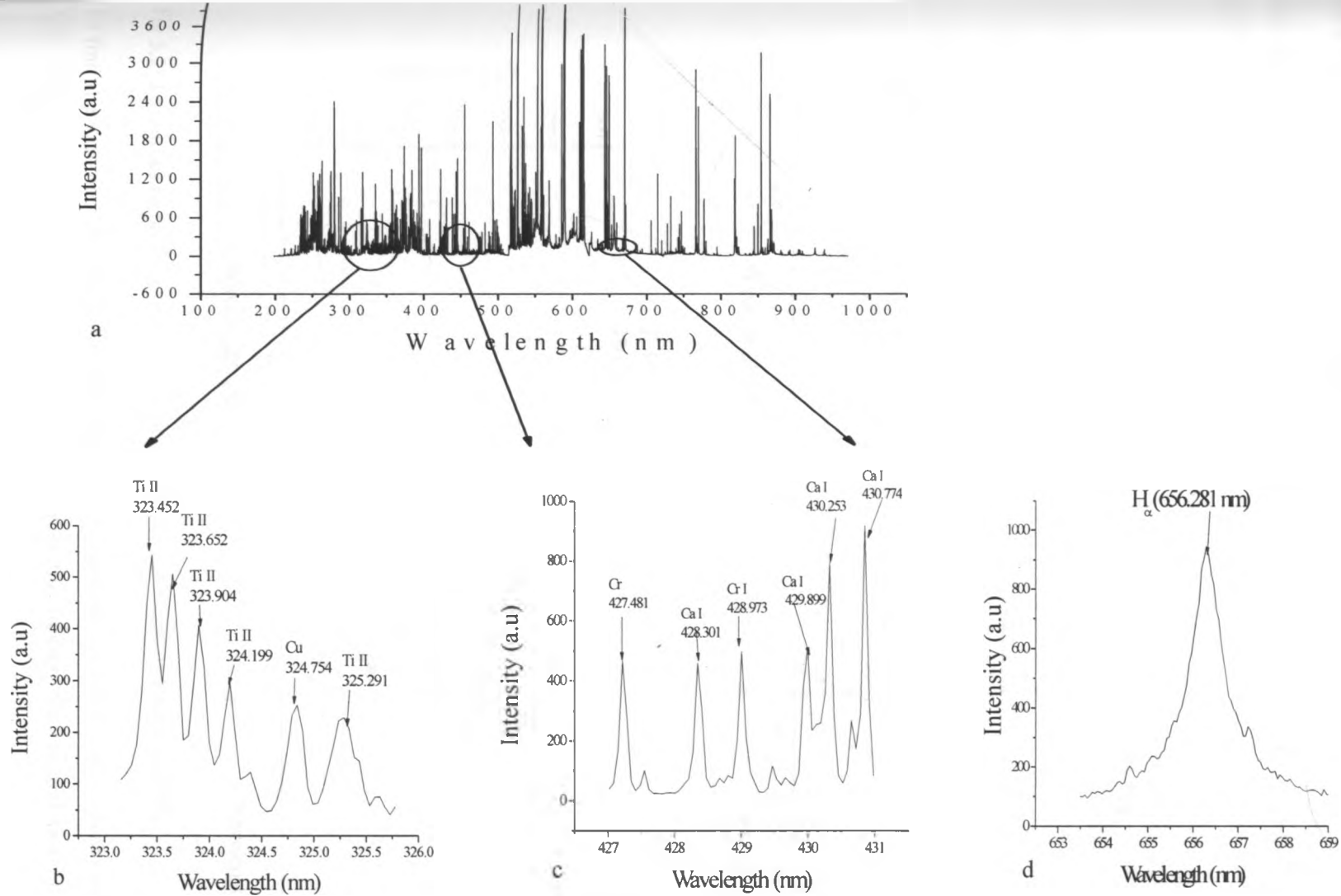


Fig 5.1: LIBS spectra for soil model showing; (a) 200-980 nm spectral range and (b - d) expanded regions of the spectrum showing some emission profiles of spiked elements and molecular bands.

5.2 Optimization of Laser Parameters for Geothermal Sample Analysis

5.2.1 Effect of Laser Pulse Energy on LIBS Intensity

The profiles of emission lines that were used to study the effect of laser pulse energy (LPE) on the intensity of the lines are shown in Fig 5.2, for the case of kaolin.

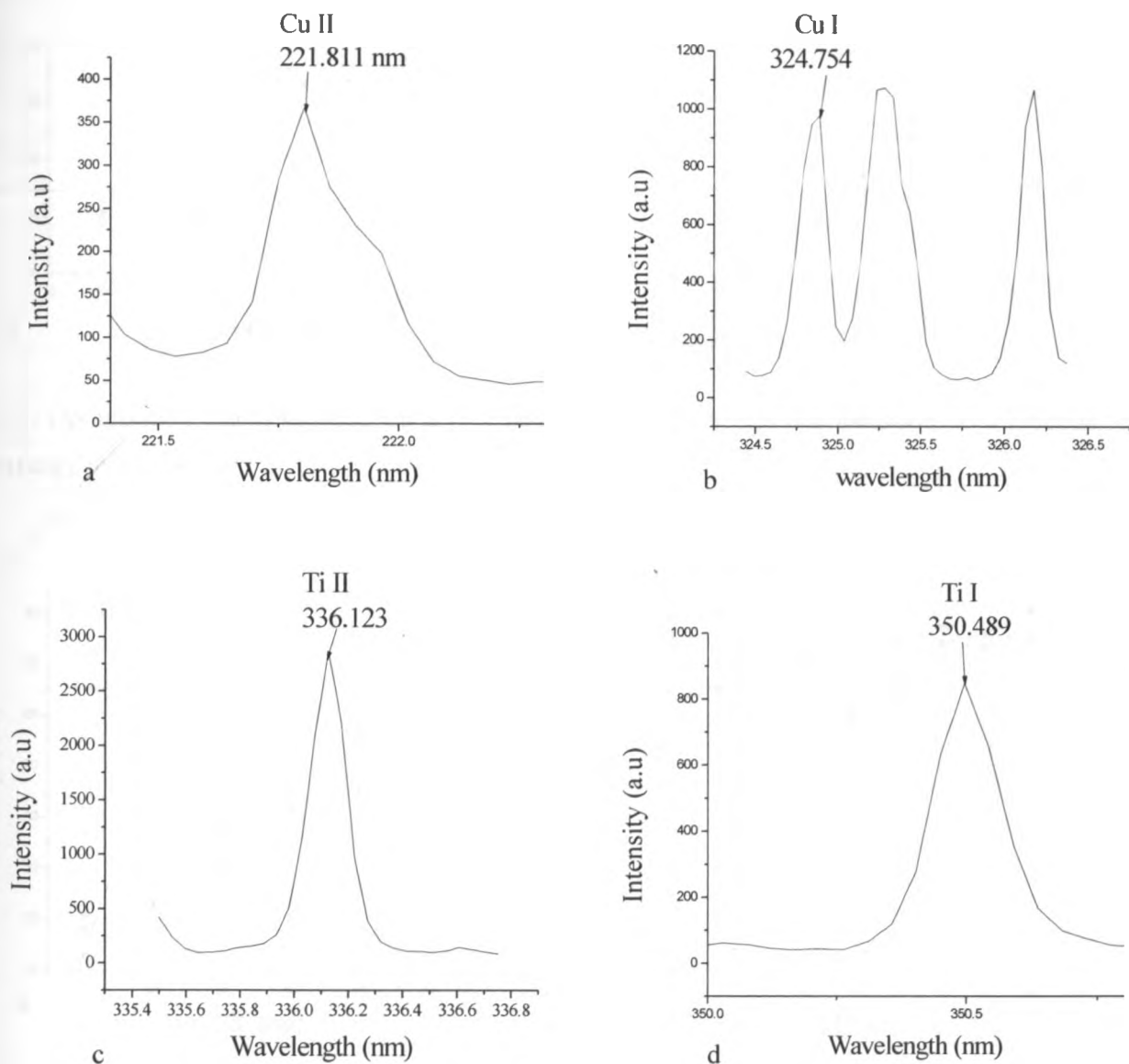


Fig 5.2: Examples of profiles of emission lines used for optimization measurements.

To find the variation of LPE with LIBS signals, four lines for Cu and Ti were monitored for kaolin at different LPE. This variation is represented in Fig5.3.1. From the figures, the spectral line intensities showed linear

dependence on the LPE up to 45 mJ then flattened off slightly as the energy was increased. From 25 mJ, the intensity increases with increase in LPE, reaching a maximum at 45 mJ then decreases slightly.

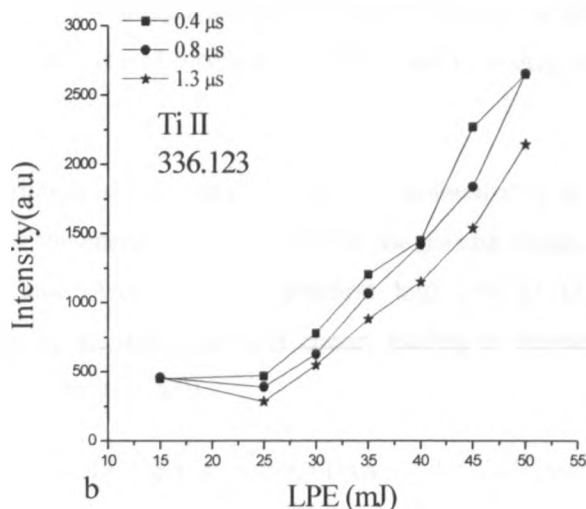
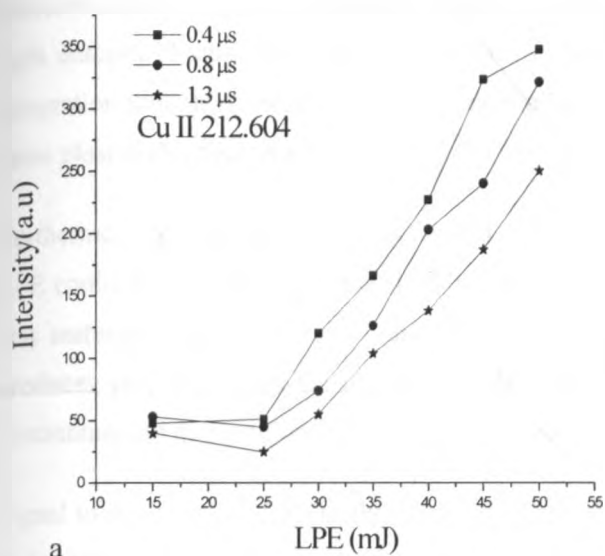


Fig5.3.1: Optimization graphs showing Cu II (212.604) and Ti II (336.123) line intensities as a function of laser pulse energy in kaolin.

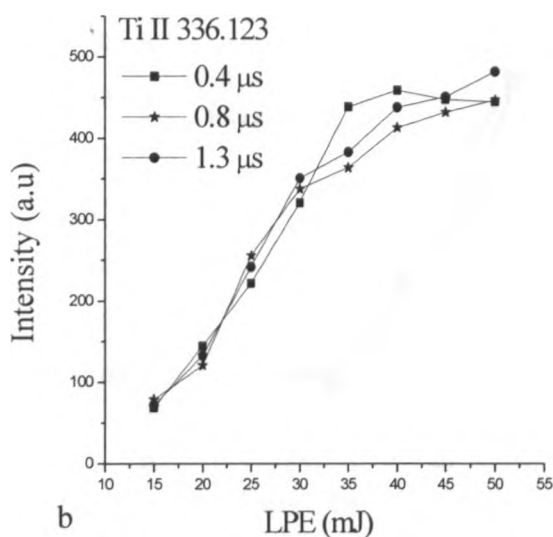
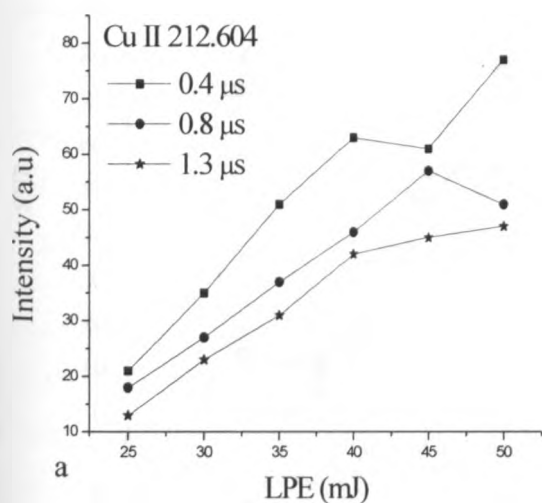


Fig5.3.2: Variation of intensity with respect to laser pulse energy for Cu and Ti lines in a rock simulate.

Unlike kaolin, the dependence of line intensity on LPE is non-uniform and has limits at 40 mJ for rock simulate. This is due to the nature of matrix such as thermo-physical/chemical matrix composition, surface reflectivity, conductivity and constituents' melting and boiling points of the rock simulate. The intensity increases

monotonically from 15 mJ, reaching a maximum value at 40 mJ for 0.4 μ s and 45 mJ at 0.8 μ s then decreases as LPE increases. The nature of Fig5.3.2 for 0.4 μ s (bending above 45 mJ) may be attributed to saturation of the detector at this line intensity. The intensity of plasma light is very high at this integration time such that the detector starts responding nonlinearly (due to large amount of light entering the detector) to the intensity of the light entering through the optical fiber. This effect reduces as the integration time increases because at higher integration time, less plasma is recorded due to large interval between observation of plasma and recording of the same plasma (Jagdish and Surya, 2007).

Furthermore, at low energy (below 25 mJ), shot to shot variation is. The non-linearity of line intensities at high LPE could also be due to plasma shielding such that most of the energy is re-absorbed by the plasma resulting in less material ablated hence less species detected (Jagdish and Surya, 2007). In addition, high LPE (> 45 mJ) produces very dense and hot plasma (~ 20000 K) that absorbs the incoming laser energy leading to increase in continuum and decrease in signal intensity (Cremers and Radziemski, 1989).

Signal to noise ratio (SNR) for these emission lines were computed by taking the ratio between the line intensities and medium noise amplitude that was obtained by averaging three spectral regions of mostly pure noise (200-205 nm, 825-834 nm, 948-952 nm) for kaolin and (200 – 205 nm, 264-269 nm, 471-479 nm) for rock simulate. These regions were selected as they were characterized by very weak emission lines whose intensities were comparable to the background. Fig 5.4.1 shows the results of variation of SNR to increase in LPE.

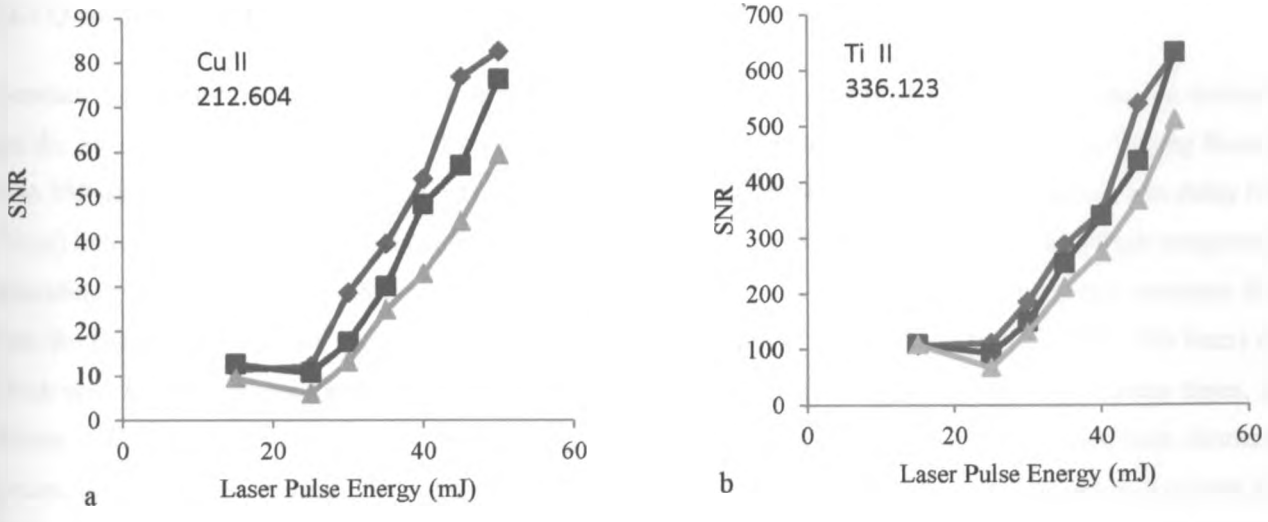


Fig5.4.1: Dependence of SNR of selected Cu and Ti lines on the laser pulse energy at 0.4 μ s (blue), 0.8 μ s (red) and 1.3 μ s (green) in kaolin.

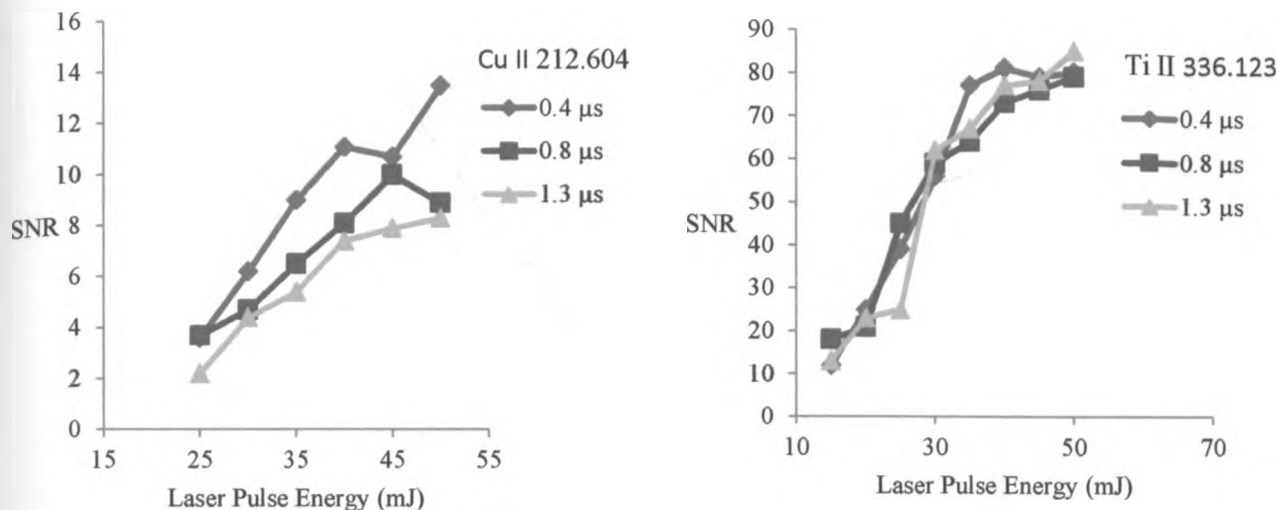


Fig5.4.2 Dependence of SNR of selected Cu and Ti lines on the laser pulse in a rock simulate at different integration times.

From Fig 5.4, SNR for Cu and Ti lines increases with the LPE and inversely with the integration times. Since the curves in Fig 5.4 show almost similar characteristics for both Cu and Ti, it can be concluded that the optimal conditions that generate LIBS signals having high SNR and non-saturated high line intensity for analysis of Cu and Ti in soil and rock matrices is achievable at low integration time and high (45 mJ) LPE. These results may be generalized for other heavy metals.

5.2.2 Q-Switch Delay (t_d)

Q-switch delay optimization was done so as to find the optimal time at which background continuum is minimum and the intensity of elemental analytical lines is optimal. Five spectra were taken at delay times ranging from 80 μs to 250 μs at intervals of 10 μs. Fig5.5 shows two spectra taken at 80 μs - 230 μs. Spectra taken at low delay time (80 μs) indicate that the background continuum is high due to inverse Bremsstrahlung caused by high temperature expanding plasma (Jagdish and Surya, 2007). From the spectra in Fig 5.6 (b), it can be seen that emission lines from the elements have peaks with low intensity at 80 μs (illustrated by Cu I 324.754 and Cu I 327.396 lines) and which are narrower, sharper and have higher intensity at 150 μs. This is due to the fact that at early times, the plasma is dominated by white light continuum which inhibits the observation of emission lines from elemental species. As the plasma expands and cools, the continuum decays away and (atomic) line emissions dominate as a result of radiative recombination of the charged particles in plasma, which becomes prominent only at lower temperatures after expansion of plasma (Cremers and Radziemski, 1989).

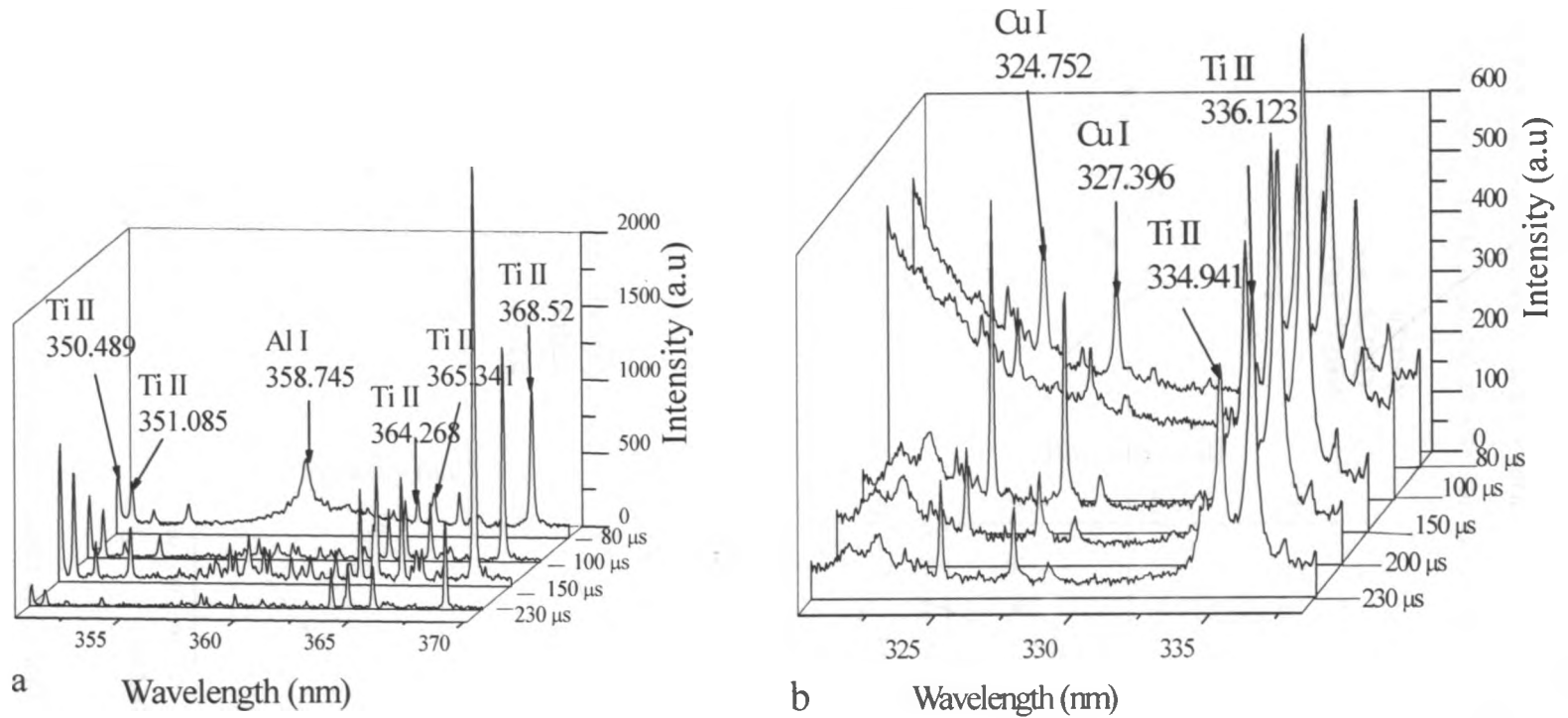


Fig 5.5: LIBS spectra showing the effect of t_d on the emission lines of elements in (a) kaolin and (b) rock simulate.

Comparison of Fig 5.5 (a) and (b) reveals that the plasma continuum dominates the spectra in early stages (80 μ s) of plasma development while the line emission, which is characteristic of elements present in a sample, becomes evident at longer (150 μ s) delay times. Therefore, considering low background continuum, higher emission line intensities and relatively low % RSD, optimal results for LIBS line intensity can be achieved at 150 μ s.

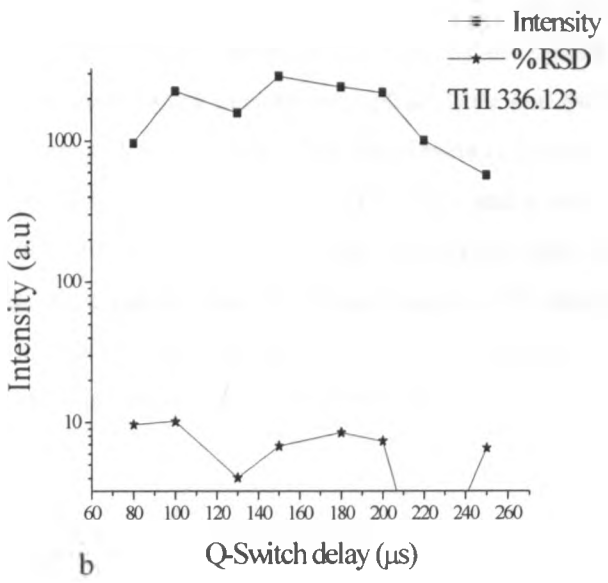
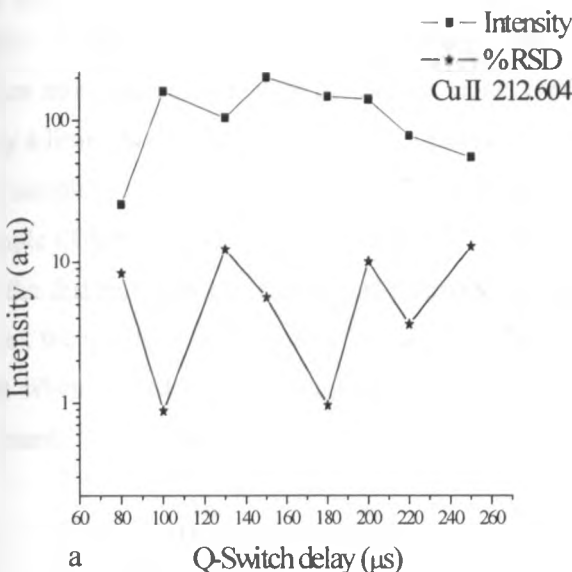


Fig 5.6.1: Optimization for LIBS intensity with respect to % RSD of Cu and Ti in kaolin as a function of delay time.

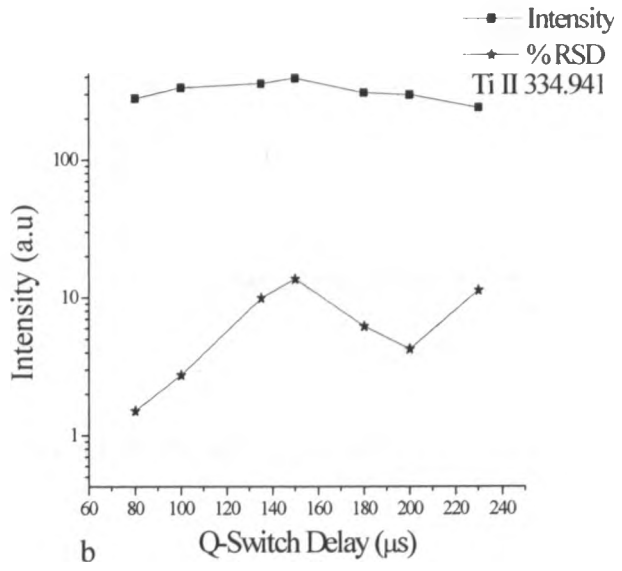
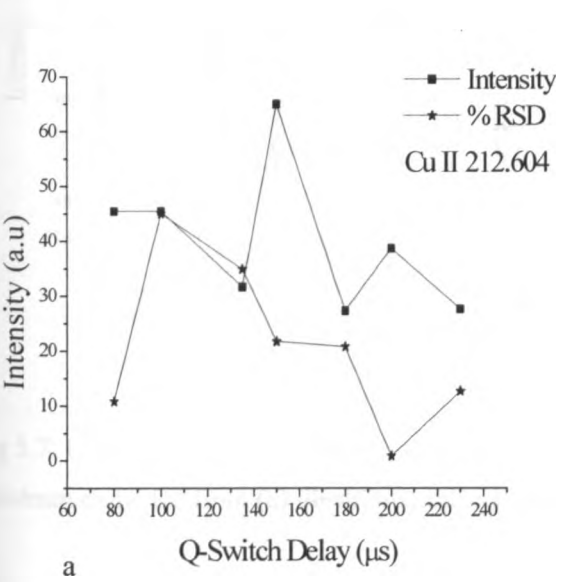


Fig 5.6.2: Optimization for LIBS intensity with respect to % RSD of Cu and Ti in synthetic rock as a function of delay time.

5.2.3 Optical Fiber-to-Sample Distance

The effect of optical fiber to sample distance was also investigated. This is because light emitted from the plasma contains qualitative and quantitative information about the species present, and as such determination of the species in a sample depends linearly on the amount of material ablated and hence the amount of light detected by the spectrometer and optical fiber. It can be seen that at a distance of 10 mm, more emission lines are observed (Fig5.7) implying that at this distance, most light emitted by the sample plasma is collected by the optical fiber hence most species detected; below this value, there is overlap between plasma and optical fiber and therefore, only a little amount of light enters the optical fiber and is detected. Above this value, the plasma is formed above the sample surface hence most of the light entering the optical fiber is due to the ablation of air and a little of the sample (Tognoni *et al.*, 2002). In Fig5.7 it is illustrated that intensity of emission lines of elements also depends on the distance between the optical fiber and the sample. As it can be seen, at optimal distance (10 mm in this case), the intensity of Cu lines (324.754 and 327.396 nm) is much higher than at other distances. This also implies that when recorded plasma light has high intensity, more species are detected hence more intense lines for elements (Muhamad, 2006).

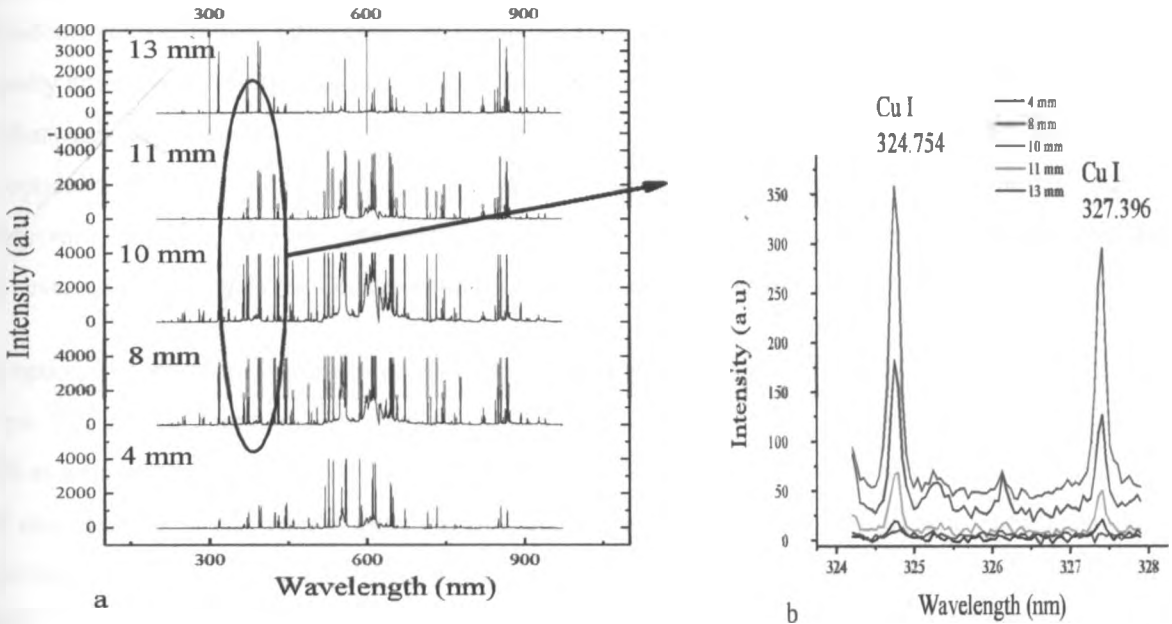


Fig 5.7: LIBS spectra (200 - 980 nm) taken at different distances from the optical fiber and (b) a section of the full spectrum extracted from (a) illustrating this variation.

5.2.4. Number of Ablations per Laser Scan

At the above laser parameters (45 mJ LPE, 0.8 μs t_g , 150 μs t_d and 10 mm optical fiber to sample distance) an average of three spectra at different points on the sample surface were acquired from kaolin and rock simulate at different number of ablation per laser scan. Intensities of emission lines at each value were evaluated (Fig 5.8). Increasing the number of ablations per laser shot results in a substantial decrease in intensities of emission lines due to increase in the crater depth that inhibits amount of plasma viewed by the optical fiber (Tognoni *et al.*, 2002; Sneddon, 2002) hence reduction in line intensities. Therefore a single ablation laser shot was found to be optimal in yielding higher line intensities.

Similar optimization results have been reported by other researchers. Gondal *et al.* (2008) studied the relationship of signal intensity and laser pulse energy, and the results showed that signal intensity increased linearly ($r^2=0.996$) with increasing pulse energy from 10 m J to 30 m J. Wisbrun *et al.* (1994) investigated the effect of repetition rates i.e. delay time(t_d) and integration time (t_w) on signal intensity and SNR using soil and sand samples, and the results showed that the optimum repetition rate for soils was 1 Hz, the optimum time parameters were element-dependent, but a common setup could be found, and t_d was more significant than t_w in controlling the LIBS signal intensity and stability. In the optimization of laser parameters for soil analysis by LIBS, Sirven *et al.* (2008) found out that emission intensity (signal) was proportional to the laser energy, when the laser-produced plasma was in the optically thin region. Furthermore, the variation in the intensity of Cr atomic lines as well as that of the background emission, with the gate delay indicated that the continuum background emission was dominant in the first several microseconds but decayed much faster than the atomic line signal.

The optimal experimental parameters for LIBS on soils and rocks were obtained at 45 mJ LPE, integration time of 0.4 μs , 150 μs delay time and 10 mm optical fiber- to- sample distance for a single ablation hence demonstrating LIBS as a rapid elemental analysis that can be applicable to *in-situ* measurements by just obtaining spectrum using only one ablation. These results aimed at optimizing the reproducibility of intensity measurements, while at the same time achieving plasma conditions where the hypotheses of LTE, stoichiometric ablation and thin plasma are fulfilled. Although the optimal conditions for rocks and soil analyses have been achieved, the best indication that LIBS has not yet overcome the experimentation stage to become a routine methodology is given by the variety of different experimental configurations reported in the literature (Tognoni *et al.*, 2002). Hence each different arrangement is the answer to the versatility of the LIBS technique.

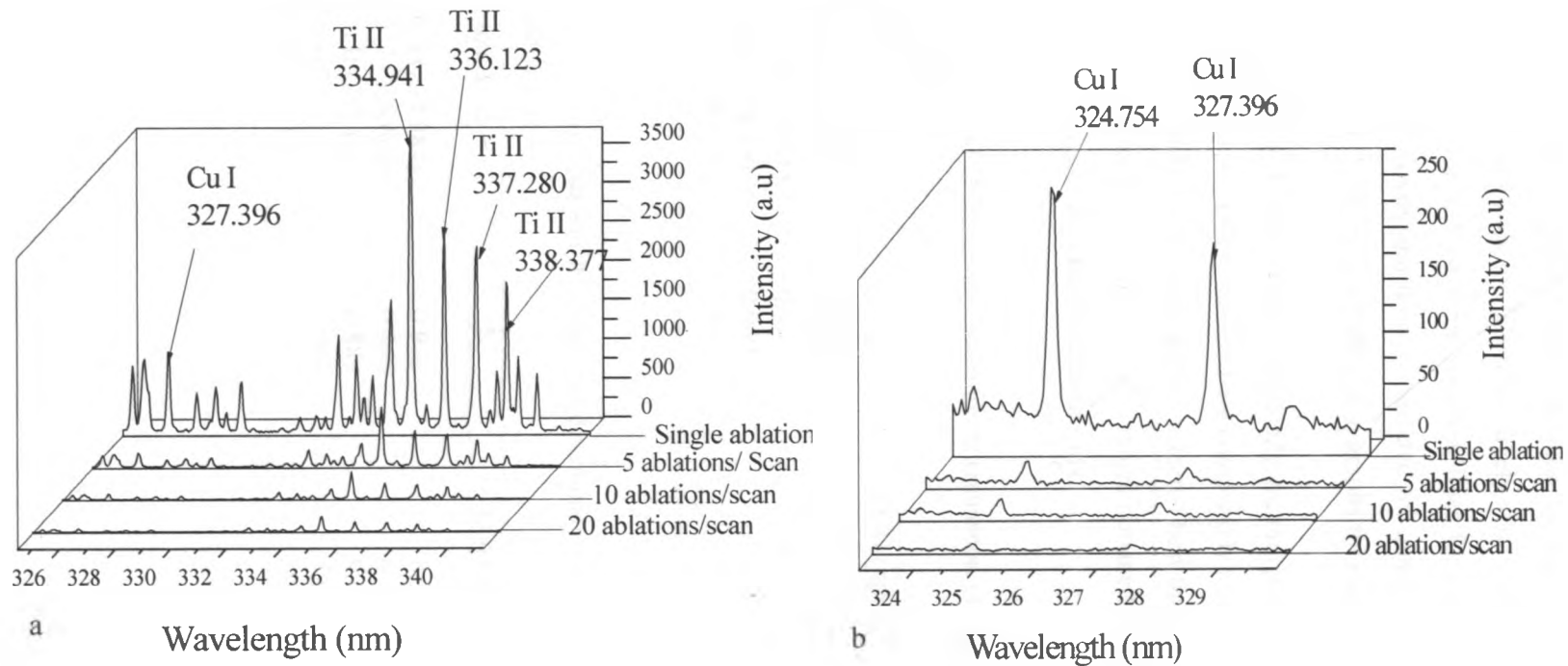


Fig 5.8: Variation of line intensity with respect to number of pulses used to obtain the spectrum of (a) kaolin and (b) rock simulate.

5.3 Calibration for Quantitative Determination of Trace Element Concentrations

Quantitative calibration (multi signal standard addition method) of soils and rocks was carried out using kaolin and synthetic rock as soil and rock models respectively. The calibration curves for the models are shown in Fig 5.9.1. Calibration curves for at least three emission lines for each element were prepared and the curves with favorably good LOD, sensitivity and R^2 were selected for quantitative analysis. The results for these parameters and the lines are shown in Table 5.2(a). Calibration graphs for elements in rock simulate are shown in Fig 5.9.2.

Calibration curves from soil show more analytically meaningful linear relationship between line intensity and trace metal concentration, and LODs obtained are comparable to those obtained by other researchers as discussed below. In this work, the best LOD obtained from selected best lines for detection of As, Cr, Cu, Pb and Ti in soil and rocks (Table 5.2 (a) and (b)). For rocks the values obtained were somewhat higher due to existence of the elements at a relatively high concentration than in soils.

Table 5.2(a) LOD and R^2 values for determination of elements in soils (from univariate calibration)

Element	R^2	LOD (ppm)	Sensitivity (Cg/ μ g)
As I 278.022	0.730	2.4	2.6
Cr II 276.258	0.908	5.1	1.5
Cu II 221.811	0.967	3.1	3.9
Pb I 280.200	0.969	7.6	20.3
Ti II 336.123	0.957	120	450

Table 5.2(b) LOD and R^2 values for determination of elements in rocks from (univariate calibration)

Element	R^2	LOD (ppm)	Sensitivity(Cg/ μ g)
As I (234.984)	0.936	8.3	1.02
Cr I (276.665)	0.846	6.1	0.85
Cu II (212.604)	0.889	9.0	1.77
Pb I (280.200)	0.944	3.0	28.59
Ti II (336.123)	0.957	180	1140

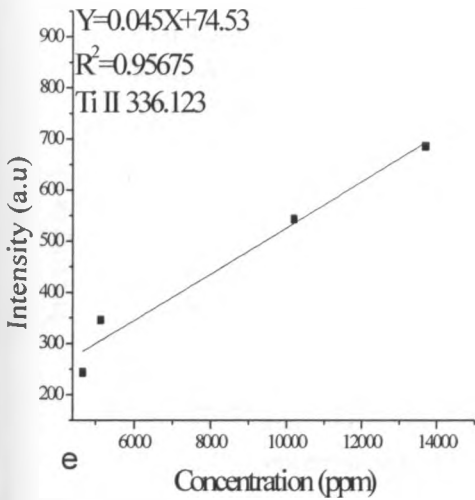
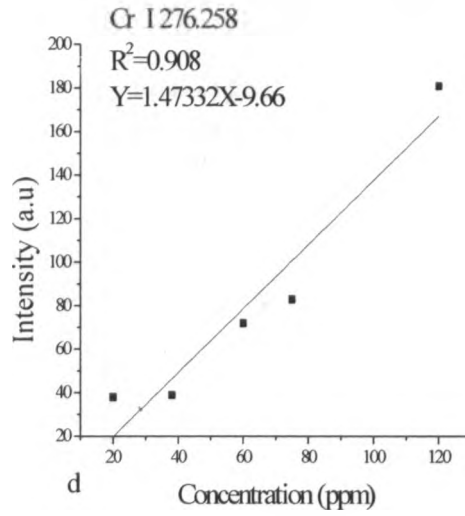
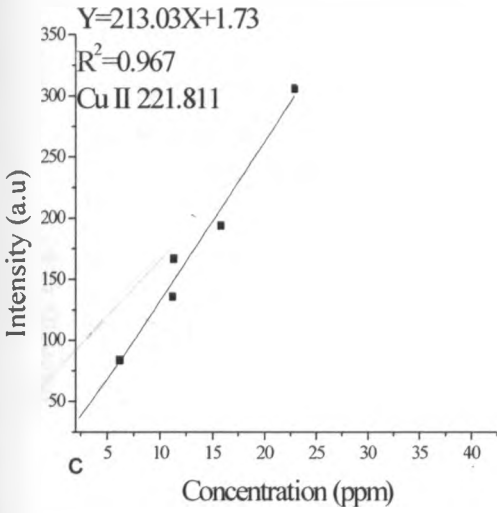
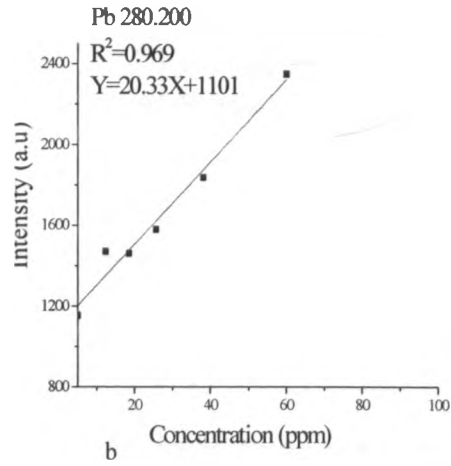
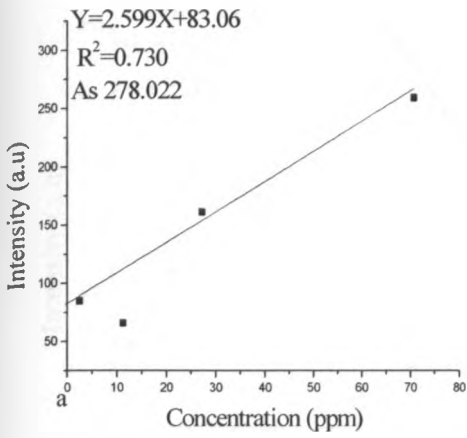


Fig 5.9.1: Examples of univariate calibration curves for As, Pb, Cr, Cu and Ti in soils.

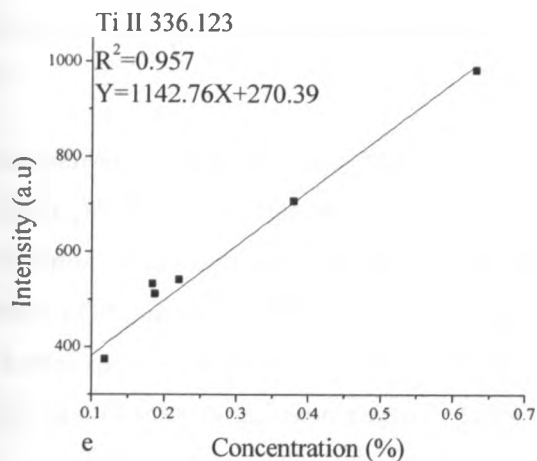
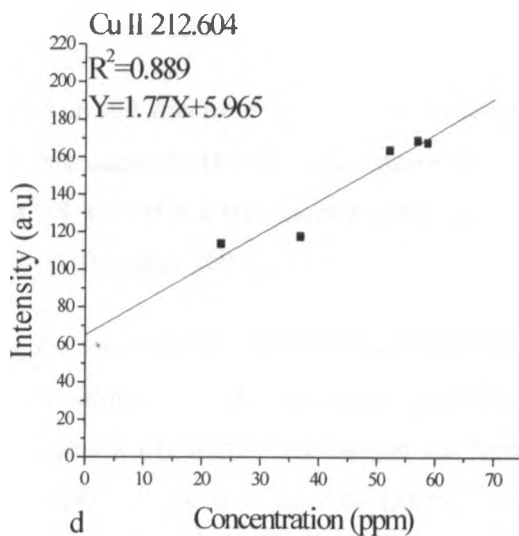
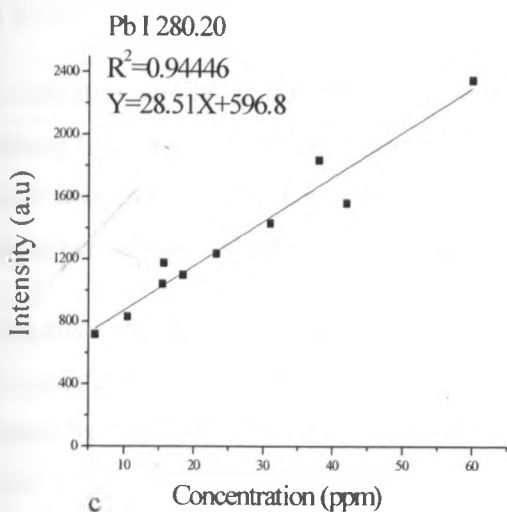
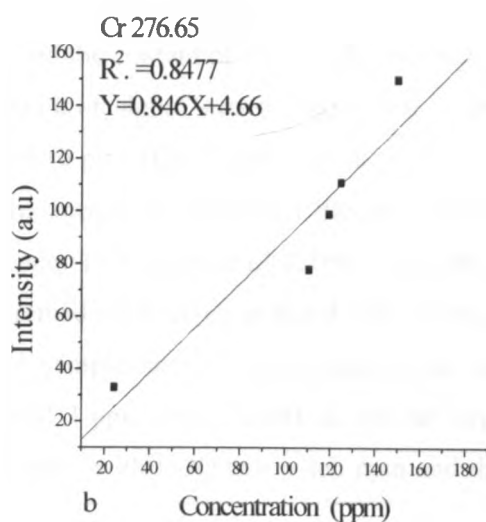
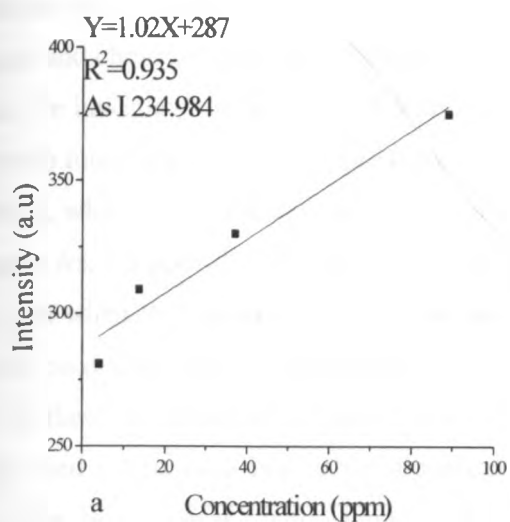


Fig 5.9.2: Examples of univariate calibration curves for As, Pb, Cr, Cu and Ti in rocks.

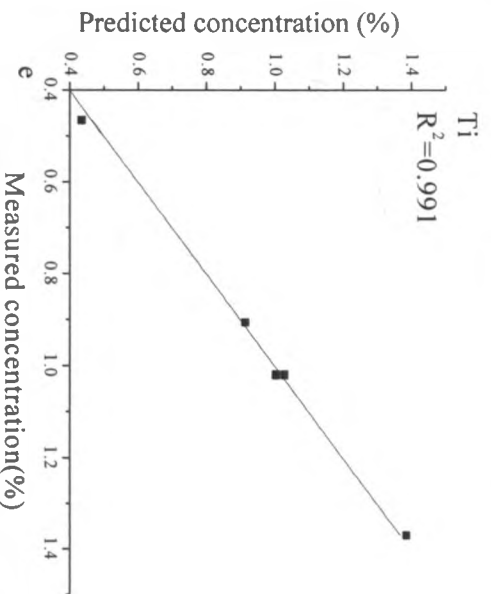
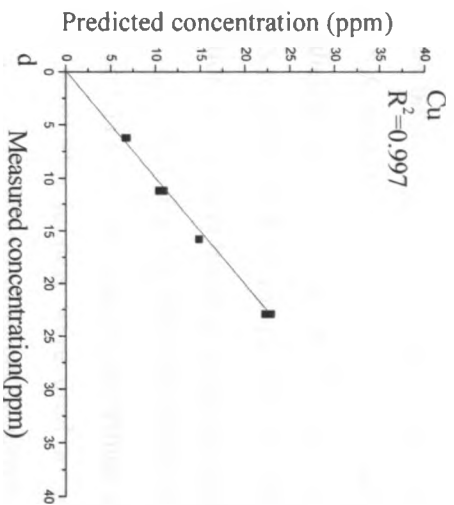
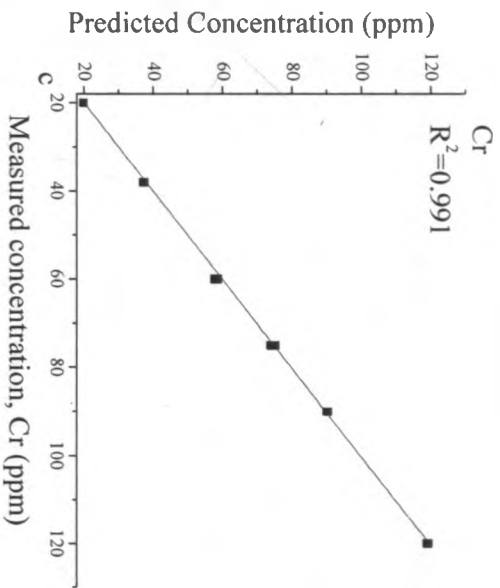
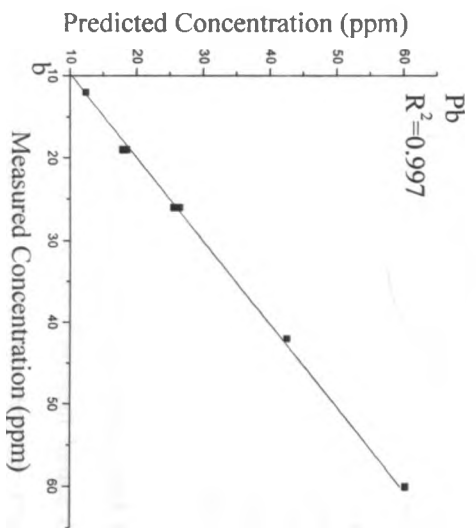
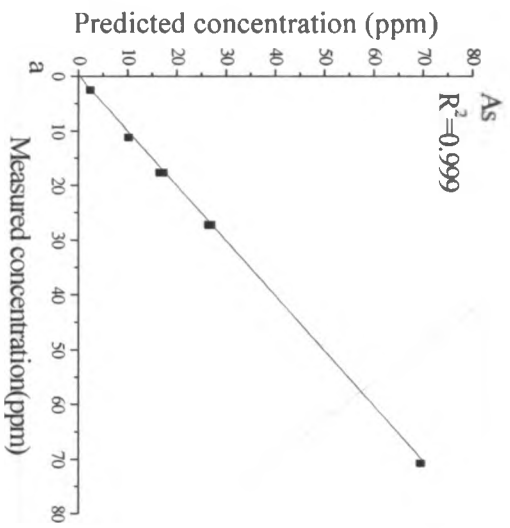
In comparison to other research carried out previously using univariate approach for LIBS in air at atmospheric pressure and choice of best line, Chengli *et al.* (2009) analyzed the content of Pb in soils and obtained the LOD of 8 ppm. On investigating the effect of delay time and gate width on signal intensity using soil samples, Wisbrun *et al.* (1994) found the LOD of 10 ppm (Pb), 20 ppm (Cu) and 10 ppm (Cr). Similar results were found by Frank *et al.* (2001), who carried out research on the analysis of heavy metals in soil using LIBS, the values obtained were 3.3 ppm- As, 2.5 ppm-Cr, 3.3 ppm Cu, 17 ppm Pb and 48 ppm Ti. Gondal *et al.* (2009) found the LOD for Cr to be 2 ppm when they carried out an online monitoring of remediation of Cr polluted soils using LIBS. In their research on determination of trace elements in volcanic rock samples using LIBS, Yamani *et al.* (2009) found the LOD of these elements to be 4 ppm (Cr), 14 ppm (Cu) and 3 ppm (Pb). Therefore we can say that the LIBS system used in this work is capable of analyzing trace elements with LOD below ten ppm and the results are in most cases lower (hence superior) to those published earlier.

5.3.1 PLS Calibration and Prediction of Trace Elements in Soils and Rocks

PLS calibration and prediction models were developed based on full spectrum (200-545 nm) and spectral regions containing line intensities of the elements of interest taking into consideration the minimum ends of the peaks for selected lines and using the Unscrambler software (version 9.8, CAMO). LIBS spectra were first averaged to one spectrum per sample and pretreated by standardization method (Richard, 2003).

The models were developed with the PLS regression using the spectral data obtained from the model (kaolin and rock simulate) samples at the concentration ranges stated in Section 4.5. Predictive ability of the PLS models was evaluated by full cross-validation. Full cross validation systematically leaves one sample out from the original samples as the validation data and uses the remaining samples as the training data (Zhe *et al.*, 2011). This procedure was repeated until every sample was used once as the validation data. Full cross-validation is a conservative model evaluation method that helps to select the model with the best predictive ability (Sirven *et al.*, 2006).

Results from the PLS analysis are presented in terms of correlation coefficients (R^2), root mean square error of calibration (RMSEC) and standard error of prediction (SEP). An independent set of spectral data (five samples with different concentrations of As, Cr, Cu, Pb and Ti) was set aside for prediction purposes so as to evaluate the capability of the model generated in predicting future similar samples. Fig 5.10 shows PLS calibration curves from partial spectra for As, Cr, Cu, Pb and Ti in soils. Regression coefficient (R^2) and the root mean square error of calibration (RMSEC) are summarized in Table 5.3



Figs.10: PLS calibration curves for As, Pb, Cr, Cu and Ti in kaolin.

Table 5.3. R² and RMSEC values for soils using PLS calibration models

Element	Full spectrum (200-545 nm)			Feature selection		R ²
	RMSEC (ppm)	SEP (ppm)	R ²	RMSEC (ppm)	SEP (ppm)	
As	3.76	11.72	0.968	0.73	3.98	0.999
Cr	92.44	136.72	0.927	2.87	5.03	0.991
Cu	1.44	1.10	0.999	0.15	0.76	0.999
Pb	0.65	1.91	0.982	0.28	0.29	0.997
Ti	2300	234.78	0.974	500	152.00	0.991

Full spectrum region of 200 – 545 nm was chosen because the region contained mostly atomic and ionic lines of the elements of interest, beyond this region, atomic lines of C, H, O and N are dominant hence contain more redundant information. Partial spectra were selected by choosing regions containing As, Cr, Cu, Pb and Ti emission lines within the 200 – 545 nm range.

It can be seen that RMSE in all PLS models with spectral regions are better (lower) than those in the full spectra model. Specifically, compared with the full spectra model, the PLS models with spectral region have lower RMSEC values while high calibration quality is maintained as indicated by SEP values (Table 5.4). The lower RMSEC value indicates that the proposed spectral region based PLS models are more robust than the full spectra based model for measuring samples with matrix out of the calibration set. This is because variables influencing concentration of these elements in the spectra are fully captured in regions containing elements while in the full spectrum, variables from other elements apart from As, Cr, Cu, Pb and Ti and noisy regions contribute to model development thus affecting the prediction results (Yang *et al.*, 2010). PLS models were used to test their applicability on standard reference materials (SRM) soil samples IAEA soil 1 having different concentrations of the elements except Ti. Results of univariate and PLS prediction of the concentrations are shown in Table 5.4 (a).

Table 5.4(a) Comparison of univariate multi signal (using best line) and PLS calibration in prediction of element concentration in SRM for soils

Sample	Method	As (ppm)	Cr (ppm)	Cu (ppm)	Pb (ppm)
Soil 1	SRM (reference)	28±3	104±9	30±6	38±7
	Univariate	46	40	36	18
	PLS (full spectrum)	14	230	15	25
	PLS (feature selection)	32	123	27	39
%RSD		9	12	7	2

* % RSD value for best model

In Table 5.4 (a), it can be seen that PLS results improved as indicated by the respective values of percent relative standard deviation, whereas classical approach had poor prediction. This is because with PLS, all the spectral regions with chemical content of the elements of interest are simultaneously taken into account and modeled with

respect to many features (line shape, intensity, spectral interference, broadening) unlike in classical approach where only the intensity of one or multi signal spectral line is considered; as such some of the important information not related to the intensity (spectral interference, line broadening) but influencing the concentration is left out (Labbe *et al.*, 2008). Therefore, for linear relationships, PLS calibration should be used in LIBS analysis of soils. PLS results using full spectrum performed very poorly because of so many variables influencing the model but not important being taken into account. That is, noise influence, interference from emission lines of other major elements present in sample e.g. Ca, Mg and spectral overlap between emission lines of different elements close together, hence affecting the modeling ability of PLS.

Furthermore, the choice of spectral regions containing emission lines for elements of interest yields models which contain main quantitative information, this helps to avoid the use of the noise in the spectrum thus becoming more robust over a wide concentration range. Similar results were obtained by Niangfang (2009) who found that PLS regression using the reduced spectral range (300-350 nm) containing Cu and Zn peaks produced the best results among all the spectral ranges, which indicated that use of the suitable spectral range in the PLS regression improved the LIBS analytical performance.

Results from this study indicate that the use of PLS significantly improves the quantitative analytical capacity of LIBS. The application of PLS in analysis of LIBS spectra has great potential for constructing robust calibration models for trace quantitative LIBS analysis and providing reliable prediction of element concentrations consistent with conclusions of previous studies (Clegg *et al.*, 2006; Labbe' *et al.*, 2008; Gottfried *et al.*, 2009; Martin *et al.*, 2010). PLS results for rocks SRM showed poor results as shown in Table 5.4 (b), this can be attributed to non-linearity in the variation of concentrations with respect to line intensities resulting from complex sample thermo chemistry, hence linear models like PLS do not yield satisfactory results. As a result, nonlinear method of calibration was carried out using ANNs.

5.3.2 ANNs Calibration for Prediction of Trace Elements in Rocks

For rock models, classical calibration showed nonlinear relationship (this can be seen from the non-uniform distribution of points and low values of R^2 in Fig 5.9.2) in variation of intensity with respect to concentration. Furthermore, normalization by internal standard of emission lines for these elements using Ca or C line could have led to improvement of the result but this was not obtained because there were no suitable lines for Ca/C to be used as internal standards. This is due to the fact that most of the lines were not near the region containing elements of interest hence not suitable for analysis. As such, calibration with neural network was performed on the data set of the simulate spectra at different concentrations.

A two layer (in – built with back propagation training function) neural network (NN) was generated for As, Cr, Cu, Pb and Ti using Matlab version 7.8 (The Mathwork, Inc). Since using full spectra requires large memory due to large a large number of data, data compression was necessary for neural networks computation. Data compression was done by selecting spectral regions of containing the elements to be analyzed. Spectral regions containing emission lines of elements studied in this work were utilized as inputs in the network while their measured concentrations were fed into the network as targets i.e. expected outputs. Back propagation training functions with Levenberg-Marquardt (LM) algorithm was used to train the feed forward networks for non-linear regression because it obtains lower mean square errors compared to other algorithms due to its faster rate of convergence hence advantageous for accurate training (Howard *et al.*, 2009).

The training session consisted of assembling training data, creating the network object, training the network and simulating the network response to new inputs. The number of neurons in the hidden layer was chosen based on the mean square error (MSE) and the training performance of each network during the training session; training was repeated several times until the best results of low MSE and satisfactory performance were achieved. Training stopped automatically when the validation error increased thereby avoiding over fitting. After developing the NN model, results were tested by simulating the output of the neural network with the measured input data which were compare to the measured outputs. These results were saved in the computer. Sample training performance plots are shown in Fig 5.12. The figure shows mean square error (MSE) starting at a higher value and decreasing to a smaller value (the network is learning). Three lines in the plot are for training, validation and testing. Three lines arise because the inputs fed into the network are divided into three sets; 60 % for training the network, 20 % for validating how well the network generalizes and 20 % to test how the network will perform on new set of data. The training stopped when validation increased for five (e.g. Fig 5.11 (a) and nine (Fig 5.11 (b)) iterations, which occurred at iteration 11 and 15 respectively. By epoch 5 (Fig 5.11 (a)) and 9 (Fig 5.11 (b)), no significant over-fitting had occurred; the test and validation sets behaved in a similar manner. Advantage of ANN over other methods is that over fitting is automatically avoided by stopping the training when validation error increases beyond the expected low limit (Howard, 2009). Calibration graphs obtained from ANN model developed are displayed in Fig 5.12.

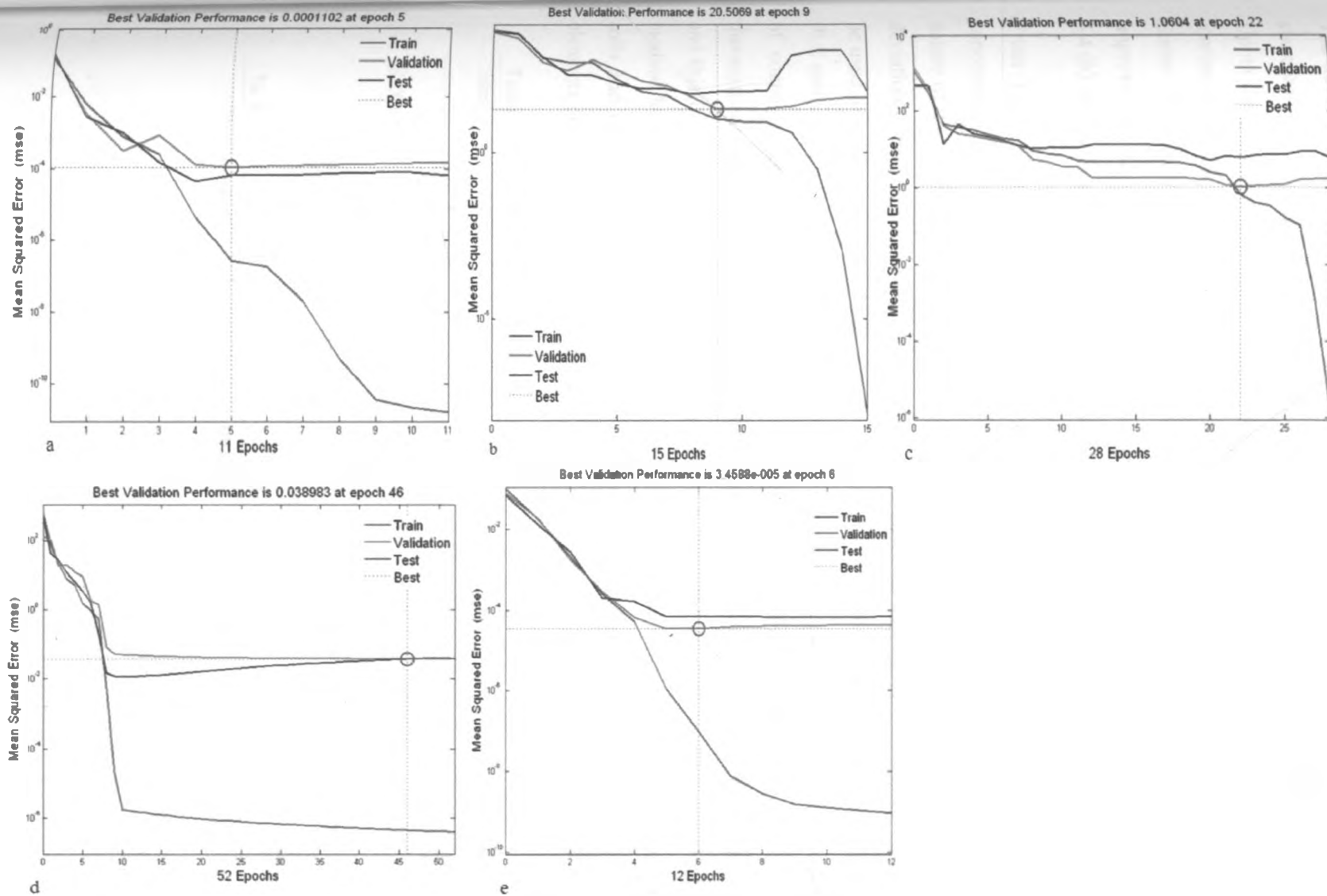


Fig5.11: Performance plots for (a) As, (b) Cr, (c) Cu, (d) Pb and (e) Ti ANNs calibration showing the training pattern of the network.

5.3.3 Validation of the PLS and ANNs Models

The developed models (ANNs and PLS) were used to predict the concentration of the above elements in rocks standard reference materials obtained from United State Geological Survey (SCO-1). SCO-1 is typical of the Upper Cretaceous silty marine shales, intermediate between fine-grained offshore shales and coarser near shore marine siltstones. The rock is medium dark-gray silty shale having thin lighter colored silty laminations. (United States Geological Survey Certificate of Analysis, Cody shale-SCO-1). Prediction from ANNs showed improvement compared to PLS result because ANN performs better in modeling nonlinear relationships. Table 5.4 (b) shows the results for three models used to predict concentration of trace elements in SRM rock samples.

From Table 5.4(b), it can be seen that not all results obtained from NN models are closer to the certified concentration of the above elements in SRM rock samples. This can be attributed to the slight difference in the nature of the simulate matrix and actual rocks as well as complex sample thermochemical properties hence slight deviation in the results. In the case of prediction the elements concentrations in rocks, ANN calibration curves can be used to predict the concentrations of As, Cr, Cu and Ti while univariate calibration methods for Pb prediction. PLS methods are linear techniques meant for solving relationships which are linear. In case of nonlinear variation of concentration in relation to spectral intensity (caused by extreme matrix effect and complex sample thermochemistry) as in the case of rocks univariate calibration graphs, the performance of PLS is less sufficient and this is why the predicted values from PLS in rocks SRM are less accurate compared to those from ANNs models. Models that yielded better results for rocks (see Table 5.4 (b)) were used to predict the concentration of soils and rocks samples respectively, from Lambwe and Olkaria. Tables 5.5 show the concentration of five elements detected in the field samples.

Table 5.4 (b). Prediction ability of different methods for elements in SRM (rocks)

Sample	Method	As (ppm)	Cr (ppm)	Cu (ppm)	Pb (ppm)	Ti (ppm)
	SRM (reference)	12±1	68±5	29±2	31±3	0.38±0.06
SCO-1	Univariate	BDL	58	9	28	0.21
	ANNs	9.17	72	25	26	0.28
	PLS (full spectrum)	BDL	139	34	7.5	0.33
	PLS (feature selection)	9	98	11	17	0.19
% RSD*		19	4	10	12	11

*Values calculated using the best model

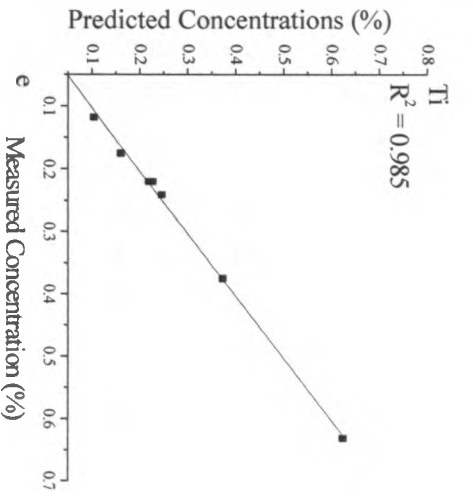
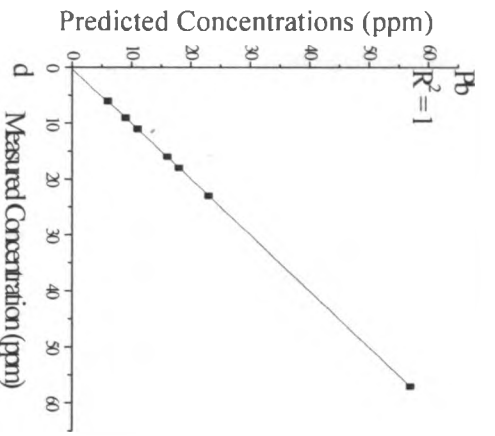
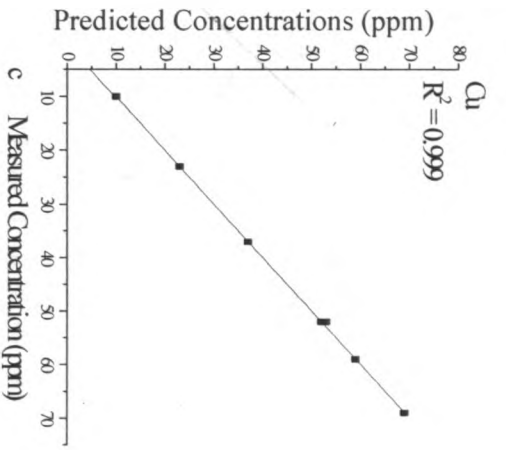
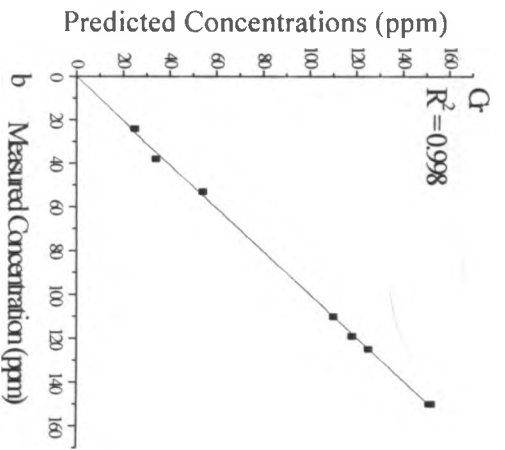
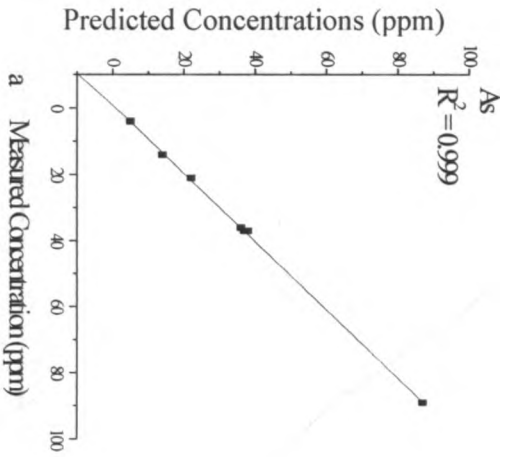


Fig 5.12: ANN calibration curves for As, Cr, Cu, Pb and Ti in rock simulate.

Table 5.5 Predicted concentration of the elements in the samples

Element Concentration (ppm) in rocks						
Category	Sample	As	Cr)	Cu	Pb	Ti (%)
HBRA (geothermal)	HGR 9	67	150	65	53	0.13
	HGR 22	26	145	54	44	0.32
	HGR 30	20	118	41	47	0.09
	HGR 34	27	145	33	44	0.14
	HGS 4	42	149	47	45	0.23
	HGS 8	12	120	31	31	0.19
	HGS 12	18	147	64	45	0.34
	HGS 22	38	127	46	44	0.32
	HGS 23	113	109	42	45	0.47
	HGS 33	139	137	120	43	0.18
HBRA (non- geothermal)	HNP 1	11	146	45	40	0.22
	HNP 2	47	149	37	29	0.18
	HNP 15	13	149	53	45	0.17
	HNP 16	20	149	71	44	0.20
	HNP 18	26	150	40	39	0.19
	HNP 19	7	149	60	44	0.18
	HNP 24	29	147	67	66	0.29
	HNS 21	17	149	56	44	0.28
	HNS 27	80	150	85	46	0.18
	HNS 29	21	150	69		0.30
NBRA (geothermal)	GSA-1	76	149	76	95	0.26
	GSA-2	13	87	84	94	0.10
	GSA-3	37	150	80	84	0.16
	GSB-2	53	55	108	91	0.03
	GSB-3	67	116	109	87	0.18

Category	Element Concentration (ppm) in soils					
	Sample	As	Cr	Cu	Pb	Ti (%)
HBRA (geothermal)	HGR 17	4	50	5	24	0.52
	HGR 24	27	100	13	17	0.73
	HGR 25	37	78	13	30	0.75
	HGR 30	15	73	11	26	0.94
	HGR 32	22	72	13	25	1.07
	HGR 34	26	75	13	27	1.43
	HGS 7	24	73	15	24	0.85
	HGS 21	54	108	22	15	0.79
	HGS 22	63	90	23	18	0.76
	HGS 23	50	88	35	29	0.91
	HGS 31	25	53	12	31	0.73
	HGS 33	38	65	13	34	0.84
	HBRA (non-geothermal)	HNP 2	17	51	10	24
HNP 14		18	52	7	26	0.72
HNP 16		36	64	13	24	0.99
HNP 17		35	51	10	33	0.38
HNP 18		12	37	4	34	0.46
HNP 20		9	31	5	32	0.61
HNS 27		20	35	8	32	0.48
HNS 29	24	36	7	35	0.47	
NBRA (geothermal)	GFA	40	40	12	12	0.60
	GFC	26	39	9	16	0.62
	GSB	32	18	8	33	0.38
	GSC	37	28	9	29	0.45

The overall range of concentrations for trace elements in rocks was as follows; As (7 -139 ppm), Cr (87- 150 ppm), Cu (33-120 ppm), Pb (30-95) and Ti (0.03 - 0.47) %. While concentrations of As, Cr and Ti are slightly higher in HBRA geothermal, Pb and Cu were found to be lower in HBRA and higher in NBRA geothermal. Elevated Pb and Cu concentration in NBRA geothermal region could have been enhanced by geothermal activities i.e. fluids which are known to contain Pb, which results to increased concentration of Pb relative to a HBRA geothermal (Ozgur, 2002).

The predicted concentrations lie within the range reported by other researchers in similar fields. Achola (2009), analyzed some radioactive elements (U, Th, K, Ti and Pb) in Lambwe rocks (HBRA non geothermal rocks) using X-ray fluorescence (XRF) technique and found that they had elevated level of Pb and Ti in the range (41 – 1560 ppm) and (0.27 - 2.2 %) respectively. Rustem (2003), carried out an analysis of major and trace element concentration in selected rocks from a hot spring (NBRA geothermal) to find the effect of these elements on human health; trace elements had varied concentration with Cr (40-152 ppm), Cu (7-32 ppm), Pb (8-110 ppm) and Ti (0.08-0.53 %).

Other researchers include: Lucia *et al.* (1998) (Cr: 35-108 ppm, Cu: 13-68 ppm and Ti: 0.18-2.36 %); Wendy and Mary (1997) (Ti: 0.14-0.25 %); Weaver *et al.* (1972) (Ti: 0.114 - 1.95 %); Hammes *et al.* (2007) (Ti: 0.11-0.85 % Cu: 16-43 ppm, Cr: 4-43 ppm, As : 40-64 ppm); Ohde (2004) (As: 13-130 ppm) and Yamani *et al.* (2009) (Cr: 285-1519 ppm, Cu: 52-380 ppm, Pb: 10-92 ppm). Hence it may be concluded that LIBS coupled with multivariate chemometrics techniques is capable of quantitative determination of trace element concentrations in HBRA geothermal field matrices (rocks).

On the other hand, the overall ranges of trace element concentrations in soils were as follows; As (4-63 ppm); Cr (18 -108 ppm); Cu (4-35 ppm); Pb (12 – 35 ppm) and Ti (0.30 - 1.43 %). Concentrations of these elements in soils were found to be generally lower than that in rocks except Ti. This is because, already elevated levels of these elements in HBRA are further enhanced by underground geothermal activities as geothermal fluids contain traces of these elements.

Research on geochemical and radionuclide of Tuzia geothermal field (NBRA geothermal) revealed that in soil samples, heavy metals were found to be in higher concentration in the vicinity of hot springs, with Cr being on average 40 ppm (Alper *et al.*, 2008). Stuart *et al.* (2004) carried out an analysis of trace elements in soils from Longonot volcano using XRF and ICP-MS; concentration of these elements were in the range of; Cr (4-53 ppm), Cu (6-49 ppm), Pb (7-24 ppm) and Ti (0.33-0.832 %). Kursad *et al.* (2002) investigated heavy metals in the volcanic soils from Turkey and detected four heavy metals to be in excess levels in the soils with Pb (40-130 ppm) and Cu (9-25 ppm). Similar results were reported by Adamo *et al.* (2003) (Cr: 45-335 ppm, Pb: 23-100

ppm), Amaral *et al.* (2006) (Ti: 0.38-0.70 %, Cu: 18-58 ppm, Cr: 22-55 ppm, Pb: 17-83 ppm), Laurent *et al.* (2003) (Cr: 52-95 ppm, Cu: 29-52 ppm, Pb: 89-155 ppm, Ti: 0.58-1.22 %) and Emmanuel *et al.* (2008) (Cr: 35-108 ppm, Cu: 6.5-164 ppm).

Correlation coefficients for the concentration of the elements in the soils and rocks are shown in Table 5.6. Correlation coefficients help in understanding the relationship between the occurrence and concentrations of the trace elements. If the correlation is close to one (positive correlation), it implies that the elements are linearly related to each other such that if one exist at higher concentration in the sample, the other element also exists at higher concentrations and vice versa. On the contrary, if the value is close to negative one (negative correlation); it means the elements are anti-correlated such that if one exists at high concentration, the other will be in low concentrations and vice versa.

Table 5.6 Pearson correlation coefficients for the elements in the samples using the mean concentrations

Soils						Rocks							
		As	Cr	Cu	Pb	Ti			As	Cr	Cu	Pb	Ti
As	HBRAG		0.7	0.8	-0.3	0.0	As	HBRAG		-0.1	0.6	0.2	0.2
	HBRANG	1.0	0.7	0.9	-0.2	0.2		HBRANG	1.0	0.5	0.3	0.0	-0.2
	NBRAG		0.0	0.6	-0.0	-0.1		NBRAG		0.3	-0.2	-0.0	0.5
Cr	HBRAG	0.7		0.6	-0.7	0.1	Cr	HBRAG	-0.1		0.3	0.3	-0.2
	HBRANG	0.7	1.0	0.8	-0.8	0.7		HBRANG	0.3	1.0	0.2	-0.3	-0.2
	NBRAG	0.00		0.7	-0.9	0.9		NBRAG	0.3		-0.6	-0.2	-0.8
Cu	HBRAG	0.8	0.6		-0.1	0.1	Cu	HBRAG	0.6	0.3		0.2	-0.0
	HBRANG	0.8	0.8	1.0	-0.6	0.5		HBRANG	-0.3	0.2	1.0	0.5	0.2
	NBRAG	0.9	0.7		-0.8	0.6		NBRAG	0.2	-0.6		-0.2	-0.5
Pb	HBRAG	-0.2	-0.1	-0.1		0.1	Pb	HBRAG	-0.2	0.3	0.2		-0.0
	HBRANG	-0.1	-0.7	-0.6	1.0	-0.9		HBRANG	-0.0	-0.3	0.5	1.0	0.6
	NBRAG	-0.0	-0.9	-0.8		-0.9		NBRAG	0.0	-0.2	-0.2		0.0
Ti	HBRAG	0.0	0.0	0.1	0.1		Ti	HBRAG	0.2	0.2	-0.0	-0.0	
	HBRANG	0.1-	0.0	0.5	-0.9	1.0		HBRANG	-0.2	-0.2	0.2	0.6	1.0
	NBRAG	0.1	0.9	0.6	-0.9			NBRAG	0.3	0.0	0.3	0.9	

Note: HBRAG - HBRA geothermal, HBRANG - HBRA non geothermal, NBRAG - Non HBRA geothermal areas.

In HBRA geothermal areas As, Cr and Cu were positively correlated but they were negatively correlated with Pb and Ti. For elements in NBRA geothermal soils, As was highly correlated to Cu and negatively with Cr, Pb and Ti. Cu and Ti were positively correlated to each other but negative with As and Pb. Ti was only correlated positively with Cr and Cu. We can therefore conclude that concentration and interrelationship of these elements are different (not high for all the elements and vice versa) in HBRA non geothermal, NBRA geothermal, and HBRA geothermal soils. Weak correlation patterns were observed in rock samples due to the distribution of the element concentrations in rocks

Therefore a HBRA geothermal area is uniquely characterized by positive correlation of As and Cr concentrations in soils while a NBRA geothermal area is characterized by negative correlation of Cu with Pb and Ti, and Pb with Cr and Ti.

Although concentrations of these elements have been found to occur naturally in soils at levels below 30 ppm, 110 ppm, 100 ppm, 200 ppm for As, Cr, Cu and Pb respectively (ANZECC/NHMRC Guidelines 1992, EPA 1986a), contaminated soils (including HBRA soils) usually contain more than the threshold values.

Ti concentration was found to be higher in soils than in rocks (by 0.62 % in HBR geothermal, 0.40 % in HBRA non geothermal and 0.37 % in NBRA geothermal areas). This could be due to rock weathering enhancement of the radionuclides and other heavy trace element concentrations in soils thereby elevating the concentration of most elements including Ti (Adel and Arabi, 2006).

Although concentration of some elements e.g. As in some samples (HGR 25, HGS 22, HGS 33, HNP 17, HNP 18, GFA, GSB and GSC) are above the recommended level, most of them (Cr, Cu, Pb) are within the range recommended by US Environmental Protection Agency (EPA 1986a) and as such, they are not yet a threat to the surrounding population.

In conclusion, LIBS coupled with multivariate calibration techniques developed have successively applied to qualitative and quantitative analysis of trace elements in geothermal field matrices. The results obtained so far indicate that LIBS is a rapid, noninvasive technique that can be used for analysis of environmental samples which in turn can help in monitoring of soil contamination.

5.4 Classification of Rocks and Soil using Chemometric techniques (PCA and SIMCA)

5.4.1 Principal Component Analysis

The data matrix obtained from LIBS spectra (full spectra: 200 – 545 nm, elemental concentrations, spectral regions containing emission lines of As, Cr, Cu, Pb and Ti) of the soil and rock samples were first pre-treated by standardization method and then subjected to PCA in order to have an overview of existing trends and discover the main property variations in the data. PCA as the basic tool for data analysis simultaneously provides a visual representation of relationships between samples and variables as well as insights into sample homogeneities and heterogeneities (Mark, 2001). In this case, all individual measurements on rocks and soils were referred to as samples, while the spectral intensities taken at each particular wavelength were referred to as variables. Using Unscrambler (CAMO) software version 9.7, PCA was performed on the pretreated spectra. A total of 6 principal components (PCs) was used which carried total explained variance of 94 %. The score plot in Fig 5.13.1 shows

the coordinates of the spectra in the plane of first and second PCs, PC1 (63 %) and PC 2 (14 %) which contains 77 % of the total spectral information.

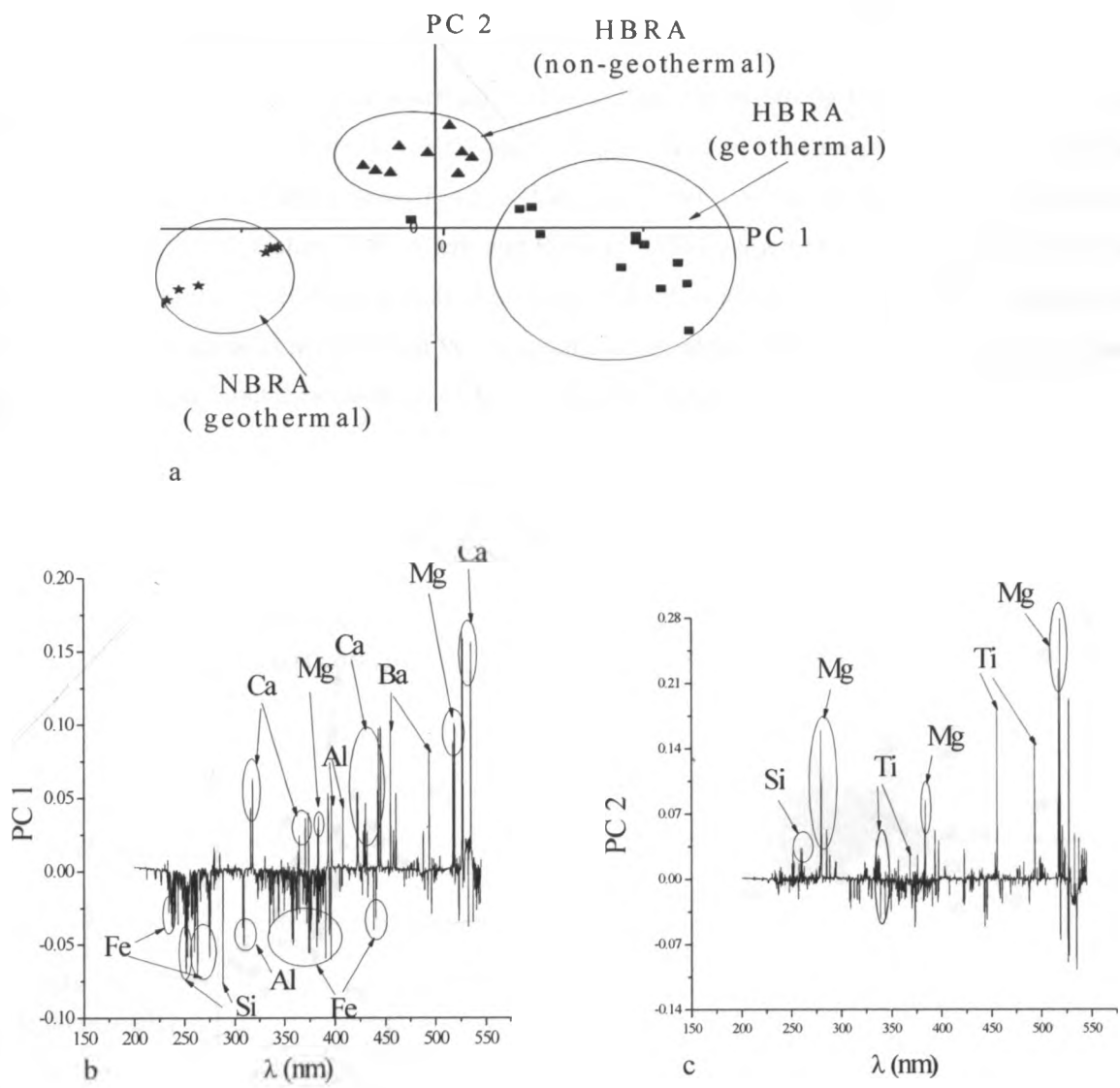


Fig 5.13.1: PCA score (a) and (b-c) loading plot for soils taken based on the full spectra.

Fig 5.13.1 shows the PC scores and loading plot for LIBS analysis of the three different classes of soils analyzed simultaneously using PCA. Clearly, the samples of each class tend to cluster together and in almost all cases are fairly well separated from the other classes. Of these, non HBRA geothermal soils appear to be the easiest to distinguish based on their distance from the other classes. It is also interesting to observe the dispersion of the HBRA geothermal soils class along the PC directions, e.g. HBRA non geothermal soils have clustered along PC 2, HBRA geothermal samples are distributed along PC 1 downwards while non HBRA geothermal soils are negatively correlated to the HBRA geothermal ones as they lie on the negative side of PC 1. Exploration of the

loading plots revealed that each of the group is characterized by different spectral signatures for elements. HBRA geothermal soils were found to contain mostly Ca, Ba and Mg (see associated wavelengths in Appendix VI). HBRA non geothermal soils on the other hand had characteristic emission lines of Ti. Strong lines of Ca and Mg are repetition and therefore their influence is captured in PC 1.

Samples from Olkaria (non HBRA geothermal) were characterized by strong lines of Al and Fe. The clustering was based on spectral features in the UV-VIS range. This is expected because previous studies have shown that soils in Lambwe valley (a HBRA area) have exchangeable high content of Na, Mg, Ca and highly alkaline (Allsops and Baldry, 1972; Bahat, 1979; Clerk and Roberts, 1986) while Olkaria (a non-HBRA) is characterized by ferruginous and silica minerals (Marshall *et al.*, 2009; Macdonald and Scaillet, 2006). From the loading plot for the full spectra, it can be concluded that PC 1 contains information (intensities) of Ca, Mg, Si, Fe and Al while PC 2 gives information about concentration of Ti and Si in the samples.

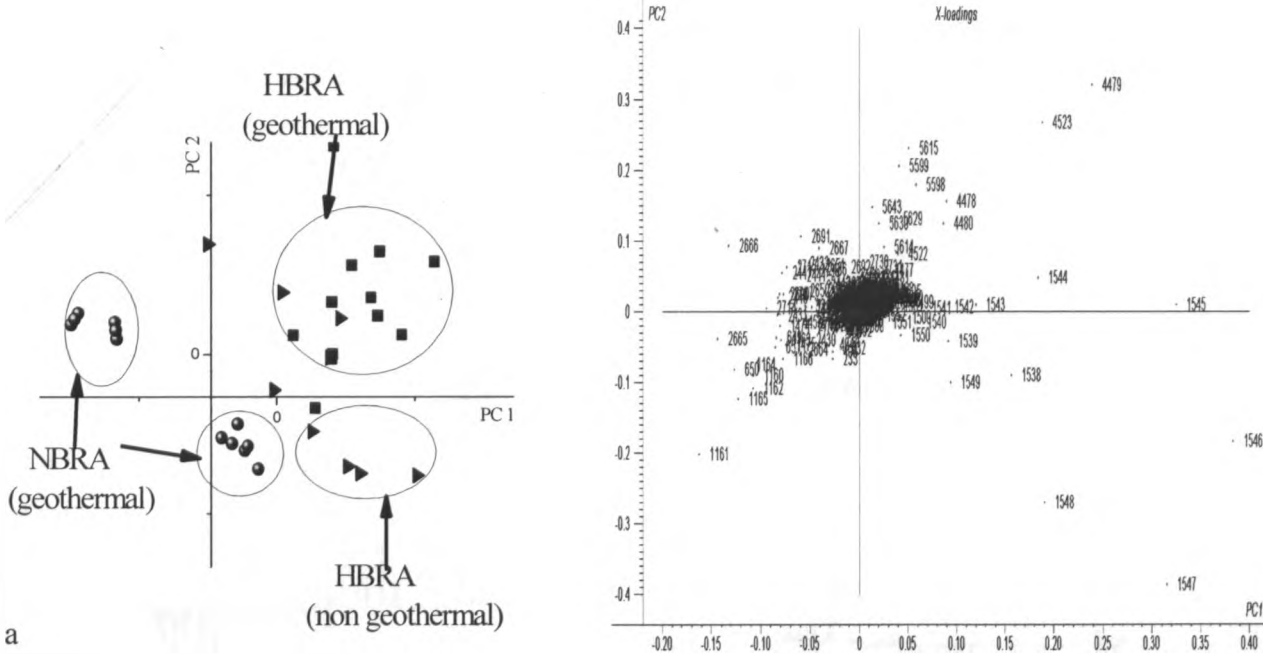


Fig 5.13.3: PCA score (a) and loadings plot for soils taken based on feature selection.

In terms of elements mentioned above (As, Cr, Cu, Pb, Ti), it can be seen that there exist four different groups, with non HBRA soils clustering in two sub groups i.e., one group far away from the rest and the other lying close to Lambwe soils. On exploration of the loading plot (on the right hand side of Fig 5.13.2 the pixel numbers represent wavelengths for the elements of interest as they occur in the LIBS spectrum), it was found that samples in the 1st quadrant (HBRA geothermal) were characterized by emission lines of Pb and Cr hence in agreement

with results obtained using full spectrum although the cause of clustering has been narrowed down to the elements of interest, i.e. As, Cr, Cu, Pb and Ti.

Soils sampled from fumaroles (Olkaria) were found to be characterized by As, Cr and Pb lines (4th Quadrant), those sampled from the streams were associated with Ti lines. Ti lines were also found to be associated with HBRA non geothermal soils. This can be seen from the clustering of the samples in 2nd quadrant. This is expected because from earlier studies, the level of Pb in rocks sampled from Lambwe valley was found to contain elevated levels of Pb and Ti, (Achola, 2009) due to the presence of NORM in carbonatites. PCA scores and loadings plot for rock samples based on the full and partial spectra are shown in Fig 5.13.3.

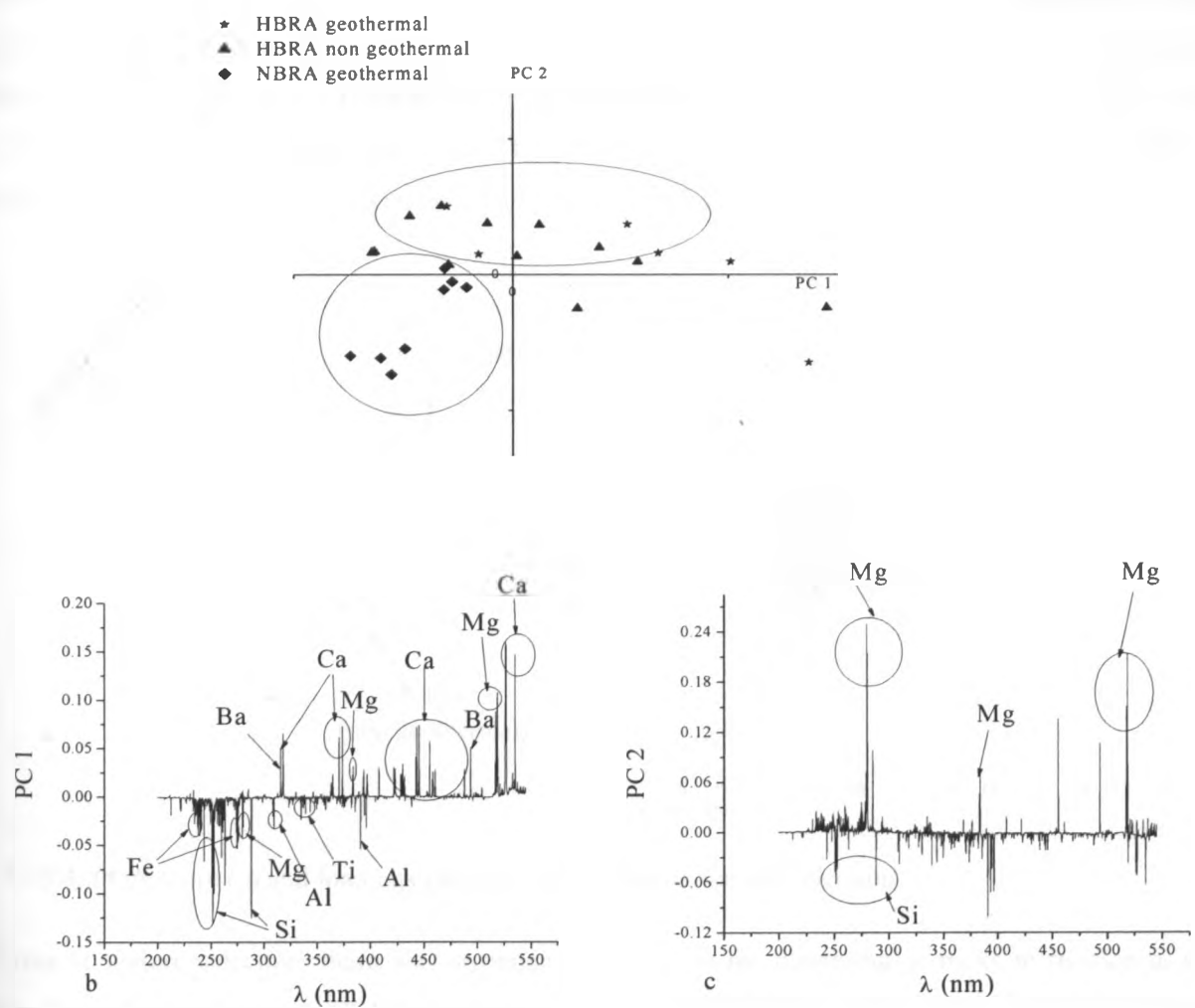


Fig 5.13.3: PCA score (a) and (b) loading plots for rocks based on the full spectra.

From the PCA score plot for rocks based on the full spectra above, there is no clear clustering. Samples from Lambwe valley are evenly distributed from PC2 downwards to PC1. Some of the samples from Olkaria have been

grouped together with those from Lambwe. But there exists a cluster of rock samples from Olkaria grouped on the 3rd quadrant. Assessment of the loading plots in indicated that rocks sampled from Olkaria (sampled in two different streams) had high concentration of Fe and Ti. Olkaria rocks having high content of Si clustered far away (this is supported by presence of silicic volcanics/trachyrhyolites in Olkaria (Williams, 1972; Marshal *et al.*, 2009)) from the others while those with high content of Fe clustered close to those from Lambwe.

Reason for clustering is because Kaniamwia escarpment in Lambwe valley largely supports ferruginous soils on rocks rich in ferro - magnesium minerals (Allsop and Baldry, 1972) thus rocks rich in Fe are found in the region. Furthermore, from the study of the loadings plots, HBRA rocks were found to be associated with strong emission lines of Ca and traces of Ba. This can be due to carbonatite rocks common in both HBRA (geothermal and non - geothermal). The high content of Ca and Mg from Lambwe rocks (Homa mountain) is mainly due to sovites and alvikites carbonatites containing calcitic and magnetitic rocks found in Homa mountain (Clerk and Roberts, 1986). From this analysis, PC1 contains chemical information of Ca, Fe and Ti while PC 2 contains that of Mg and Si. The scores and loading plots in the Fig 5.13.4 were plotted with respect to the region of the spectrum containing emission lines of five elements (As, Cr, Cu, Pb and Ti).

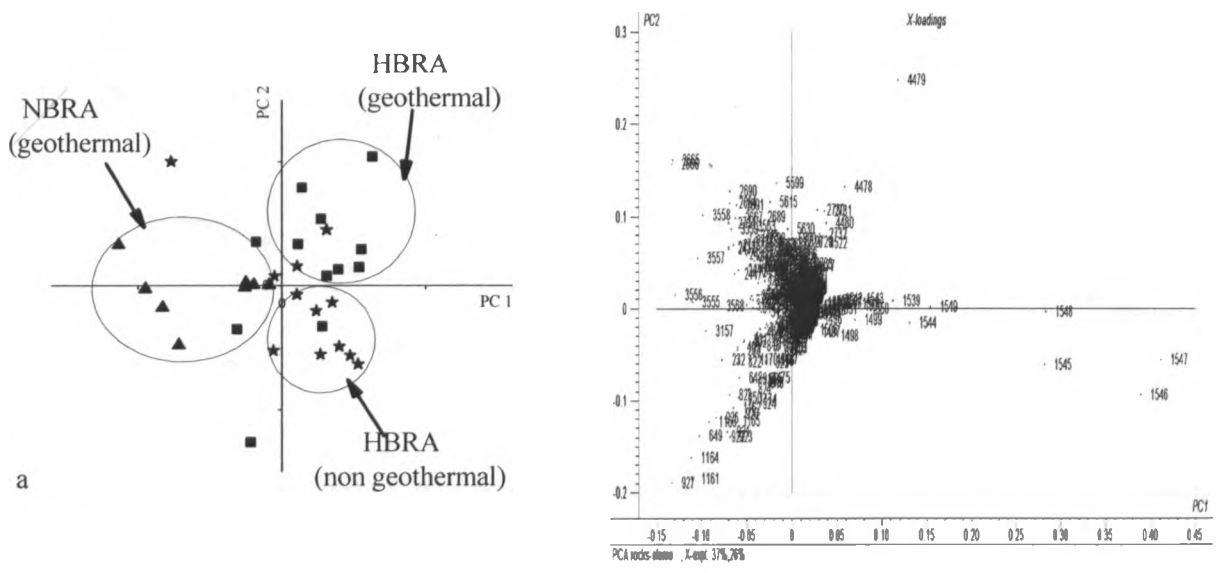


Fig 5.13.4: PCA score (a) and loadings plot for rocks based on feature selection.

In terms of feature selection, there was no much difference in the clustering of rocks in relation to sources of origin. From the loading plot, HBRA geothermal rocks were characterized by Ti lines. HBRA non geothermal which do not show clear clustering were associated with emission lines of Cu and Pb. The cluster of non HBRA geothermal close to Lambwe rocks group was found to be characterized by the presence of Ti while some samples

were clustered in accordance with As. It should be noted that the rocks from Olkaria (non HBRA geothermal) were sampled from two different springs thus the different in spectral features of trace elements.

From the score plots for soils and rocks, the three classes for soils are correctly discriminated based on intensities of As, Cr, Cu, Pb and Ti; but for rocks, those from Lambwe (HBRA geothermal and HBRA non geothermal) were not well classified due to similar characteristics of most emission lines of Ti and Cu. It was also observed that there was not much difference of the results using the entire spectrum and spectral regions of emission lines. This means that classification of samples depends on intensities of atomic components strongly influencing the distribution of elements in the samples.

PCA results based on the predicted concentrations of As, Cr, Cu, Pb and Ti are shown in Fig 5.13.5 and Fig 5.13.6 for soil and rocks.

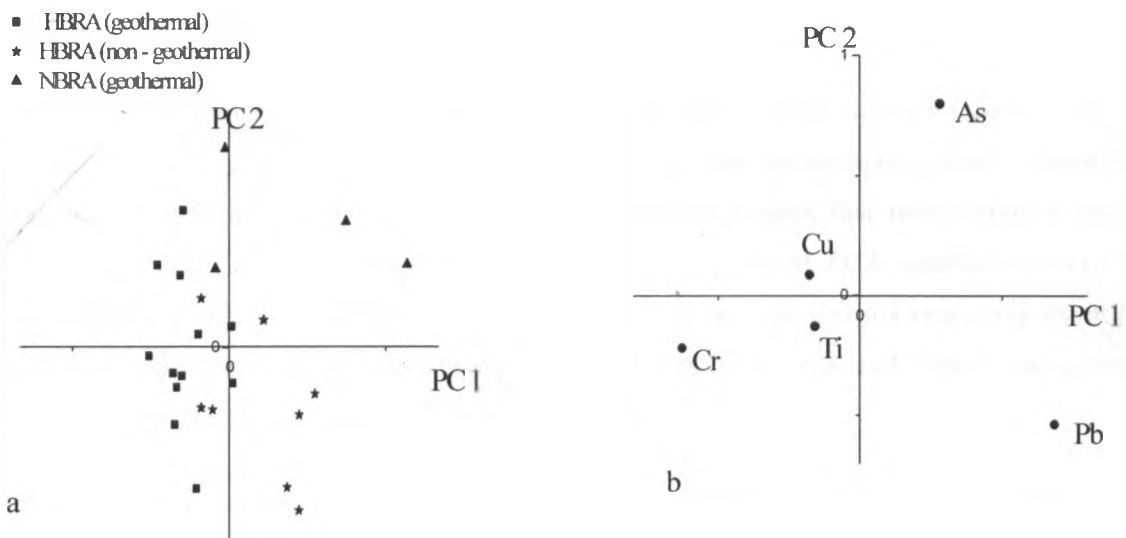


Fig 5.13.5: Scores (a) and loading (b) plots for soils analyzed using predicted concentrations of five elements.

From the plots in Fig 5.14.7 and Fig 5.14.8, although there was no clear clustering for soils, association of trace elements with sources of soils origin can be seen. HBRA geothermal soils are mostly characterized by the concentrations of Cr, Ti and Cu; HBRA geothermal are influenced by Pb concentrations; while NBRA geothermal are classified by the concentrations of As. In rocks on the other hands, HBRA rocks have clustered together, being characterized by As and Ti concentrations. NBRA exhibit no clear cluster although they are characterized by Pb and Cu concentrations.

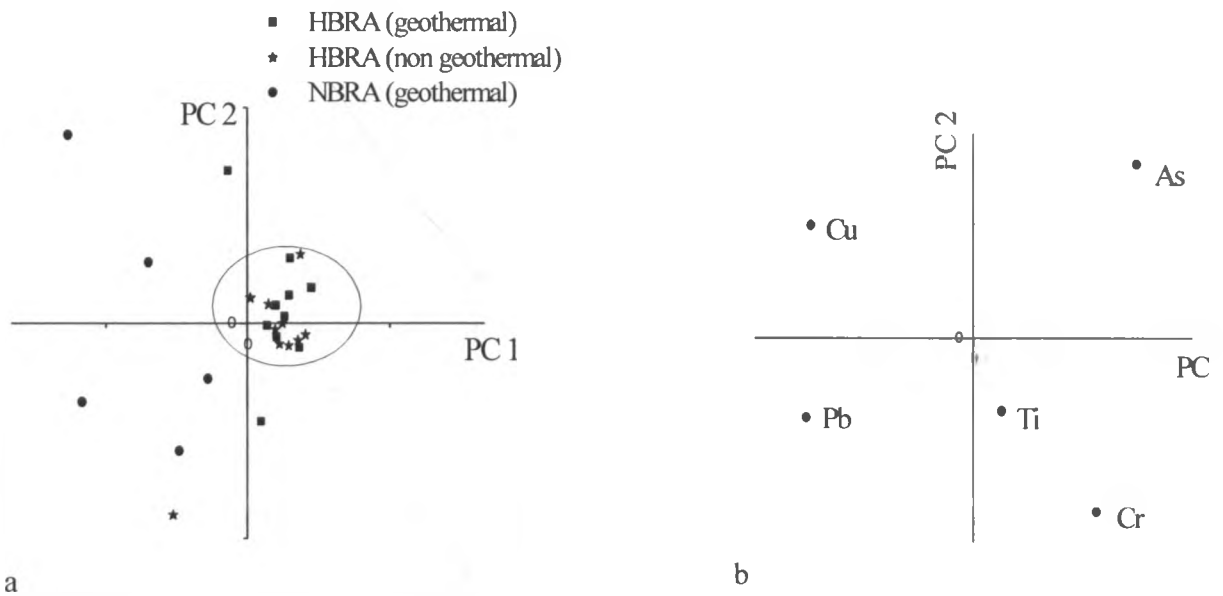


Fig 5.13.6: Scores (a) and loading (b) plots for rocks analyzed using predicted concentrations of five elements.

From all the PCA score plots, it can be said that use of full spectrum for discrimination of soils and rocks with respect to sources of origin gave satisfactory results as there was a clear distinction of sample classes based on the origin. Probably because full spectra contain more chemical components that have strong influence on the samples such that trace element's contribution to clustering is minimal PCA enables one to identify and discriminate a HBRA geothermal, HBRA non geothermal and a NBRA geothermal area using spectra from soils but it cannot be relied on to correctly identify rocks from HBRA geothermal and HBRA non geothermal (this might be due to strong influence of major elements in carbonatite rocks).

Based on these results it can reasonably be concluded that LIBS spectra provide vital information e.g. spectral signatures for atoms, elements and molecular components which can be used in routine monitoring analysis for variations in soils from different environmental sources e.g. HBRA geothermal, HBRA non geothermal and NBRA geothermal. Also PCA has helped to identify primary elements i.e. Ca, Mg, Fe and Si in soils and rocks which help in distinguishing between HBRA geothermal, HBRA non geothermal and NBRA geothermal area. On the contrary, while PCA is a valuable tool for recognizing similarities and differences between sample types based on specific chemical signature criteria, it does not automatically provide class memberships of unknown samples due to its unsupervised nature.

To assign class membership, SIMCA technique was employed. Assigning class membership is more important because it simplifies the task of determining similarities and differences between samples by providing

information on whether a sample belongs to a particular class or not based on the probability calculated from F-value of that sample in relation to already existing classes.

5.4.2 SIMCA Classification of Soil and Rock Samples

SIMCA was opted for, to identify samples as belonging to multiple (overlapping) classes and not constrained to producing a classification of samples into strictly discrete (non-overlapping) classes because it enabled independent modeling of the classes as opposed to an overall variance modeling as performed in PCA (Ashwin *et al.*, 2011).

In the first step, a PCA classification model was developed (based on atomic spectra from full spectral range of 200- 545 nm) in which the training set consisted of HBRA geothermal samples as class 1, HBRA non geothermal sources as class 2 and non HBRA geothermal samples as class 3. With LIBS data (pre - treated by standardization), a SIMCA model with 5 PCs for each class (explained variance > 97 %) and 5 % as the significance level for critical distance was the one that provided the best results. In each class, two thirds of samples were randomly selected as training set while the remaining third were set aside to be used as test set. Figure 5.14 shows Cooman's plots for the classification model constructed with the training set of three classes mentioned above.

In the Cooman's plot for soil, SIMCA has clearly distinguished Olkaria (non HBRA geothermal) soils (2nd quadrant) from Lambwe soils (HBRA geothermal and HBRA non geothermal soils) which is further illustrated by larger (> 0.3) sample to model distance. All the three categories of soils were within the limits of their class as none of the samples was located in the region of the Cooman's diagram common to the two classes. The prediction capacity of the SIMCA model was determined by analyzing the set of external test samples (12 for HBRA geothermal, 9 for HBRA non- geothermal, 5 for NBRA geothermal) that had not been used at any time to generate the model and the results are displayed in the classification table shown in Table 5.7. From Table 5.7, nearly all the samples were correctly classified (100 % correct classification) except those from HBRA geothermal class (some samples from a NBRA geothermal class exhibit similar characteristics as those from HBRA area due to the present of similar content of Fe to those from HBRA as seen in PCA score plot in Fig 5.13.2. One sample from this class was not classified in any group (false negative) but most (11) were correctly classified. The overall classification of 96 % was achieved for all the samples.

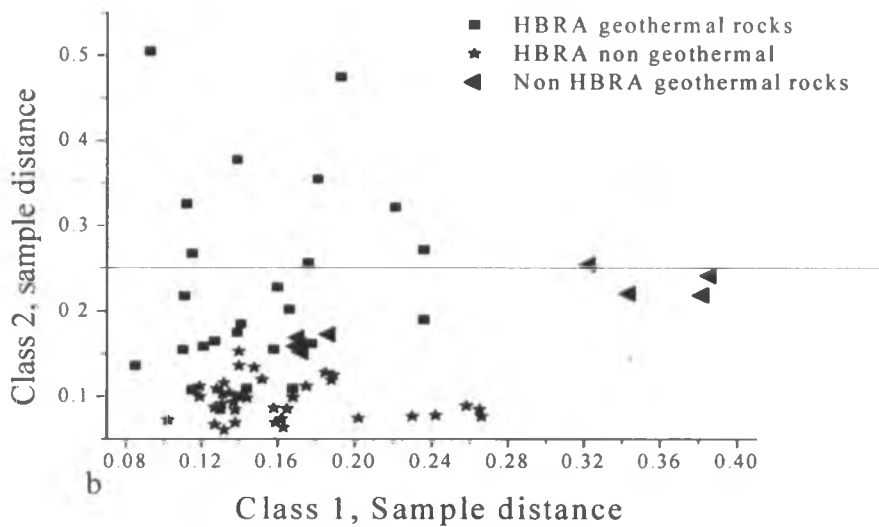
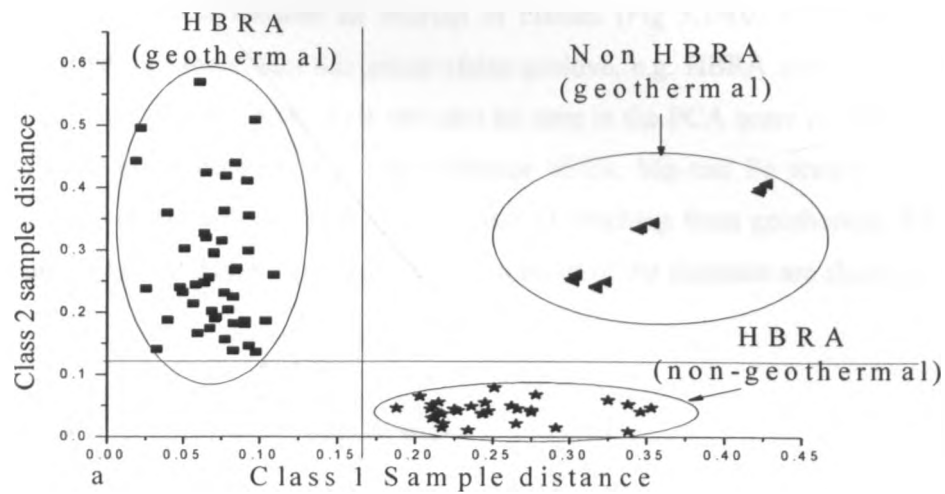


Fig. 5.14: Cooman's plot for classification models developed for; (a) soils and (b) rocks.

Table 5.7(a) SIMCA test set results (soils)

Class	No. in class	Correct	% correct
HBRA (geothermal)	12	11	92
HBRA (non- geothermal)	9	9	100
NBRA (geothermal)	4	4	100
Total	25	24	96

Table 5.7(b) SIMCA training set results (rocks)

Class	No. in class	Correct	False positive
HBRA (geothermal)	39	39	39
HBRA (non- geothermal)	47	47	47
NBRA (geothermal)	8	8	8

SIMCA classification for rocks showed an overlap of classes (Fig 5.14(b) and Table 5.7(b) such that most samples were classified into more than one group (false positive, e.g. HBRA geothermal rocks and non HBRA geothermal rocks in the Cooman's plot). This can also be seen in the PCA score plot (Fig 5.13.3) in which there lacks a clear cluster. This is because of strong influence of Ca, Mg and Fe present in carbonatite rocks that overshadows influence of elements such as As, Cu, and Ti resulting from geothermal activities. Classification results for soils and rocks based on the predicted concentrations of the elements are shown in Fig 5.15.

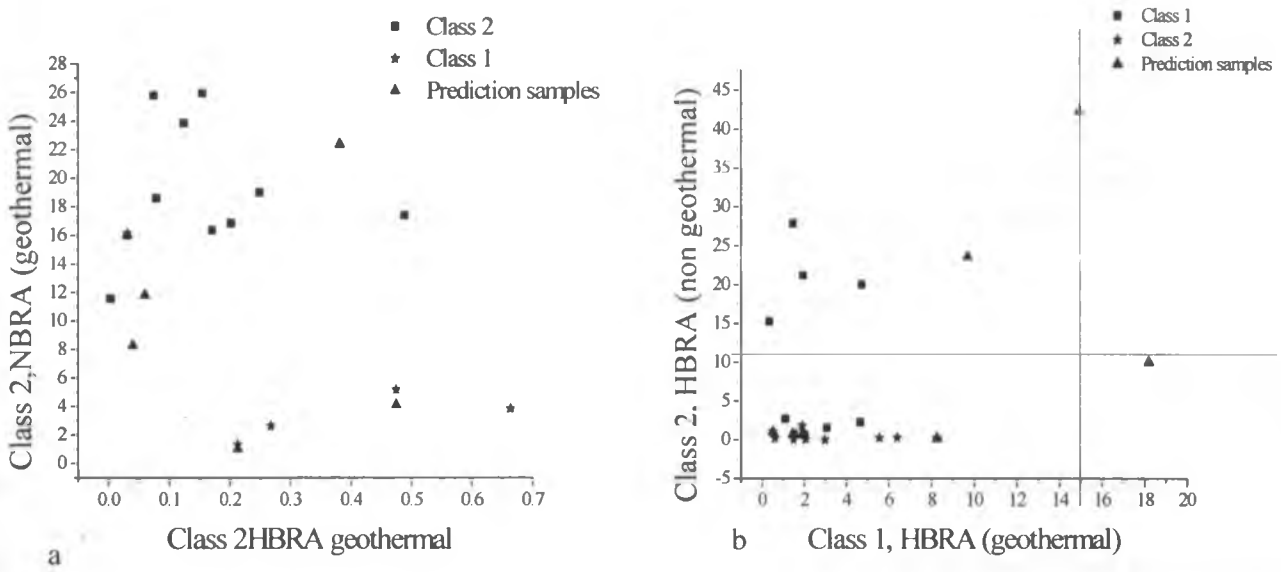


Fig 5.16: SIMCA classification results based on predicted concentrations for (a) soils and (b) rocks.

As seen previously, classification based on predicted concentration did not yield satisfactory results because most samples have been misclassified i.e. classified in more than one group as seen in the plots.

To test the applicability of SIMCA models in classification of future samples, an independent set of field samples which were sampled from a different HBRA region (Bala hills) at a different period of time (2007) was prepared. Single LIBS spectra from the samples were acquired and used for classification. It turned out that soils were 99 % correctly classified while rocks had 90 % classification as some of the rocks were doubly classified (false positive). The models having performed well in an independent set of samples proved that the models can be used for classification of future samples with > 90 % correct classification. The classification results for the independent set are shown in Fig 5.16.

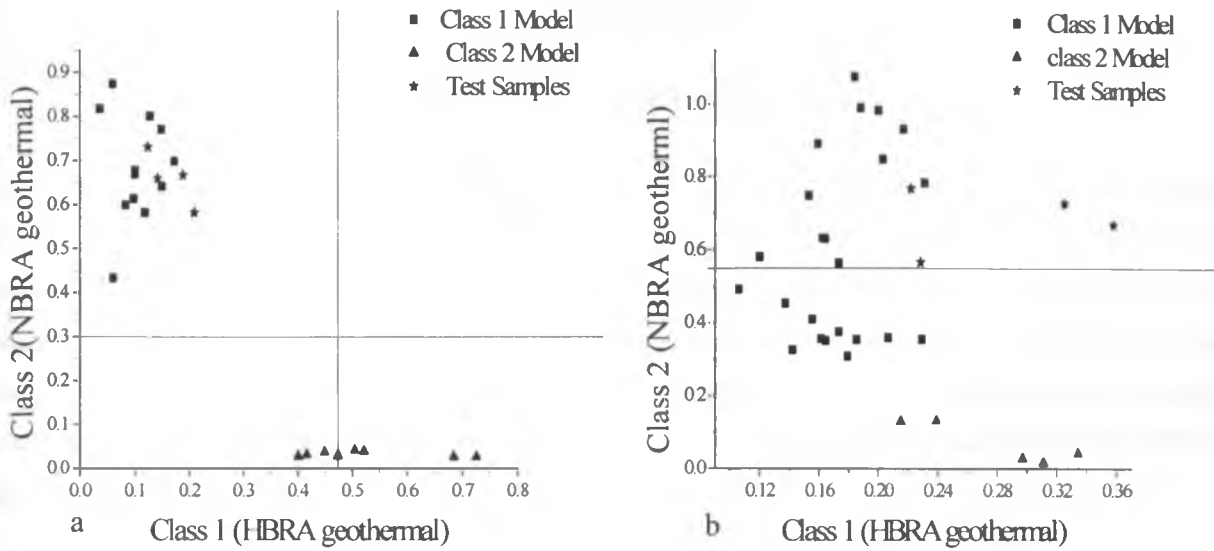


Fig 5.16: SIMCA prediction results for an independent set of (a) soils and (b) rocks.

As it can be seen, soil and rocks samples lay close to the HBRA geothermal sample classes. This is true because the independent set of samples were obtained from a HBRA geothermal source five years earlier than the model samples. Therefore SIMCA technique has proved to be a perfect tool to use in environmental modeling.

SIMCA technique improved the classification from PCA model; it is also more reliable than PCA because a sample is only classified to a class for which there is a high membership probability. With this model, spectra from any unknown sample can be used to determine if the unknown sample comes from a HBRA geothermal, HBRA non geothermal or non-HBRA geothermal source. This will make it easy to identify geothermally active areas in the future without having to go through the tiresome process of well geothermal potential determination.

In conclusion, the models developed for both calibration and classification have been utilized to interpret HBRA geothermal reservoir characteristics through the correlation of the trace element concentrations and the clustering of samples according to spectral signatures of major elements i.e. Ca, Fe, Mg and Si as well as trace elements. Classification models developed can be used for geothermal prospecting instead of the normal method of geothermal temperature gradient determination. Predicted concentrations have indicated that the trace elements levels are within the acceptable limit hence not a threat to the surrounding population and environment.

CHAPTER SIX

CONCLUSION AND FUTURE PROSPECTS

In this work, Chemometric -LIBS techniques have been developed and employed for quantitative and explorative analysis of HBRA geothermal field matrices. Firstly, optimization measurements were carried out on laser parameters namely; Q-Switch delay, integration time, sample-to- optical fiber distance, LPE and the number of laser ablations per scan required in order to obtain optimal LIBS spectra for quantitative analysis of trace atomic signature in HBRA geothermal soils and rocks. Multi- signal standard addition (classical method) was performed by spiking different trace concentrations of As, Cr, Cu, Pb and Ti in kaolin and rock simulate to mimic real soils and rock samples respectively.

The performance of obtained calibration curves was tested and used to predict concentration of these elements in certified reference materials. Results obtained demonstrated the application of multivariate calibration techniques in quantitative analysis of trace element concentrations in soils and rocks using chemometrics. PLS and ANNs were performed on LIBS spectra to develop calibration models which were used to predict concentration of trace elements in geothermal field matrices. Classification techniques PCA and SIMCA were applied on soil and rock spectra from HBRA geothermal field matrices for purpose of finding the similarities and differences between HBR geothermal, HBRA non geothermal and NBRA geothermal matrices.

Optimization parameters have been established for the quantitative analysis of soils and rocks using the multi – signal univariate calibration technique. Parameters namely LPE, integration time were found to depend on the nature of matrices under investigation. LIBS proved to be potentially viable in quantitative characterization of geothermal field matrices (soils and rocks). With LIBS, it was possible to detect and identify viable analytical lines for As, Cr, Cu, Pb and Ti which were used for quantitative analyses of these elements in the matrices.

Univariate calibration curves developed from the emission lines intensity were not satisfactory in prediction of element concentrations in the field matrices due to the limitation of using intensity of a single line per element and as such, multivariate chemometrics techniques (PLS and ANNs) were developed. In LIBS spectra, intensity of emission lines is not linearly dependent on the concentration of element species in the sample due to factors such as matrix effect, spectral interferences and broadening mechanisms involved in plasma evolution; as a result, it was important to perform calibration using multivariate chemometrics techniques, which take into consideration all the underlying factors. Results from univariate analysis of simulate soils and rocks indicate that univariate calibration is not sufficient to overcome inter-element effects and non - linear relationships between elements concentration and their LIBS intensity.

Limits of detection were determined and found to be favorably good (below 10 ppm for trace elements) hence with LIBS; it is possible to detect the elements in soil and rock matrices at low levels. The advantage of using PLS is that the full spectral information for the elements of interest are used and as such, factors not related to the species concentration but affecting the species e.g. spectral interference and line broadening are accounted for in the quantitative model. In classical calibration method, there is a great challenge on the time taken to compute the intensity of all lines for element and the choice of which lines to be used. Furthermore, a lot of time is spent in generating calibration curves for the lines of elements, especially for elements having many lines like Ti.

PLS and ANNs calibration models have been developed which are more accurate than SAM as they can easily and simultaneously predict concentration of trace elements analyzed in different samples using a single LIBS spectrum of a soil and rock sample. PLS showed improved prediction in soils but did not perform well in rocks due to nonlinear characteristics of LIBS spectra for rocks arising from the thermo physical and thermochemical properties in the rock simulate. Therefore, PLS technique was found to be suitable in solving linear problems while ANNs was best for nonlinear problems.

It was also found that concentration of the trace elements was different in three categories of classes of samples studied with HBRA geothermal area having higher concentration of the five elements compared to HBRA non geothermal and NBRA geothermal area. This may be due to enhanced radioactivity in HBRAs. In a HBRA geothermal soil, As was found to be highly correlated to Cr, but negatively correlated in NBRA geothermal soil. Cr was negatively correlated to Ti in HBRA and positively correlated in geothermal area. Pb was strongly anti-correlated to Cr and Cu in a geothermal soil but less correlated in HBRA. Therefore, to characterize and explore a field as geothermal or not using the concentrations, the correlation of these elements should be determined and assessed.

PCA performed better on samples classification using full spectra than in cases of spectral regions containing five elements. This is because major elements (Ca, Mg, Fe and Si associated with geothermal and HBRA activities) that strongly influence clustering vary in the three classes discussed so far i.e. HBRA geothermal, HBRA non-geothermal and NBRA geothermal. In comparison to PCA, SIMCA showed even better classification capability as it clearly distinguished samples in relation to their origin based on atomic spectra of UV-VIS spectral range.

SIMCA and PCA were successfully applied to classify and distinguish the origin of the geothermal field matrices (HBRA, or non-HBRA) based on LIBS atomic signatures in a manner applicable to geothermal resource characterization and environmental impact modeling. Classification models developed by SIMCA could be used in future for geothermal prospecting by making it easier to identify geothermally active areas without going through time consuming processes like geothermal gradient determination. It has also been found that the

concentrations of trace metals (As, Cr, Cu, Pb and Ti) in the soil and rocks vary from one source to the other in all the three classes of sampling, being higher in HBRA geothermal. Their concentrations (in soils) were such that they do not pose any environmental risk or health hazard to human beings (although they are high in HBRA areas, they are still within the acceptable levels).

It is concluded from the present study that in the soil and rock samples of the Lambwe Valley, the concentrations of the heavy trace metals analyzed were nominal and do not pose any potential health hazard to the general public. However, this data may provide a general baseline level for the area studied and may also serve as a guideline for future measurement and assessment of trace elements in the case of any abnormal health hazards from the area. A HBRA geothermal area is uniquely characterized by elevated levels of As and Cr concentrations in relation to low concentrations of Ti and vice versa in soils; while a NBRA geothermal area has negative correlation of Cu with Pb and Ti, Pb with Cr and Ti.

REFERENCES

- Achola, S. 2009: Radioactivity and Elemental Analysis of Carbonatite Rocks from Parts of Gwasi Area, South Western Kenya. MSc. thesis. *University of Nairobi*
- Adamo, P., Denaix, L., Tembile, F and Zampella, M. 2003: Characterization of Heavy Metals in Contaminated Volcanic Soils of Solofrana River Valley (Southern Italy). *Geoderma* 117, 347-366.
- Adel, G and Arabi, A. 2006: Naturally Occurring Radioactive Materials from the Aluminium Industry: A Case Study: The Egyptian Aluminium Company, Nag Hammady, Egypt. *Journal of Radiological Protection* 26, 415-422.
- Allsopp, R and Baldry, D. 1972: A General Description of the Lambwe Valley Area of South Nyanza District, Kenya. *Bull. Org. Mond. Sante.* 47, 691-697.
- Amaral, A., Cruz, J and Rodrigues, A. 2006: Baseline Levels of Metals in Volcanic Soils of Azores (Portugal). *Soil and Sediment Contamination* 15, 123-130.
- Andrez, M., Vincenzo, P and Israel, S. 2006: Laser Induced Breakdown Spectroscopy (LIBS). Fundamentals and Applications. *Cambridge University Press* New York, 153-160.
- Australian and New Zealand Environment and Conservation Council and the National Health and Medical Research Council (ANZECC/NHMRC) Guidelines 1992.
- Aragón, C., Aguilera, J and Peñalba, F. 1999: Improvements in Quantitative Analysis of Steel Composition by Laser-Induced Breakdown Spectroscopy at Atmospheric Pressure using an Infrared Nd: YAG Laser. *Applied Spectroscopy* 53 (10), 1259 – 1267.
- Ashwin, K., Myakalwara, S., Ishan, B., Narahara, C., Venugopal, R., P. and Manoj, K. 2011: Laser-Induced Breakdown Spectroscopy-Based Investigation and Classification of Pharmaceutical Tablets using Multivariate Chemometric Analysis. *Talanta* 87, 53– 59.
- Bahat, D. 1979: Interpretation on the Basis of Hertzian Theory of a Spiral Carbonatite Structure at Homa Mountain, Kenya. *Tectonophysics.* 60, 235 – 246.
- Bansi, L., Zheng, H., Yuer, F and Singh, P. 2004: Parametric Study of Pellets for Elemental Analysis with Laser-Induced Breakdown Spectroscopy. *Applied Optics* 43 (13), 2792-2796.

- Baranwala, V., Sharma, P., Sengupta, D., Sandilya, K., Bhaumik, K and Sahac, K. 2006: A New High Background Radiation Area in the Geothermal Region of Eastern Ghats Mobile Belt (EGMB) of Orissa, India. *Radiation Measurements* 41, 602 – 610.
- Barber, C. 1974: The Geochemistry of Carbonatites and Related Rocks from Two Carbonatite Complexes, South Nyanza, Kenya. *Lithos* 7, 53-63.
- Barbini, R., Calao, F., Fantoni, R., Palocci, A., Capitelli, F and Vander Steen, H. 2000: Laser- Induced Breakdown Spectroscopy. Proceedings of EARSeL- SIG- Workshop. *Lidar* 124-129.
- Bhagal, P. 1985: Reservoir Models of the Olkaria Geothermal Project (1975-1985). *Proc. World Geoth. Congress* 2000, Kyusu- Tohoku, Japan, May 28 - June, 985-989.
- Boersema, J., Stipe, C., Hensley, B and Buckley, S. 2010: Laser Induced Breakdown Spectroscopy of Steel: A Comparison of Univariate and Multivariate Calibration Methods. *Applied Spectroscopy*. 64 (2), 154-160.
- Bousquet, B., Sirven, J.-B and Canioni, L. 2007: Towards Quantitative Laser-Induced Breakdown Spectroscopy Analysis of Soil Samples. *Spectrochimica Acta Part B*. 62, 1582 – 1589.
- Boyle, J. 1999: Isotope- Source ED-XRF Analysis of Geological Materials using Gas Filled Proportional Counters: Signal Deconvolution using Simulated Peak Shapes. *X- Ray Spectrom.* 28, 178-182.
- Bruno, S and Ray, M. 2003: Experimental Constraints on the Relationships between Peralkaline Rhyolites of the Kenya Rift Valley. *Journal of Petrology* 44(10), 1867-1894.
- Capitelli, F. Colao, F., Provenzano, R., and Fantoni, R. 2002: Determination of Heavy Metals in Soils by Laser Induced Breakdown Spectroscopy. *Geoderma* 106, 45–62.
- Castle, B., Talabardon, K., Smith, W and Winefordner, J. 1998: Variables Influencing the Precision of Laser- Induced Breakdown Spectroscopy Measurements. *Applied Spectroscopy* 52 (5), 649-657.
- Chase, B., Munson, A., Frank, C., Thuvan, P., Kevin, L and Andrzej, W. 2005: Investigation of Statistics Strategies for Improving the Discriminating Power of Laser-Induced Breakdown Spectroscopy for Chemical and Biological Warfare Agent Stimulants. *Spectrochimica Acta Part B*. 60, 1217 – 1224.
- Chengli, X., Jidong, L, Pengyan, L., Jie, L and Lin, Z. 2009: Correction and Analysis of Pb Content in Soil by Laser Induced Breakdown Spectroscopy. *Chinese Optics Letters* 7 (6), 545-548.

- Christoph, L., Ji-hyun, K., Christian, S., Eun-Joung, K., Kyoung-Woong, K., and Kihong, P. 2009: Quantitative Analysis of Arsenic in Mine Tailing Soils Using Double Pulse-Laser Induced Breakdown Spectroscopy. *Spectrochimica Acta Part B*. 64, 1105–1110.
- Ciucci, A., Palleschi, V., Barbini, R., Colao, F., Fantoni, R., Palucci, A and Ribezzo, S. 1996: Trace pollutants analysis in soils by time resolved laser induced breakdown spectroscopy technique. *Appl. Phys. B*. 64, 185-190
- Clegg M., Sklute, M., Dyar, J., Barefield J and Wiens, R. 2006: Multivariate Analysis of Remote Laser-Induced Breakdown Spectroscopy Spectra Using Partial Least Squares, Principal Component Analysis, and Related Techniques. *Spectrochim. Acta. B*. 64, 79 - 88.
- Clarke, M., Flegg, M., Le Bas, M. and Sutherland, D. (1979): Homa Mountain I: Ijolites and Associated Fenites. In Carbonatite-Nephelinite Volcanism: An African Case History. London: John Wiley and Sons.
- Clarke, M and Roberts, B. 1986: Carbonated Melilitites and Calcitized Alkalicarbonatites from Homa Mountain, Western Kenya: A Reinterpretation. *Geol. Mag.* 123 (6), 683-692.
- Clegg , S., Sklute, E., Darby, M., Barefield, J and Roger, C. 2009: Multivariate Analysis of Remote Laser-Induced Breakdown Spectroscopy Spectra using Partial Least Squares, Principal Component Analysis and Related Techniques. *Spectrochimica Acta Part B*. 64, 79–88.
- Costa, J., Alves, M and Ferreira, E. 2009: Principal Component Analysis on Quantitative Image Analysis to Predict Effects of Toxic in Anaerobic Granular Sludge. *Bioresource Technology* 100, 1180-1185.
- Cremers, D and Radziemski, J. 1989: Laser-Induced Plasmas and Applications .Marcel Dekker, New York
- Cremers, D., Ebinger, M., Unkefer, P., Breshears, D., Susan, A and Ferris, J. 2001: Measuring Total Soil Carbon with Laser Induced Breakdown Spectroscopy (LIBS). *J. Environ. Qual.* 30, 2202-2206.
- Cremers, D and Radziemski, J. 2002: Handbook of Laser-Induced Breakdown Spectroscopy. John Wiley and Sons, Chichester.
- Ctvmickova, T., Cabalin, L., Laserna, J., Kanicky, V and Nicolas, G. 2009: Laser Ablation of Powdered Samples and Analysis by Means of Laser- Induced Breakdown Spectroscopy. *Applied Surface Science* 255, 5329-5333.

- Dalyander, P., Gornushkin, B and Hahn, W. 2008: Numerical Simulation of Laser Induced Breakdown Spectroscopy: Modeling of Aerosols Analysis with Finite Diffusion and Vaporization Effects. *Spectrochimica Acta Part B*. 63, 293-304.
- David, M and Melgaard, K. 2001: New Classical Least-Squares/Partial Least-Squares Hybrid Algorithm for Spectral Analyses. *Applied Spectroscopy* 55 (1), 1-8.
- Deans, T and Roberts, B. 1984: Carbonatite Tuffs and Lava Clasts of the Tinderet Foothills, Western Kenya: A Study of Calcified Natrocarbonatites. *J. geol. Soc. London*. 141, 563 – 580.
- Dimitra, N., Kristine, L and Michael, S. 2000: Dual- Pulse Laser Induced Breakdown Spectroscopy using a Pre-Ablation Spark for Enhanced Ablation and Emission. *Applied Spectroscopy* 54 (9), 1270-1274.
- Diyun, C., Zeping, T., Zhiqiang, Z and Wenbiao, X. 2012: Natural Radioactivity Levels in Topsoil from the Pearl River Delta Zone, Guangdong, China. *Journal of Environmental Radioactivity* 103, 48 – 53.
- Dolle, C., Schade, W., Hartmann, R and Horn, R. 2001: Laser Induced Breakdown Spectroscopy for Soil Diagnostics. *European Journal of Soil Science* 52, 305-312.
- Doucet, F., Belliveau, T., Fortier, L and Hubert, J. 2007: Use of Chemometrics and Laser-Induced Breakdown Spectroscopy for Quantitative Analysis of Major and Minor Elements in Aluminum Alloys. *Applied Spectroscopy* 61 (3), 327-331.
- Doucet, F., Faustino, P., Sabsabi, M and Lyon, R. 2008: Quantitative Molecular Bands Emission using Laser Induced Breakdown Spectroscopy and Chemometrics. *J. Anal. At. Spectrom.* 23, 694-701.
- Emmanuel, D., Macary, H and Virginia, K. 2008: Sources of Very High Metal Content in Soils of a Volcanic Island (La Ré Union). *Journal of Geochemical Exploration* 88, 194-197.
- Environmental Protection Agency (EPA). 1986a: Ground Water Issue: Behaviour of Metals in Soils.
- Eppler, S., Cremers, D., Hickmott, D., Ferris, J and Koskelo, C. 1996. Matrix Effects in the Detection of Pb and Ba in Soils using Laser-Induced Breakdown Spectroscopy. *Applied Spectroscopy* 50 (9), 1175 – 1181.
- Faber, N., Song, X-H and Hopke, P. 2003: Sample-Specific Standard Error of prediction for Partial Least Squares Regression. *Trends in Analytical Chemistry* 22 (5), 330-334.

- Ferreira, E., Jesu, A., De Bora, M., Milori, P., Ednaldo, J., Roberto, J., Lasheras, B., Beatriz, M., Justiniano, C And Ladislau, M. 2009: Multiple Response Optimization of Laser-Induced Breakdown Spectroscopy Parameters for Multi-Element Analysis of Soil Samples. *Applied Spectroscopy* 63 (9), 1081 – 1088.
- Ferrer, A., Aguado, D., Santiago, V., José, M and Zarze, M. 2008: PLS: A Versatile Tool for Industrial Process Improvement and Optimization. *Applied Stochastic Models Bus. Ind.* 24, 551-567.
- Fichet, P., Toussaint, A and Wagner, J. 1999: Laser-Induced Breakdown Spectroscopy: A Tool for Analysis of Different Types of Liquids. *Applied Physics A*. 69, S591-S592.
- Fitria, H., Soeffady, W and Tahir, S. 2008: Geochemical Characterization of Volcanic Soils from Tawao, Sabah. *Geological Society of Malaysia. Bulletin* 544, 33-36.
- Flegg, M., Clarke, G., Sutherland, D. and Le Bas, J. 1977: Homa Mountain II: The main carbonatite centre. In *Carbonatite-Nephelinite Volcanism: An African Case History*. London: John Wiley and Sons.
- Frank, H., Noll, R., Peter, W., Falk, H and Becker, C. 2001 : Analysis of Heavy Metals in Soils Using Laser Induced Breakdown Spectroscopy Combined with Laser Induced Fluorescence. *Spectrochimica Acta Part B*. 56, 933-945.
- Giakoumaki, A., Mellesanaki, K and Demetrios, A. 2007: Laser- Induced Breakdown Spectroscopy (LIBS) - Applications and Prospect. *Anal Bioanal Chem*. 387, 749-760.
- Gondal, M., Hussain, T., Yamani, Z and Baig, A. 2009: On-Line Monitoring of Remediation Process of Chromium Polluted Soil using Laser- Induced Breakdown Spectroscopy. *Journal of Hazardous Materials* 163, 1265-1271.
- Gottfried, L., Harmon, S., Lucia, F and Miziolek, W. 2009: Multivariate Analysis of Laser-Induced Breakdown Spectroscopy Chemical Signatures for Geomaterial Classification. *Spectrochim. Acta. B*. 64, 1009 - 1019.
- Hannes, B and Reusser, E. 2010: Mineralogical and Geochemical Characterization of Ashes from an Early Phase of the Explosive September 2007 Eruption of Oldonyo Lengai (Tanzania). *Journal of Africa Earth Sciences* 58, 752-763.
- Howard, D., Mark, B and Hagan, M. 2009: Neural Network Toolbox: User's Guide. The MathWorks, Inc, US.
- HR2000: High-Speed Fiber Optic Spectrometer: Installation and Operation manual (2010). *Ocean Optics. Inc.*

- Hybl, J. 2003: Laser Induced Breakdown Spectroscopy for Detection and Classification of Biological Aerosols. *Applied Spectroscopy* 57, 1207-1215.
- ICRP. 1991: Recommendations of the International Commission on Radiological Protection, ICRP Publication 60.
- Jagdish, P and Surya, N. 2007: Laser Induced Breakdown Spectroscopy. Elsevier, Amsterdam.
- Jean, S., Maichen, P and Salle, B. 2008: Analytical Optimization of Some Parameters of a Laser- Induced Breakdown Spectroscopy Experiment. *Spectrochimica. Acta. Part B.* 63, 1077-1082.
- Jorado, A and Castro, M. 2003: Chemometric Approach to Laser- Induced Breakdown Spectroscopy Analysis of Gold Alloys. *Applied Spectroscopy* 57 (3), 349-352.
- Jose', L., Pavo, N., Carmelo, G., Pinto, M., Esther, F., Bernardo, M. and Armando, G. 2003: A Method for the Detection of Hydrocarbon Pollution in Soils by Headspace Mass Spectrometry and Pattern Recognition Techniques. *Anal. Chem.* 75, 2034-2041.
- Katleen, V., Claudia, F., Rene, V., Ignasi, Q., Manuela, H and Margui, E. 2008: Application of High Energy Polarized Beam Energy Dispersive X-Ray Fluorescence Spectrometry to Cadmium Determination in Saline Solution. *Journal of Analytical Atomic Spectroscopy* 23, 1034-1037.
- Kebwarol, I., Rathorel, N., Hashiml, O and Mustapha, O. 2011: Radiometric Assessment of Natural Radioactivity Levels around Mrima Hill, Kenya. *International Journal of the Physical Sciences* 6 (13), 3105-3110.
- Kemal, E., Markandey, M and Singh, P. 2010: Elemental Analysis of Slurry Samples with Laser- Induced Breakdown Spectroscopy. *Applied Optics* 49 (13), 21-26.
- Kursad, M., Kilicel, F., Kaa, K., Tuncer, I and Uygan, T. 2002: Heavy Metals in Soils, Vegetables and Fruits in Endermic Upper Gastro Intestinal Cancer Region of Turkey. *Environmental Toxicology* 13, 175-179.
- Labbe, N., Isabel, M., Andre, M., Madhari, z., Timothy, M and Rial, G. 2008: Extraction of Information from LIBS Spectral Data by Multivariate Analysis. *Applied Optics* 47 (13), G158-G165.
- Laurent, P., Francois, G., Peter, Sand Didier, L. 2003: Formation of Radioactivity Enriched Soils in Mountain Area. *Journal of Environmental Radioactivity* 68, 215-233.

- Liang, X., Valery, B., Vladimir, G and Israel, S. 1997: Absolute Analysis of Particulate Materials by Laser-Induced Breakdown Spectroscopy. *Analytical Chemistry* 69, 2103 - 2108.
- LIBS 2500 plus. 2008: Laser Induced Breakdown Spectroscopy: Installation and Operation Manual. *Ocean Optics. Inc.*
- Liwana, Z and Feng, Y. 2008: Controlled Calibration Method for Laser- Induced Breakdown Spectroscopy. *Chinese Optics Letters* 6 (1), 5-8.
- Loppi, S and Ilaria, B. 2000: Lichens and Mosses as Biomonitors of Trace Elements in Areas with Thermal Springs and Fumarole Activity. *Chemosphere* 41, 1333- 1336.
- Lucia, C., Massimo, M., Gioranni, O. and Tilton, G. 1998: The Geochemistry of Volcanic Rocks from Pantelleria Island, Sicily Channel: Petrogenesis and Characteristics of the Mantle Source Region. *Journal of Petrology* 39 (8), 1453-1495.
- Macdonald, R. and Scaillet, B. 2006: The Central Kenya Peralkaline Province: Insights into the Evolution of Peralkaline Salic Magmas. *Lithos* 91, 59–73.
- Maesschalck, R., Candolfi , A., Massart, L and Heuerding, S. 1999: Decision Criteria for Soft Independent Modelling of Class Analogy Applied to Near Infrared Data. *Chemometrics and Intelligent Laboratory Systems* 47, 65–77.
- Mangala, J. (1987): A Multi- Channel X-Ray Fluorescence Analysis of Fluorspar Ore and Rocks from Mrima Hill, Kenya. MSc. Thesis, *University of Nairobi*
- Mangala, J and Patel, P. 1994: Elemental Analysis of Carbonatite Samples from Mrima Hill, Kenya, by Energy Dispersive X-Ray Fluorescence (EDXRF) Spectroscopy. *Nuclear Geophysics* 8 (4), 389 – 393.
- Marini, F., Bucci, R., Magri, A and Magri, D. 2008: Artificial Neural Networks in Chemometrics: History, Examples and Perspectives. *Microchemical Journal* 88, 178-185.
- Márcio, J., Juliana, C., Roberto, K., Harrop, G., Celio, P., Mário, C., Ugulino, A., Ricardo, M and Chibad, K. 2009: Classification of Brazilian Soils by using LIBS and Variable Selection in the Wavelet Domain. *Analytica Chimica Acta*. 642, 12–18.
- Mark, H. 2001: Data analysis: Multi linear Regression and Principal Component Analysis. Handbook of Near-Infrared Analysis (*D. A. Burns and E. W. Ciurczak, eds*), 129–184.

- Marshall, S., Macdonald, R., Rogers, N., Fitton, J., and Hinton, W. 2009: Fractionation of Peralkaline Silicic Magmas, The Greater Olkaria Volcanic Complex, Kenya Rift valley. *Journal of Petrology* 50, 323-359.
- Markandey, M., Kemal, E., Eseller, F and Yueh, P. 2009: Multivariate Calibration of Spectra obtained by Laser Induced Breakdown Spectroscopy of Plutonium Oxide Surrogate Residues. *Spectrochimica Acta Part B*. 64, 1212–1218.
- Martin, Z. and Cheng, D. 2000: Detection of Chromium Aerosol using Time-Resolved Laser-Induced Plasma Spectroscopy. *Applied Spectroscopy* 54 (9), 1279-1285.
- Martin, M., Labbe., Andre', N., Wullschleger, D., Harris, R and Ebinger, H. 2010: Novel Multivariate Analysis for Soil Carbon Measurements using Laser-Induced Breakdown Spectroscopy. *Soil Sci. Soc. Am. J.* 74, 87 - 93.
- Marwa, A., Hisham, I., Asmaa, E., Walid, T and Mohamed. A. 2004: LIBS Limit of Detection and Plasma Parameters of Some Elements in Two Different Metallic Matrices. *Anal. At. Spectrom.* 19, 489-494.
- Maya, I., Young, T., Madhavi, Z., Nicole, L., Andre, N and Rials, T. 2008: Extraction of Information from Laser Induced Breakdown Spectroscopy Spectral Data by Multivariate Analysis. *Applied Optics* 47, 158-169.
- McCall, G. 1958: Geology of the Gwasi Area, Ministry of Commerce and Industry, *Geology Survey of Kenya*, Dept. No. 45.
- Mohammed, A., Nasr, M., Zulfqar, A and Zain, H. 2009: Determination Of Trace Elements In Volcanic Rock Samples Collected From Cenozoic Lava Eruption Sites Using LIBS. *Journal of Environmental Science and Health Part A* 44, 528–535.
- Mohanty, K., Sengupta, D., Das, K., Saha, K and Van, K. 2004: Natural Radioactivity and Radiation Exposure in the High Background Area at Chhatrapur Beach Placer Deposit of Orissa, India. *Journal of Environmental Radioactivity* 75, 15-33.
- Muhammad, S. 2006: Plasma Diagnostics of Zn, Cd and Hg using Laser Induced Breakdown Spectroscopy. Ph. D thesis, Quaid-i-Azam University, Pakistan.
- Muller, K and Stege, H. 2002: Evaluation of the Analytical Potential of Laser- Induced Breakdown Spectroscopy for Analysis of Historical Glasses. *Archeometry* 45 (3), 421-433.

- Mustapha, A., Patel, J and Rathore, S. 1999: Assessment of Human Exposure to Natural Sources of Radiation in Kenya. *Radiation Protection Dosimetry* 82 (4), 285–292.
- Ningfang, Y. 2009: Elemental Analysis of Soils Using Laser-Induced Breakdown Spectroscopy (LIBS), MSc. thesis, *University of Tennessee*, Knoxville Trace: Tennessee Research and Creative Exchange.
- Nilesh, R., Rai, A., Kumar, A and Surua, T. 2008: Detection Sensitivity of Laser- Induced Breakdown Spectroscopy for Cr II in Liquids. *Applied Optics* 47 (31), 105-110.
- Ohde, S. 2004: Instrumental Neutron Activation Analysis of Carbonatites from Homa Mountain, Kenya. *Journal of Radioanalytical and Nuclear Chemistry* 260 (1), 213 - 218.
- Özgür, N. 2002: Geochemical Signature of Kizildere Geothermal Field, Western Anatolia. *Turkey International Geology Review*.44, 153-163.
- Pastorelli, S., Perello, P., Dematteis, A., Martinotti, G and Marini, L. 1999: Exploration and Exploitation of the Low- Enthalpy Geothermal Resources in Alpine China. *Materials and Geo –environment* 50, 285-288.
- Patel, J. 1991: Environmental Radiation Survey of the Areas of High Natural Radioactivity of Mrima Hill of Kenya. *Discovery and Innovation* 3 (3), 31-36.
- Paul, G. and Laurie, D. 1989: Raw Materials Testing using Soft Independent Modeling of Class Analogy Analysis of Near- Infrared Reflectance Spectra. *Analytical Chemistry* 61 (2), 139-144.
- Pichahchy, A., Cremers, D and Ferris, J. 1997: Elemental Analysis of Metals under Water using Laser-Induced Breakdown Spectroscopy. *Spectrochimica Acta Part B*.52, 25-39.
- Richard G. 2003: Chemometrics Data Analysis for the Laboratory and Chemical Plant. University of Bristol, *John Wiley and Sons*.
- Rodrigues, M., Gornushkin, B., Heitmann, M., Almirall, R., Smith, W and Omenetto, N. 2008: Laser- Induced Breakdown Spectroscopy as a Tool for Discrimination of Glass for Forensic Applications. *Anal Bioanal Chem*. 391, 1961-1968.
- Romanenko, S and Stromberg, G. 2007: Modelling of Analytical Peaks: Peaks Modifications. *Analytical Chimica Acta*. 581, 343-354.

- Rosalba, G., Marcella, D., Olga, P., Giorgio, S and Alessandro, G. 2010: Laser Induced Breakdown Spectroscopy for Elemental Analysis in Environmental, Cultural Heritage and Space Applications: A Review of Methods and Results. *Sensors* 10, 7434 – 7468.
- Rusten, P. 2003: The Effect of Human Health on Hydrogeochemical Characteristics of Kirkgecit and Ozancik Hotsprings, Canakkale, Turkey. *Environmental Geochemistry and Health* 25, 205-217.
- Sabsabi, M., Motto-Ros, V., Laville, S and Lui, S.2009: Laser Induced Breakdown Spectroscopy with Artificial Neural Networks for Material Identification. *Planet Space. Sci.* 10, 1016-1022.
- Samek, O., Lambart, J., Liska, M., Kaiser, J., Novotny, K., Hergenroder, R and Kukhlevsky, S. 2006: Femtosecond Spectrochemical Analysis of Plant Samples. *Laser Physics Lett.* 3 (1), 21-26.
- Shiwani, P and Rai, A. 2008: Laser- Induced Breakdown Spectroscopy: A Versatile Tool for Monitoring Traces in Materials. *Journal of Physics* 70 (3), 553-563.
- Simiyu, G and Mwakio, T. 2000: Concentrations of Trace Elements in Waters, Soils, and Plants of the Olkaria Geothermal Field, Kenya. *Proceedings World Geothermal Congress*, 681-684.
- Stanley, J. 1979: Radioactivity Surveys. *Virginia Divisional of Minerals Resources* 25 (2), 9-14.
- Sirven, J-B., Bousquet, B., Canioni, L and Sarger, L. 2006: Laser-Induced Breakdown Spectroscopy of Composite Samples: Comparison of Advanced Chemometrics Methods. *Anal. Chem.*78, 1462-1469.
- Sneddon, J. 2002: *Advances in Atomic Spectroscopy*. Elsevier Science B.V, Amsterdam. 7, 303-315.
- Snezana, D and Onjia, A. 2007:Classification of Soil Samples according to Geographic Origin using Gamma-Ray Spectrometry and Pattern Recognition Methods. *Applied Radiation and Isotopes* 65, 218–224.
- Stavropoulos, P., Angelopoulos, G and Papamantellos, S. 2004: Laser- Induced Breakdown Spectroscopy using Nanosecond and Picosecond lasers. *Spectrochimica Acta Part B.* 59, 1885-1892.
- Stefano, L and Ilaria, B. 2000: Lichens and Mosses as Bio Monitors of Trace Elements in Areas with Thermal Springs and Fumaroles Activity (Mt. Amiata, Central Italy). *Chemosphere* 41, 1333-1336.
- Stuart, C., Peter, E., Steve, B., and Chris, J. 2004: Rates and Timescales of Fractional Crystallization from ^{238}U - ^{20}Th - ^{226}Ra Disequilibria in Trachyte Lavas from Longonot Volcano, Kenya. *Journal of Petrology* 45 (9), 1747-1776.

- Sun, Q. 2000: Applications of Laser-Induced Plasma Spectroscopy to Human Tissue, Plants and Ores. Ph.D. thesis. *University of Florida*
- Termizi, A., Ramlia, A., Wahab, M., Husseina, A and Khalik, W. 2005: Environmental ^{238}U and ^{232}Th Concentration Measurements in an Area of High Level Natural Background Radiation at Palong, Johor, Malaysia. *Journal of Environmental Radioactivity* 80, 287–304.
- Tiwari, M., Singh, R and Sawtney, J. 2001: Analysis of Stainless Steel Samples by Energy Dispersive X-Ray Fluorescence (EDXRF) Spectrometry. *Bull. Mater. Sci.* 24, 633-638.
- Tognoni, E., Palleschi, V., Corsi, M and Cristoforetti, G. 2002: Quantitative Micro-Analysis by Laser-Induced Breakdown Spectroscopy: A Review of the Experimental Approaches. *Spectrochimica Acta Part B.* 57, 1115–1130.
- UNSCEAR. 2000: Sources and effects of ionizing radiation. Report to the General Assembly. New York: United Nations Scientific Committee on the Effects of Atomic Radiation.
- Vincent, M., Alexander, S., Gordon, R and Osinski, A. 2008: Quantitative Multi-Elemental Laser-Induced Breakdown Spectroscopy Using Artificial Neural Networks. *Journal of the European Optical Society Rapid Publications* 3, 08011 (1-5).
- Virendra, S, Agrawal, H., Joshi, C., Sudershan, M and Sinha, K. 2011: Elemental Profile of Agricultural Soil by the EDXRF Technique and Use of the Principal Component Analysis (PCA) Method to Interpret the Complex Data. *Applied Radiation and Isotopes* 69, 969–974.
- Weaver, S., Seal, J and Gibson, L. 1972: Trace Elements Data Relevant to the Origin of Trachytic and Pantelleritic Lavas in East African Rift System. *Contr. Mineral and Petrol.* 36, 181-194.
- Wei, L., Zha, Y., Tao, Z and Hew, C. 1993: Epidemiological Investigation in High Background Radiation Areas of Yangjiang, China, Ramsar 3-7, *IAEA Vienna*, 523-547.
- Wei, L. 1980: Health Surveys in High Background Radiation Areas in China. *Science* 209, 887-880.
- Wendy, A and Mary, R. 1998: Genesis of Silicic Peralkaline Rocks in an Ocean Island Settings by Crustal Melting and Open System Processes: Socorro Island, Mexico. *Journal of Petrology* 138 (9), 1137-1166.
- Williams, J. 1972: The Kenya Rift Volcanics: A Note on Volumes and Chemical Composition. *Tectonophysics* 85-96.

- Wisbrun, R., Schechter, I. and Niessner, R. 1992: Laser-Induced Breakdown Spectroscopy for Detection of Heavy Metals in Environmental Samples. *Society of Photo-Optical Instrumentation Engineers* 1716, 2-15.
- Yamani, H., Ahmed, Z., Gondal, M and Nasr, M. 2009: Determination of Trace Elements in Volcanic Rock Samples Collected from Cenozoic Lava Eruption Sites using Laser- Induced Breakdown Spectroscopy. *Journal of Environmental Science and Health* 44, 528-535.
- Yang, N., Eash, S., Lee, J., Madhavi, Z., Zhang, S., Walker, F and Jae, Y. 2010: Multivariate Analysis of Laser- Induced Breakdown Spectroscopy Spectra of Soil Samples. *Soil Sci.* 175, 447-452.
- Ying, L., Beller, R and Masoud, N. 1993: Chemometrics Data Analysis using Artificial Neural Networks. *Applied Spectroscopy* 47 (1), 12-23.
- Zhe, W., Jie, F., Lizhi, L., Weidou, N and Zheng, L. 2011): A Multivariate Model Based on Dominant Factor for Laser-Induced Breakdown Spectroscopy Measurements. *J. Anal. At. Spectrom.* 26, 2289–2299.

APPENDICES

Appendix I: Profiles of emission lines for elements used in generating calibration curves

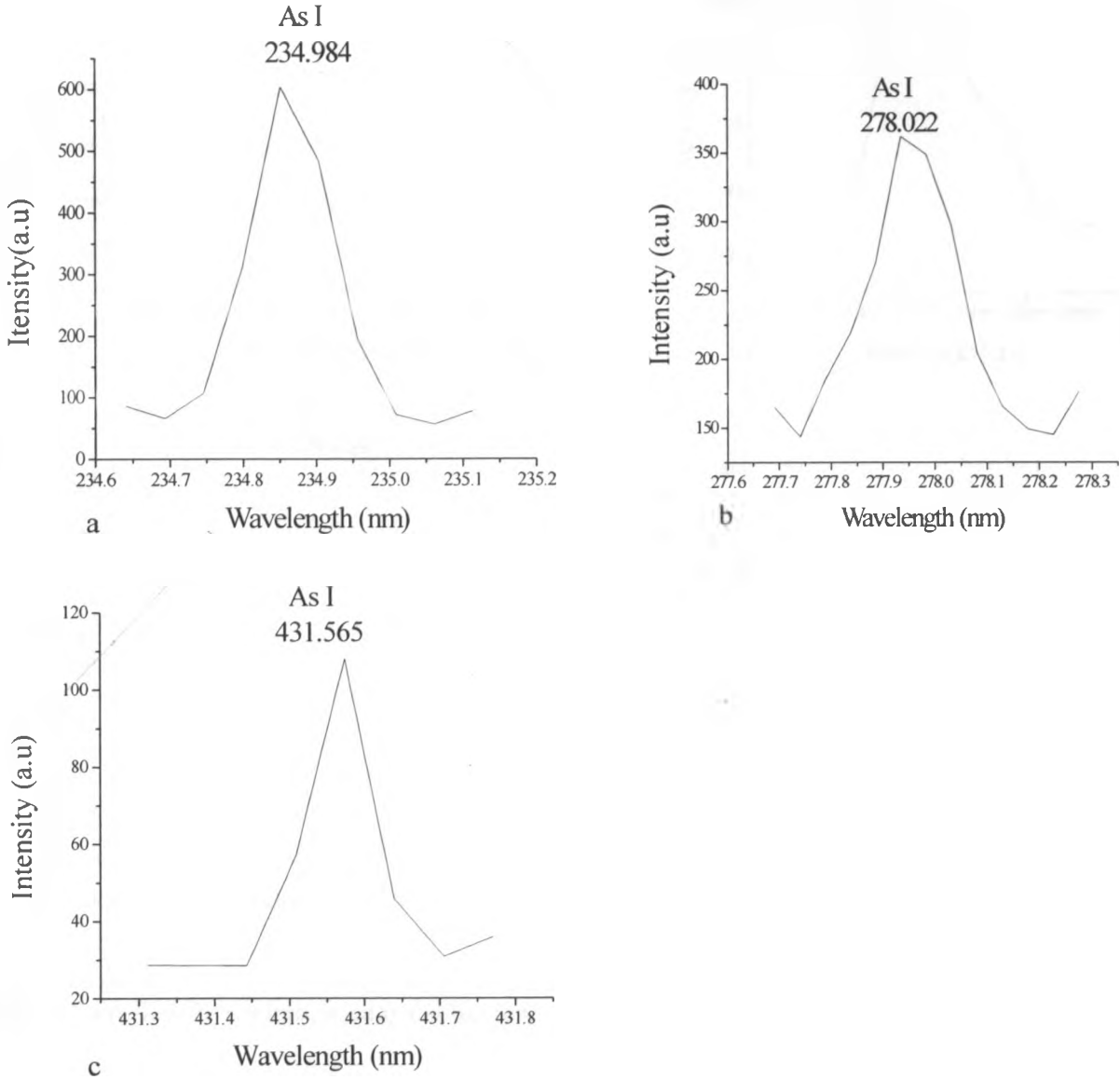


Fig I (i): Profiles of As lines used for univariate calibration.

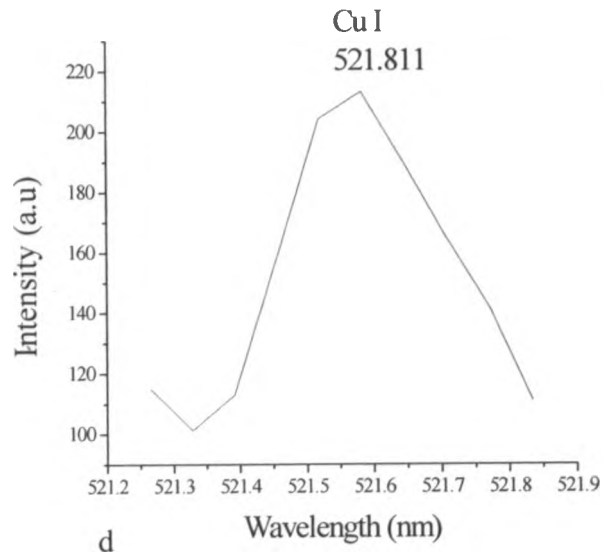
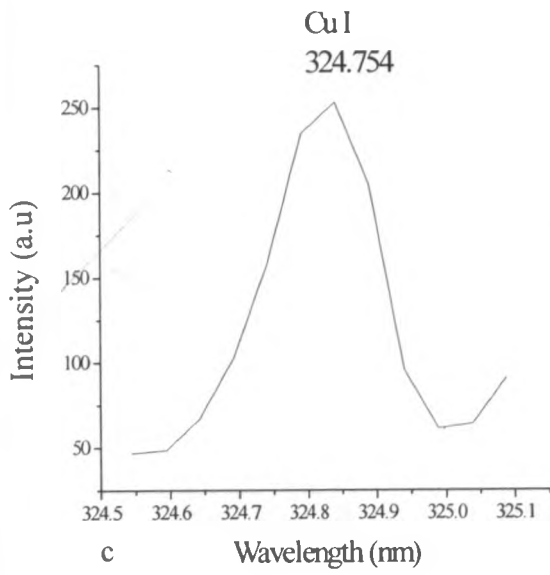
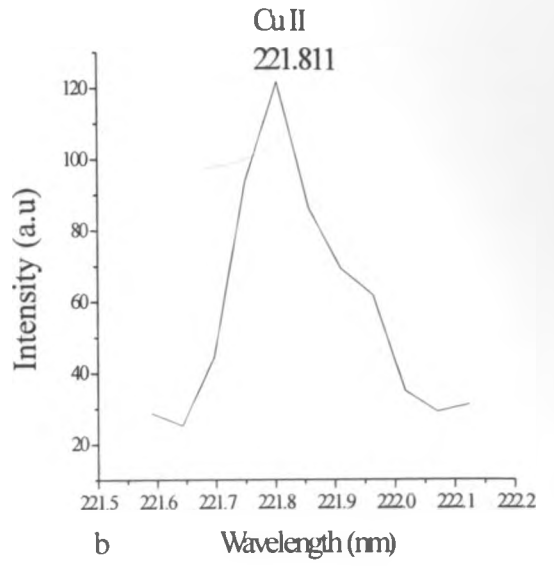
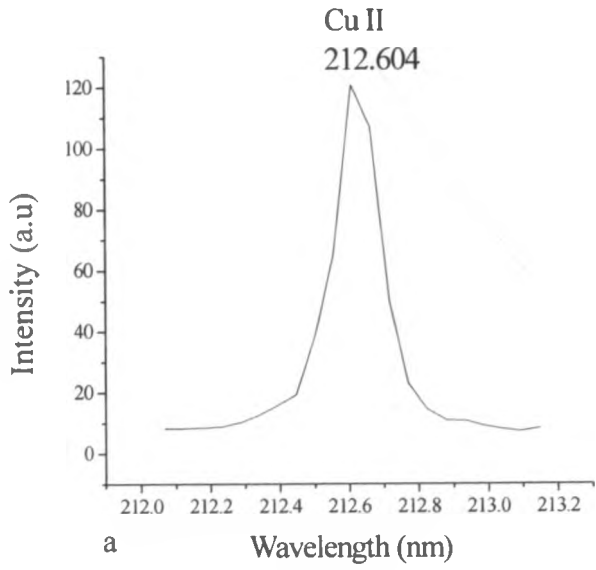


Fig I (ii): Profiles for Cu lines used in calibration.

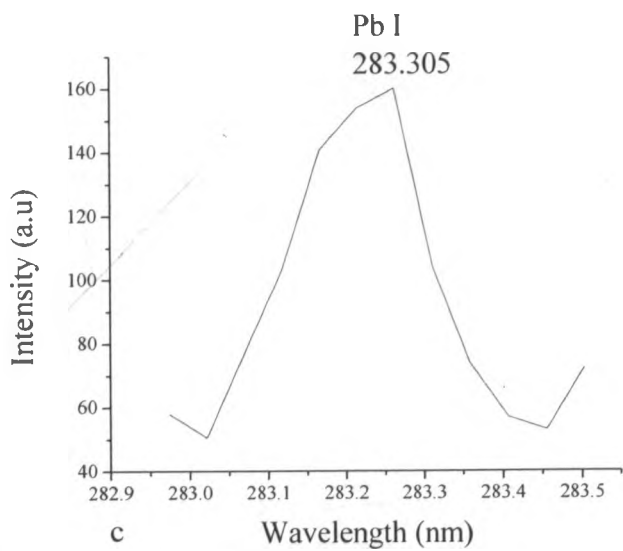
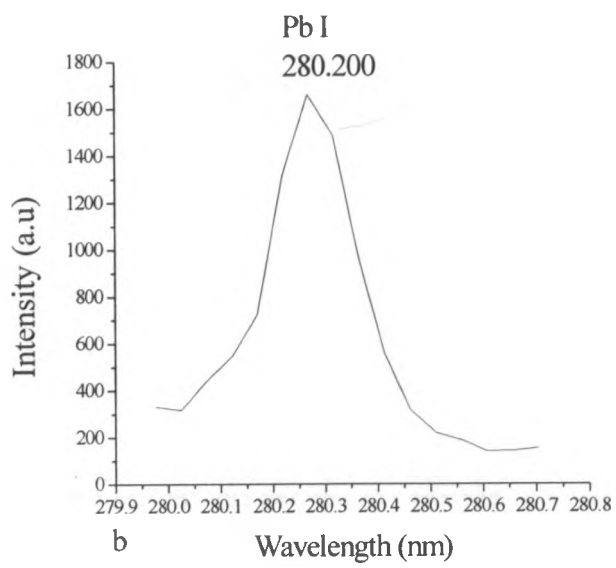
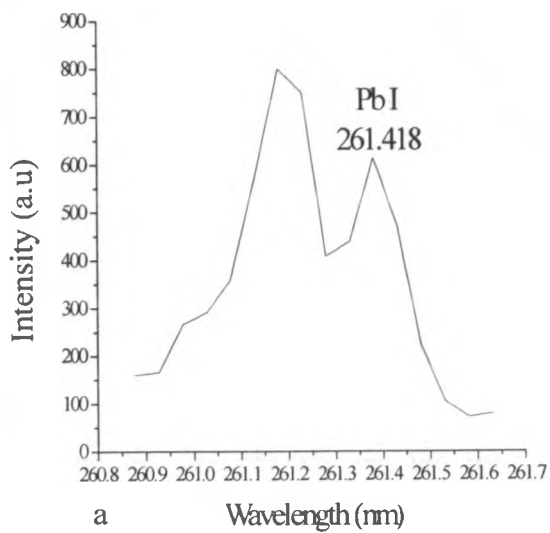


Fig I (iii): Profiles for Pb lines used for univariate calibration.

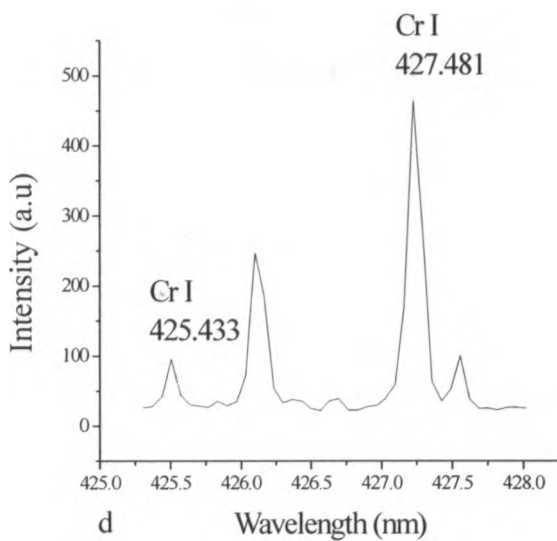
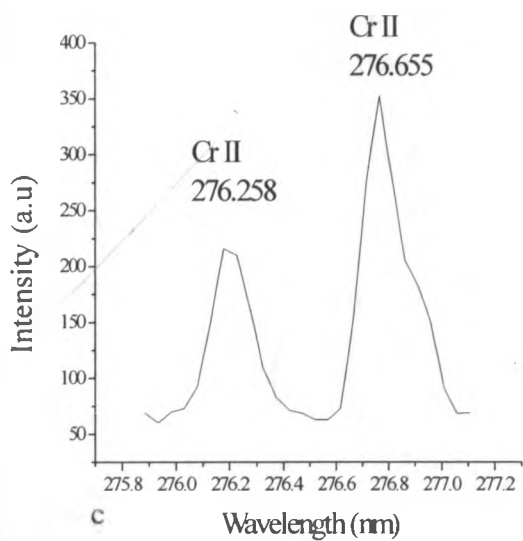
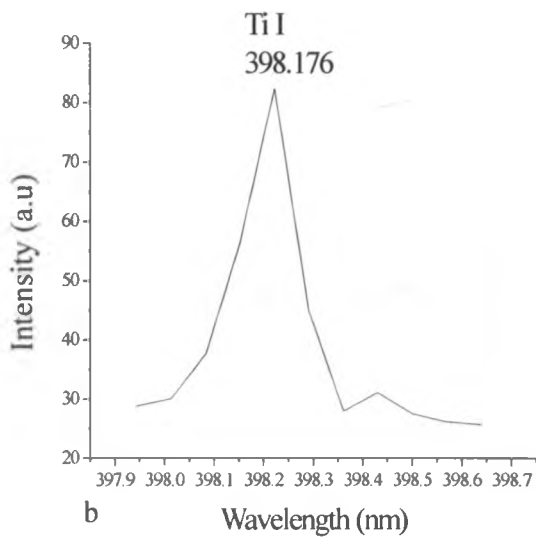
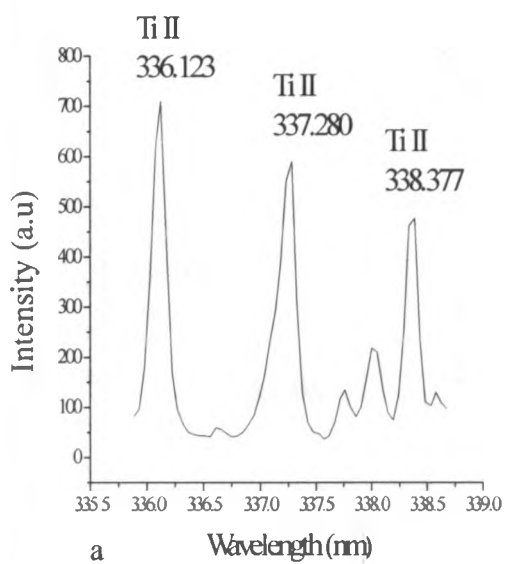


Fig I (iv): Profiles for Ti and Cr lines used in univariate calibration.

Appendix II: Examples of LIBS spectra for geothermal matrices

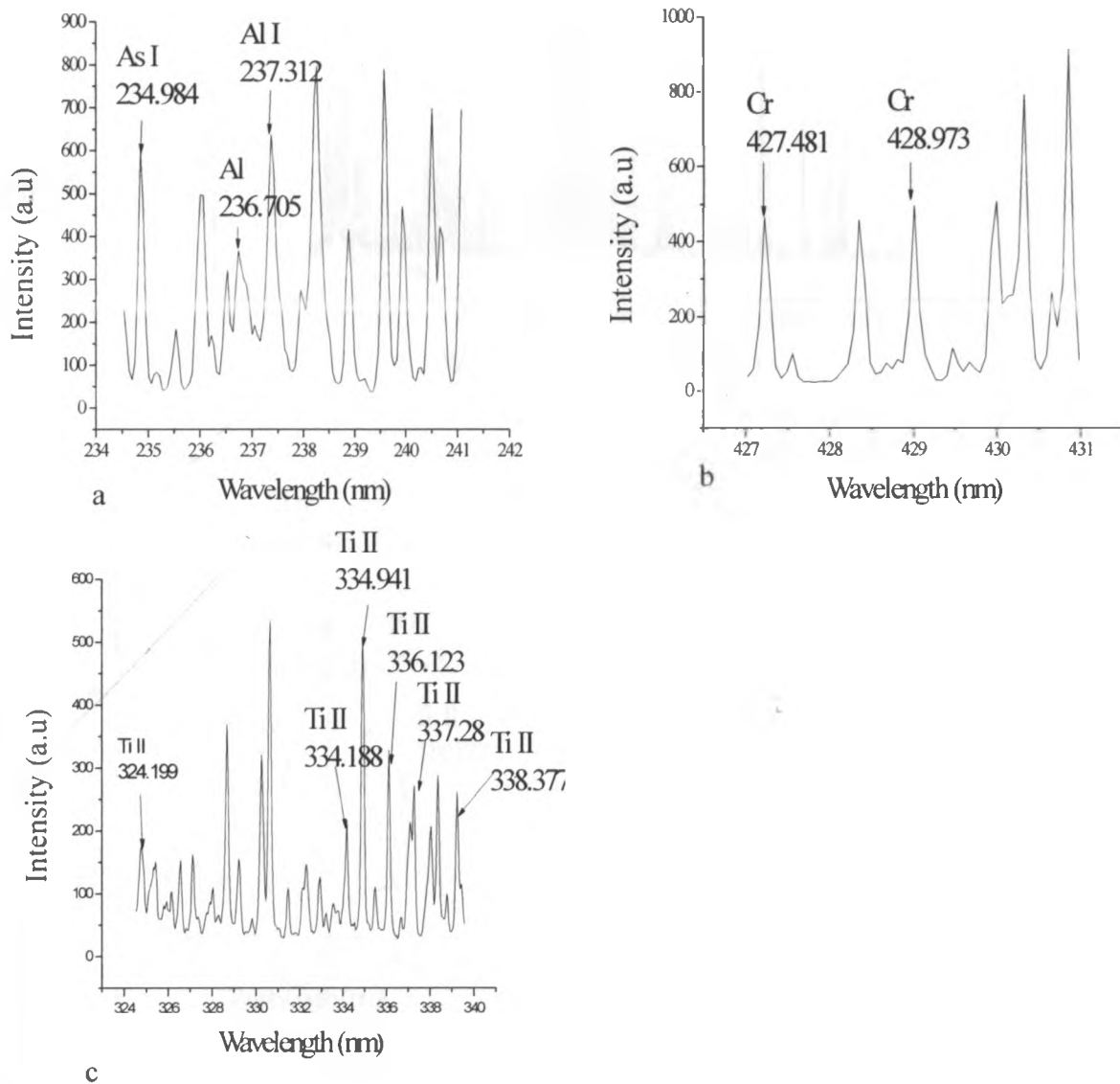


Fig II (i): Spectrum for a soil taken from a HBR geothermal active river in Lambwe valley.

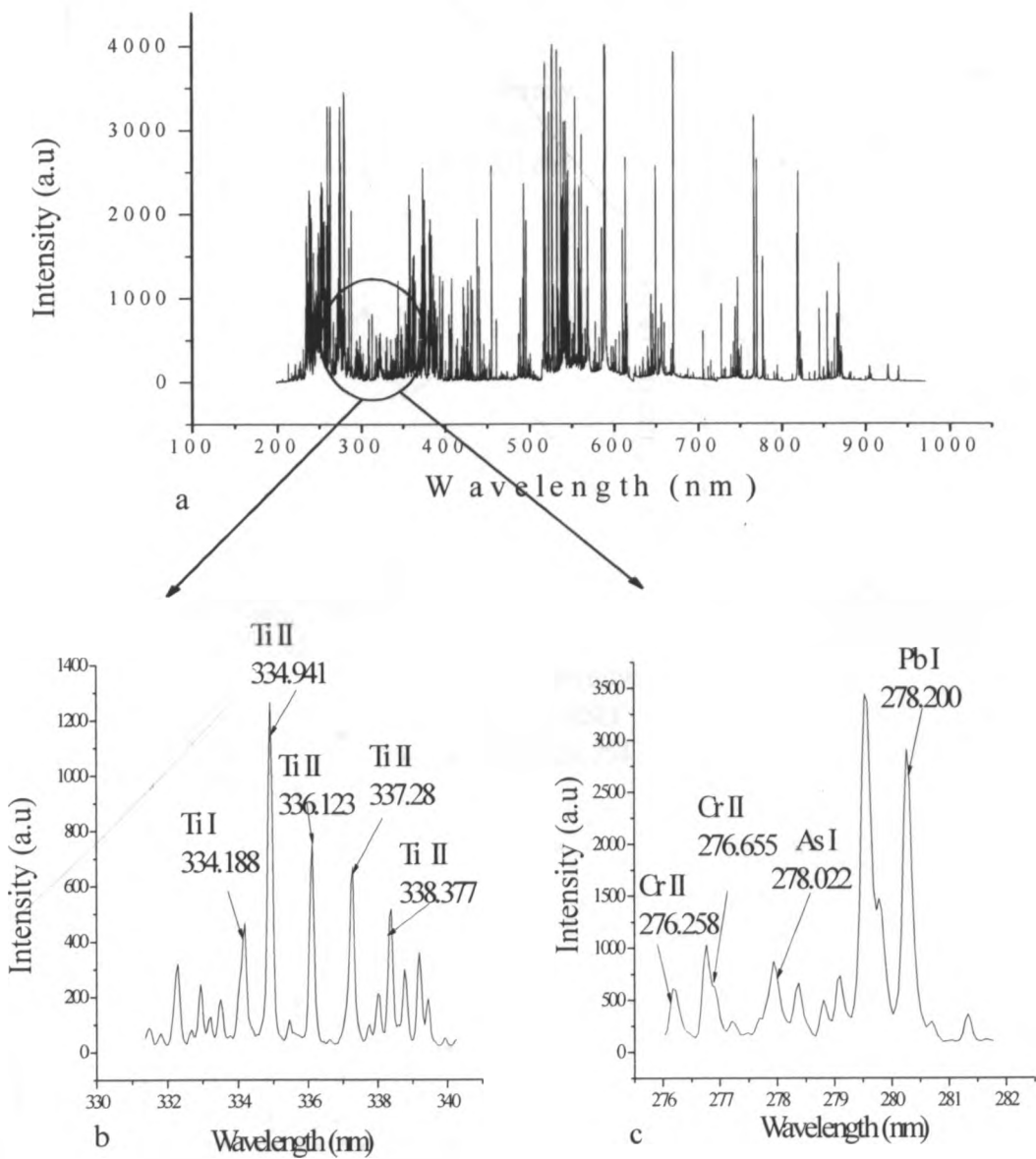


Fig II (ii): Spectra for a rock taken from a HBRA geothermal source in Lambwe valley.

Appendix III: Optimization graphs for different elements in model matrices

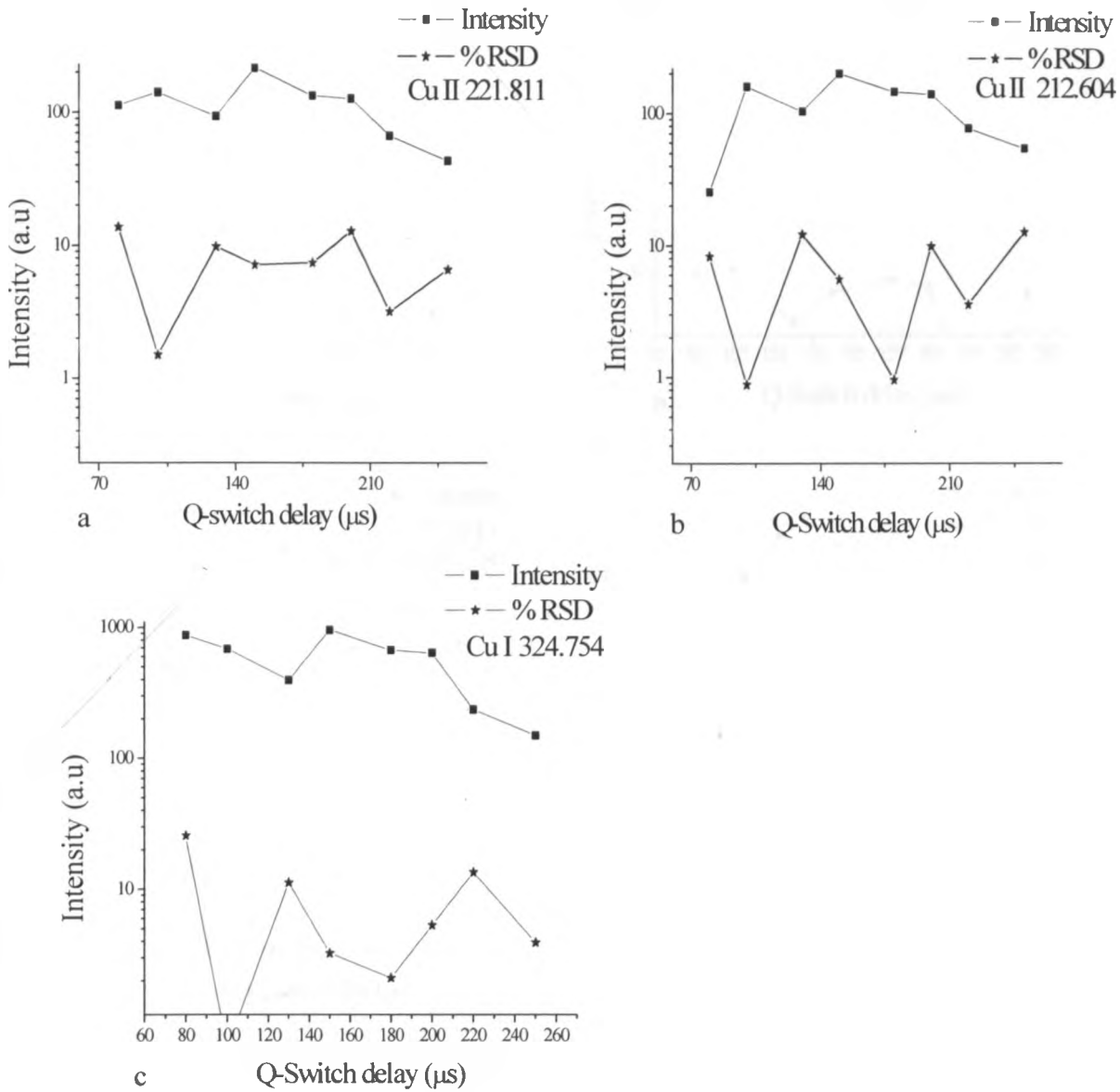


Fig III (i): Optimization graphs showing the variation of LIBS intensity and % RSD of Cu lines in kaolin at different delay times.

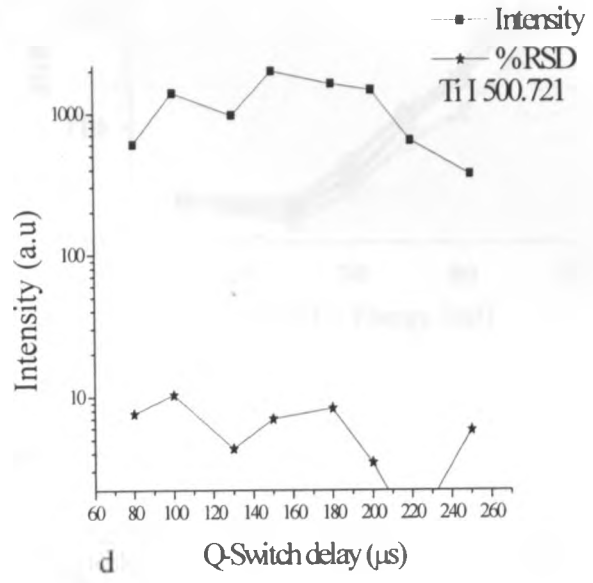
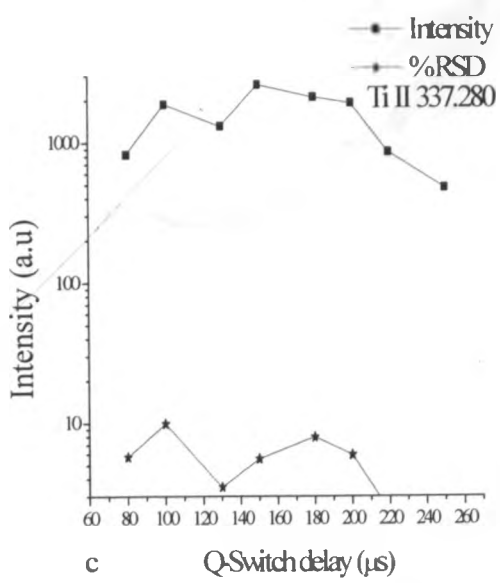
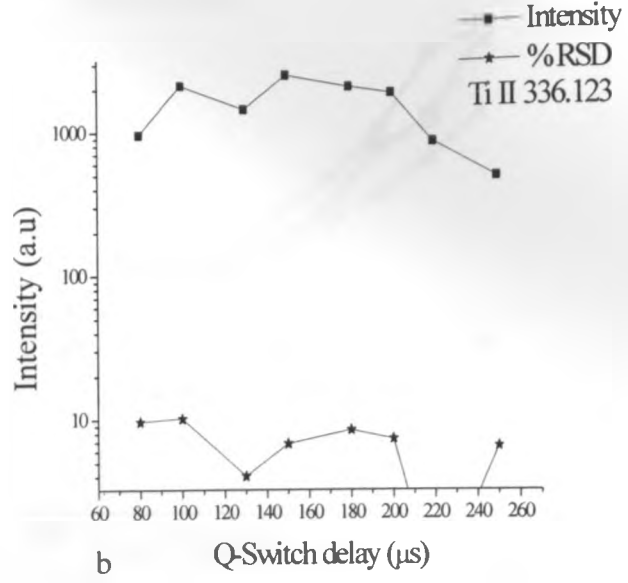
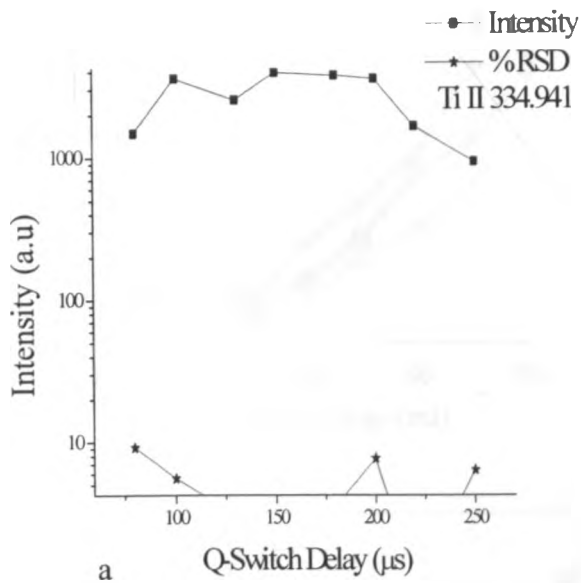


Fig III (ii): Optimization graphs showing the variation of LIBS intensity and % RSD of Ti lines in kaolin at different delay times.

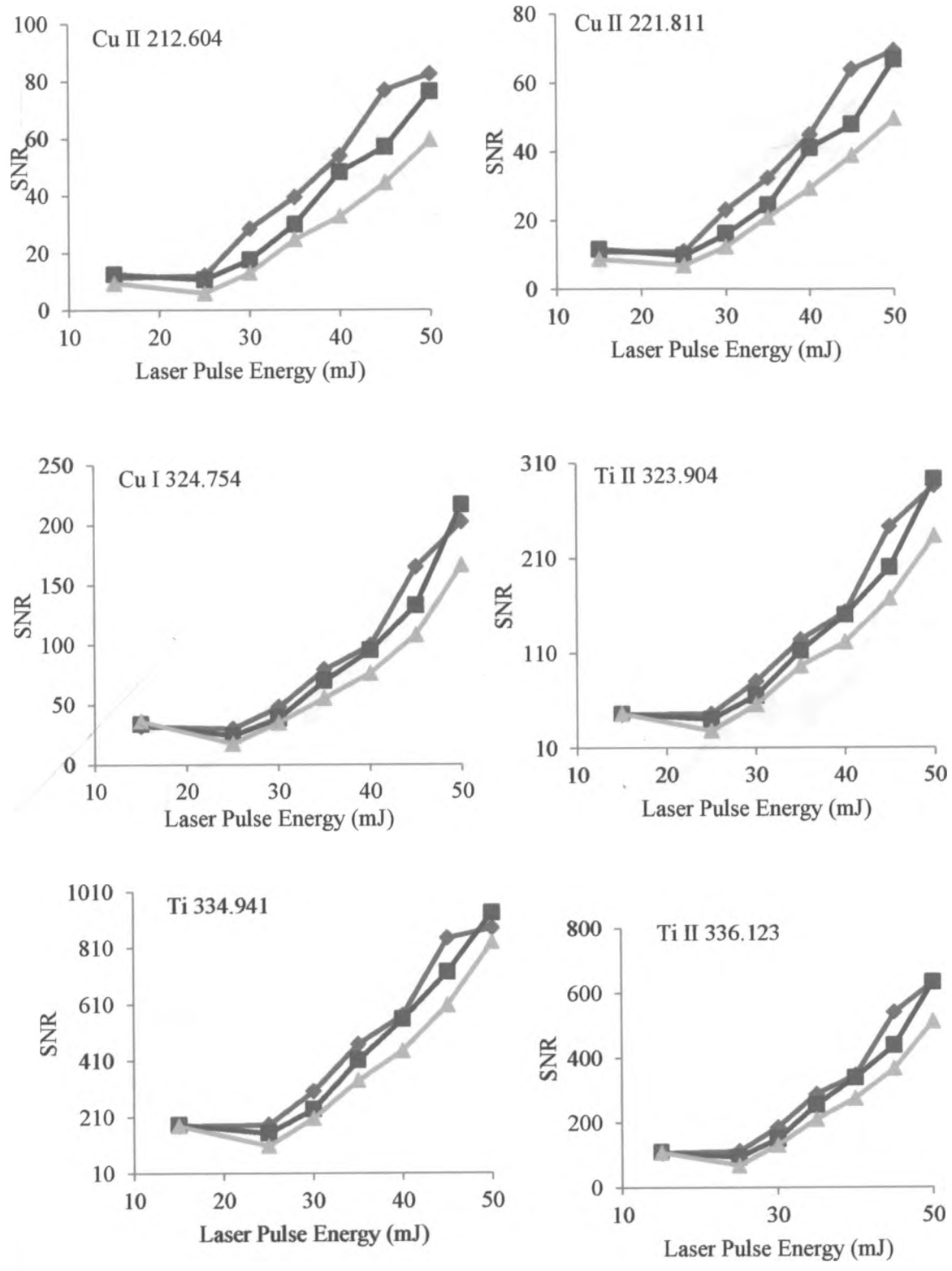


Fig III (iii): Optimization graphs for Cu and Ti lines in kaolin. The graphs show the variation of SNR with respect to the laser pulse energy at 0.4μs(blue rectangles), 0.8μs(red rectangles) and 1.3μs (green triangles).

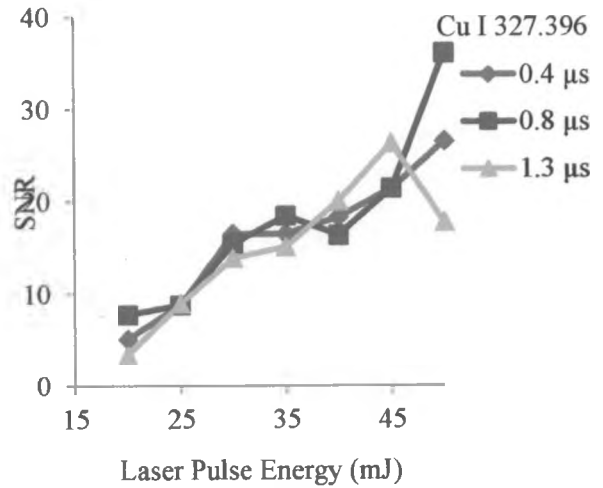
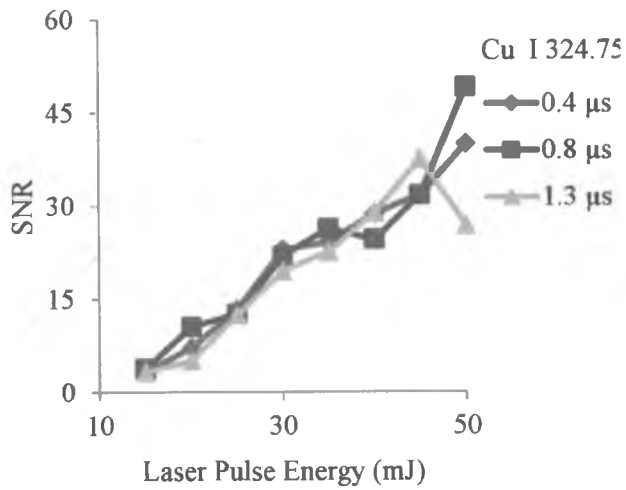
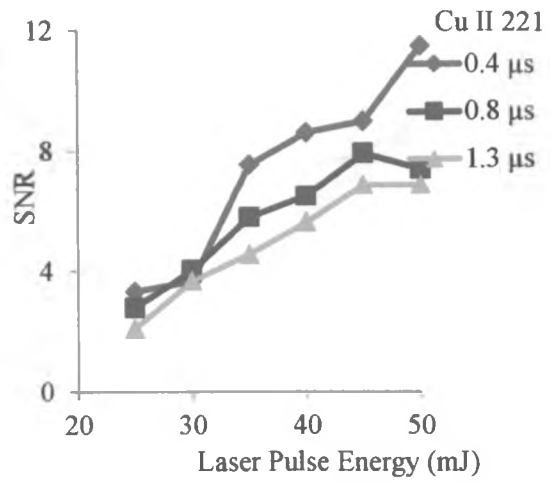
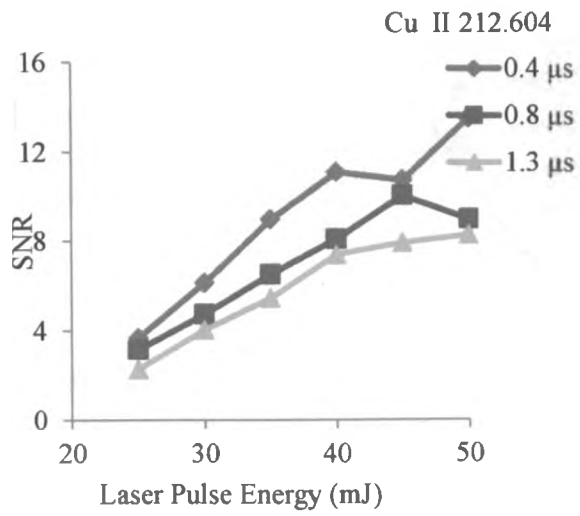


Fig III (iv): Optimization graphs showing the variation of SNR of Cu lines in a rock simulate at different laser pulse energy.

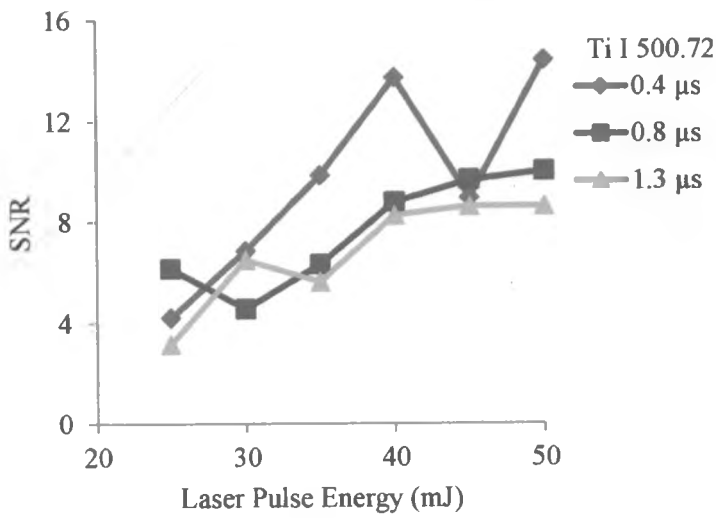
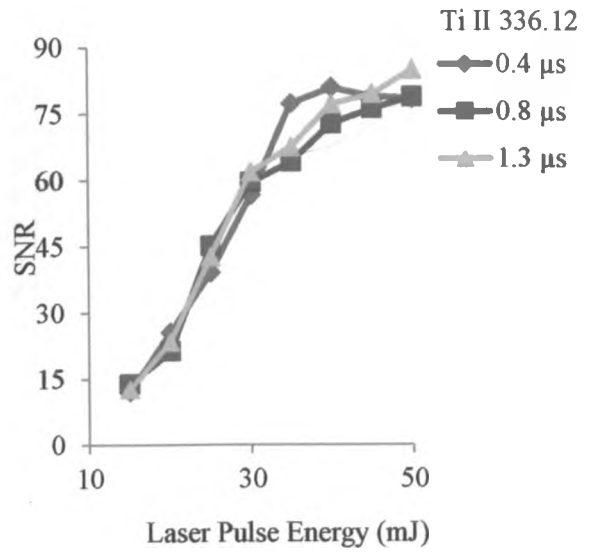
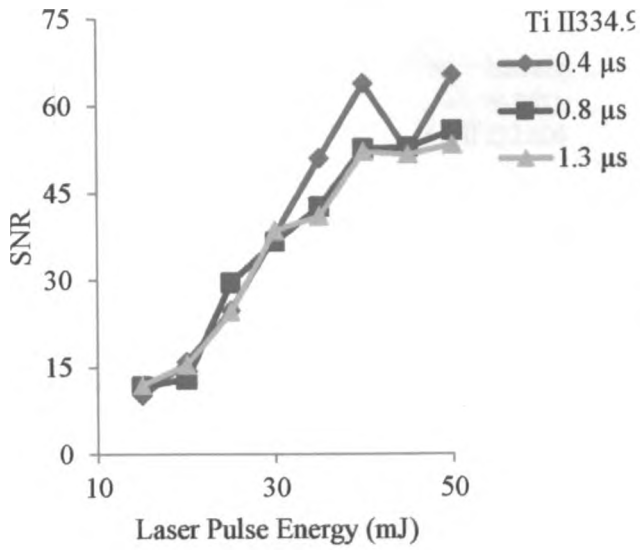


Fig III (v): Optimization graphs showing the variation of SNR of Ti lines in a rock model at different laser pulse energy.

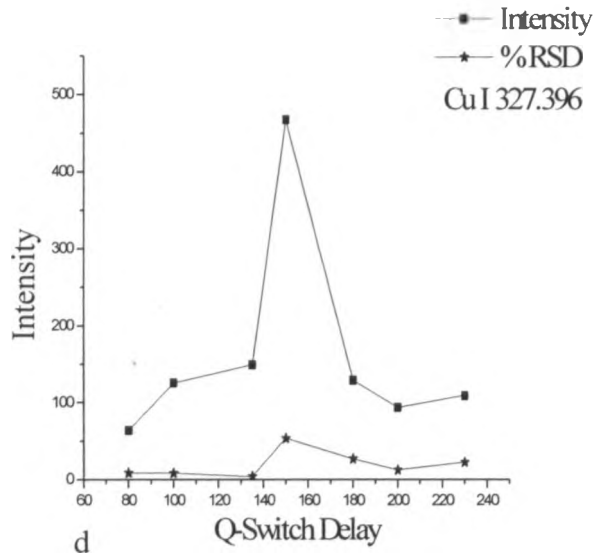
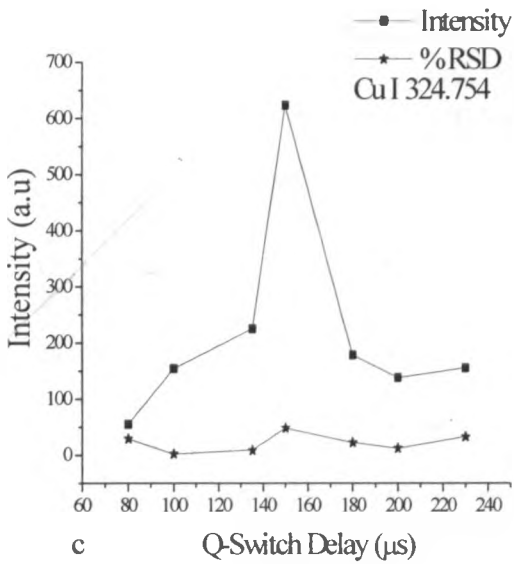
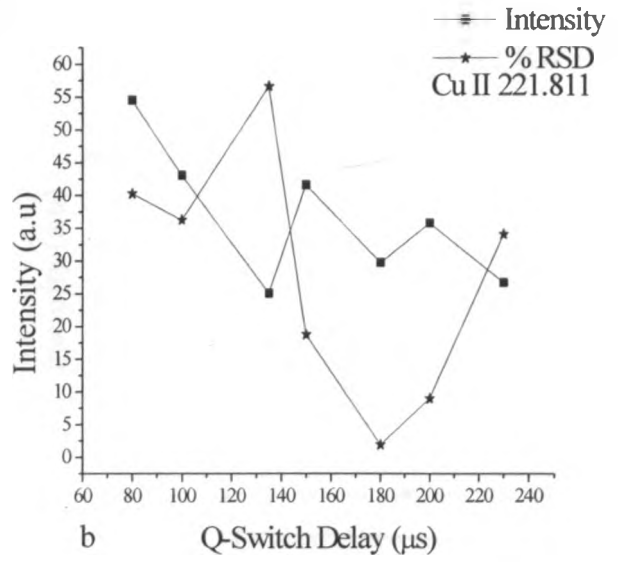
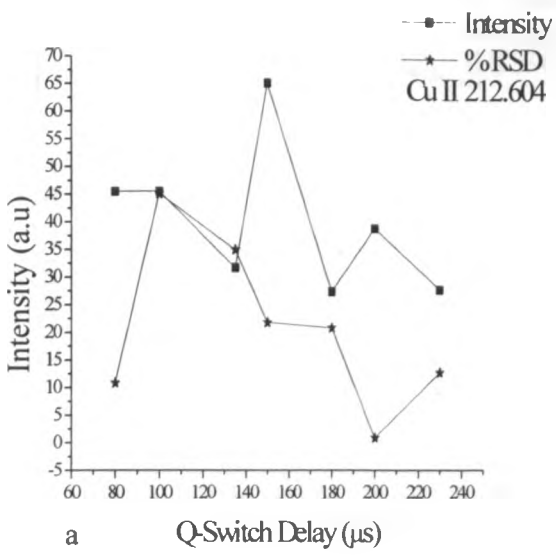


Fig III (vi): Optimization graphs showing the variation of LIBS intensity and % RSD of Cu lines in a rock simulate at different delay times.

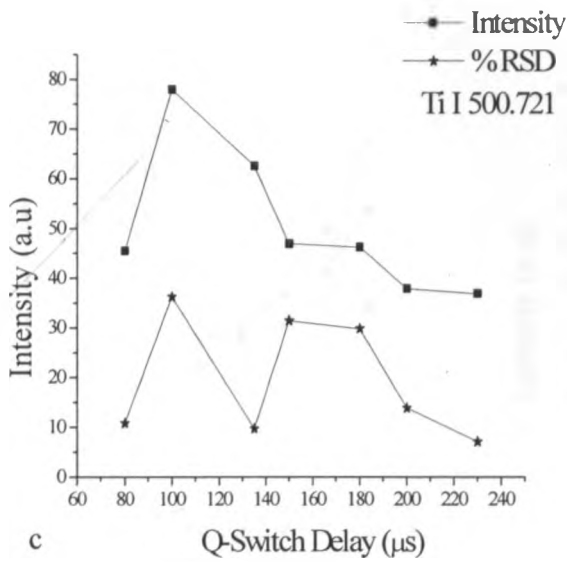
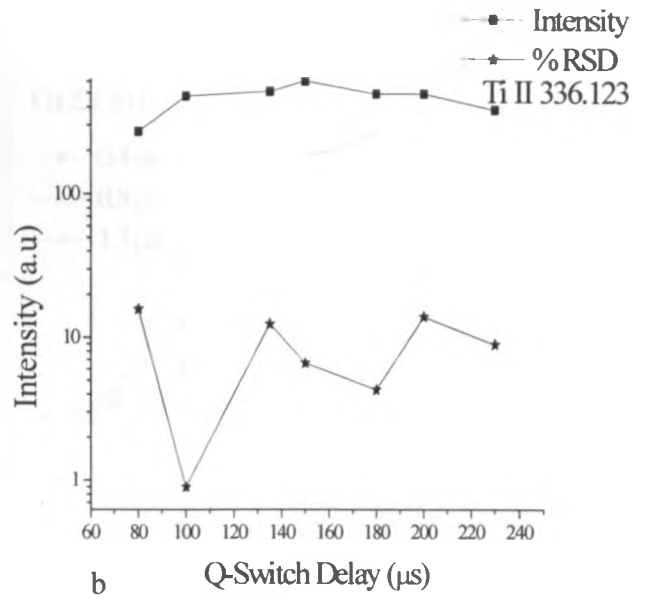
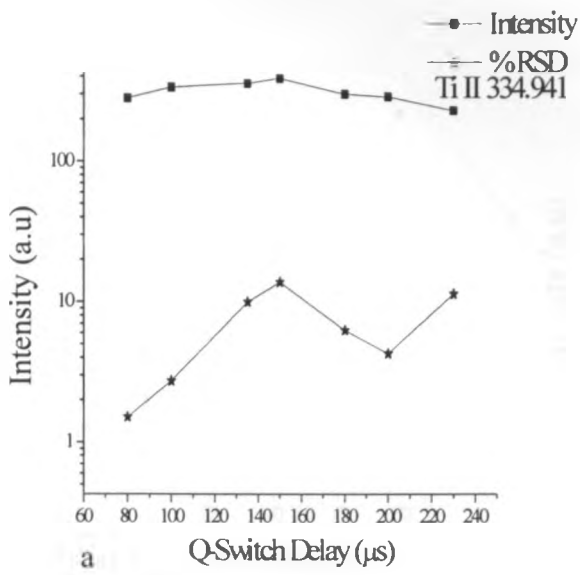


Fig III (vii): Optimization graphs showing the variation of LIBS intensity and Relative standard deviation of Cu lines in a rock simulate at different delay times.

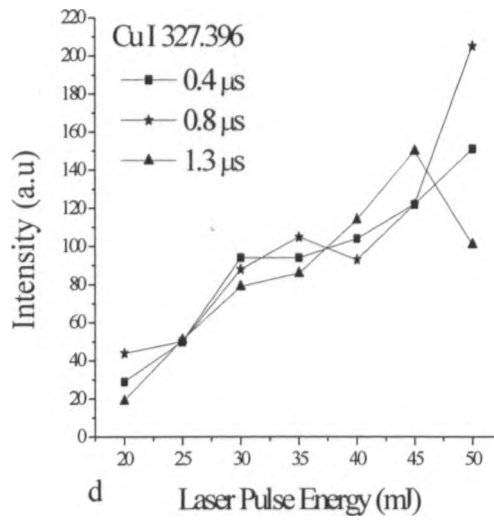
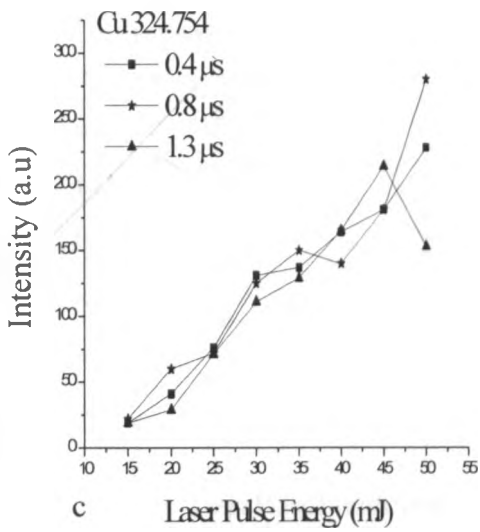
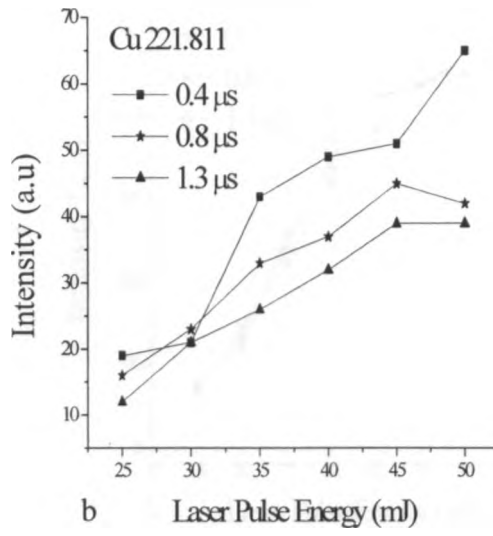
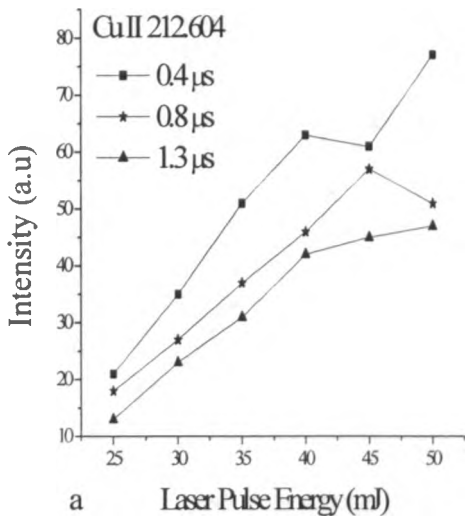


Fig III (viii): Variation of intensity with respect to laser pulse energy for Cu lines in a rock simulate.

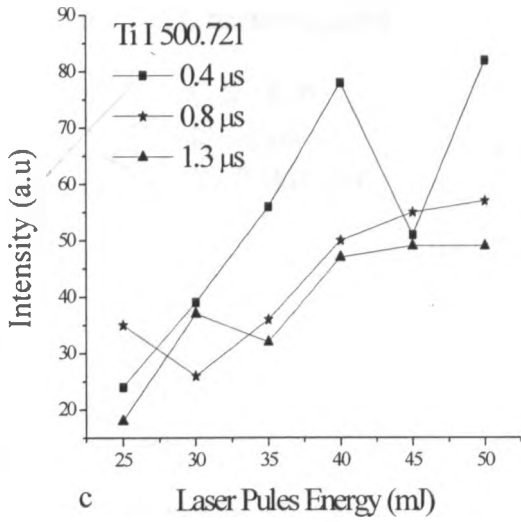
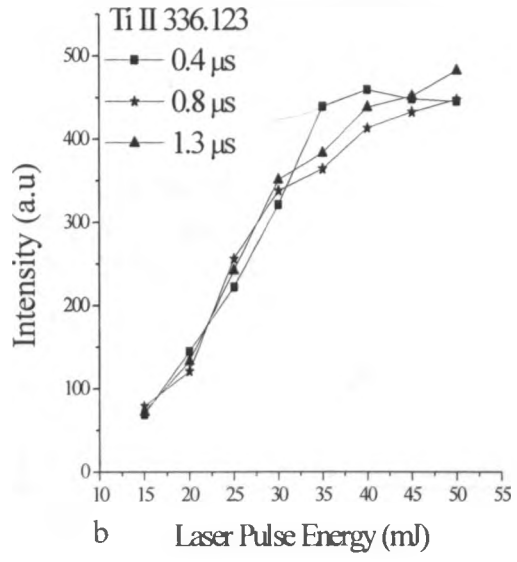
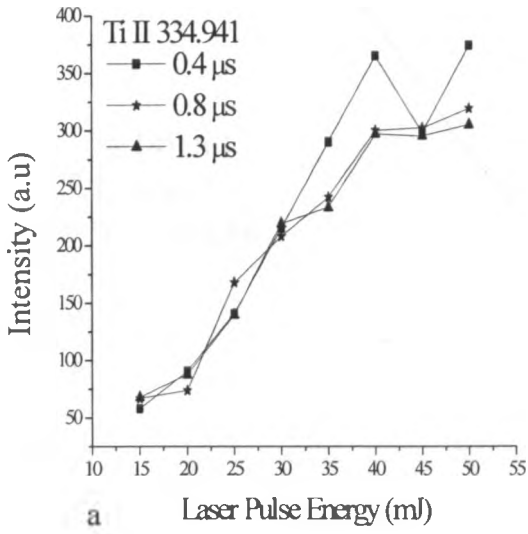


Fig III (ix): Variation of intensity with respect to laser pulse energy for three titanium lines in a rock simulate.

Appendix IV: Classical calibration curves for different elements in the sample matrices

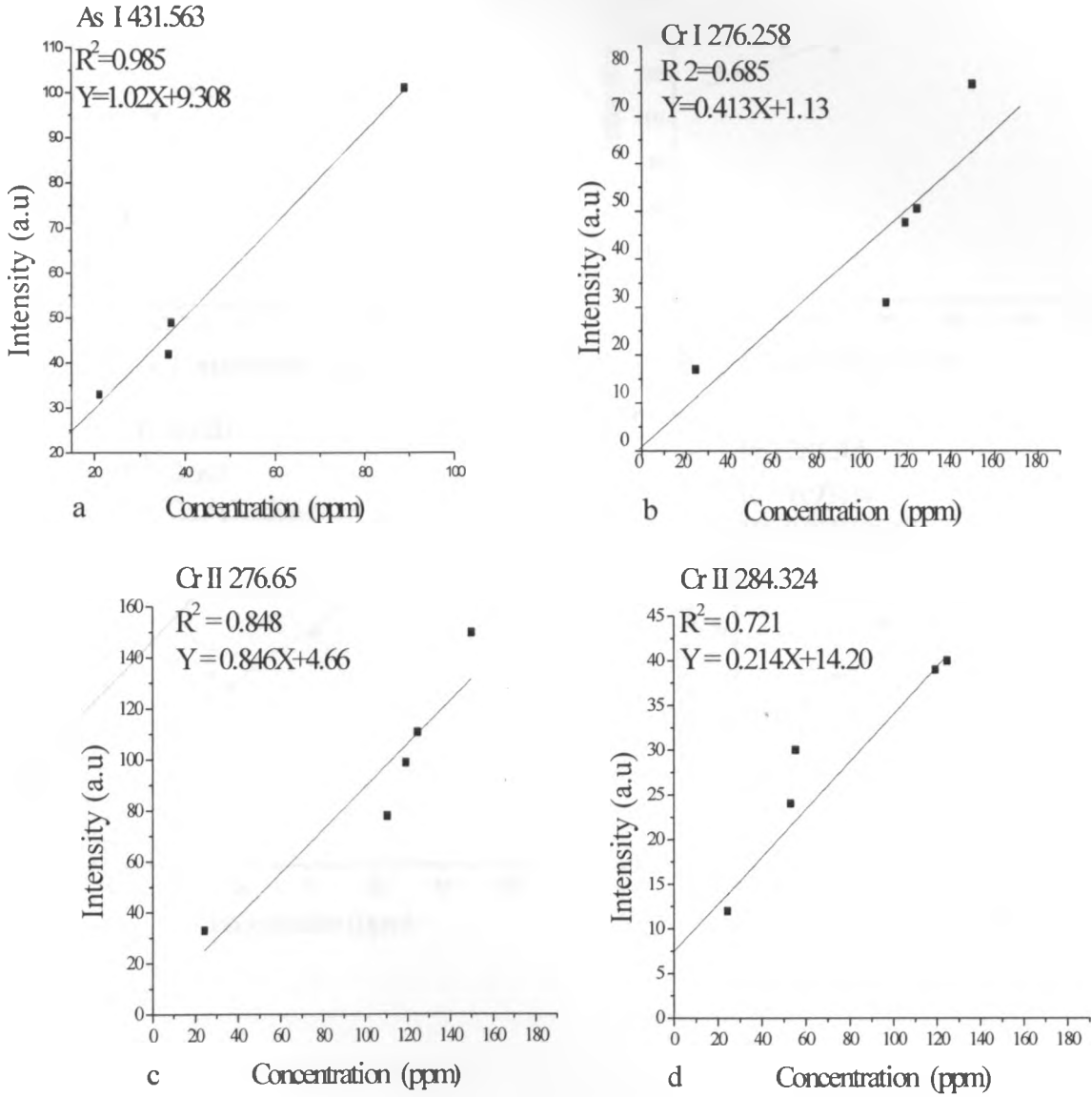
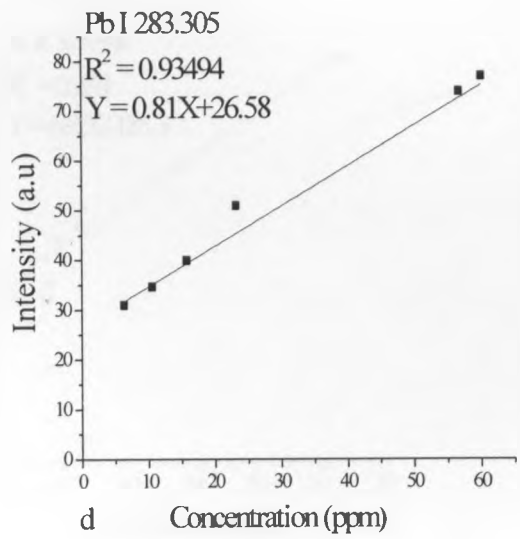
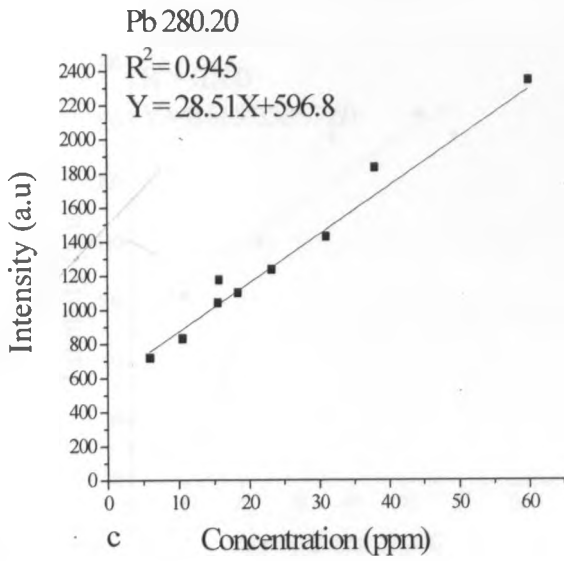
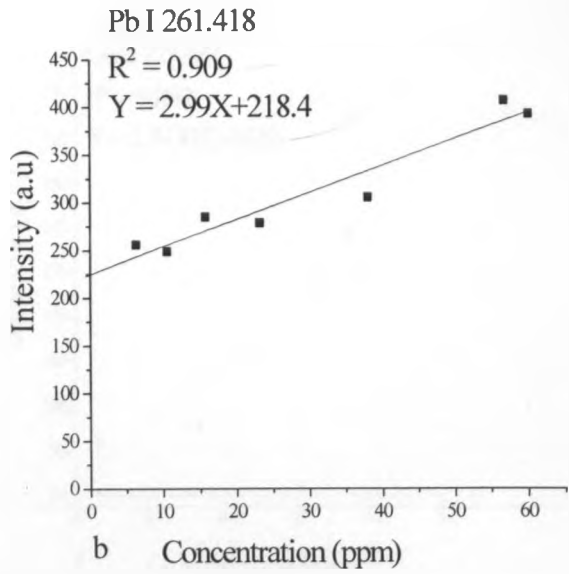
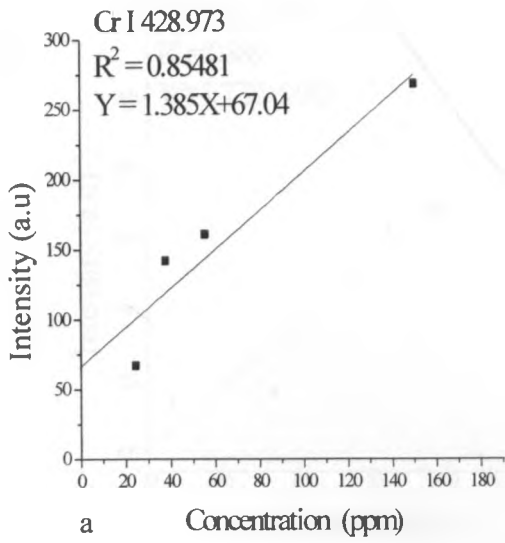


Fig IV (i): Calibration curves for As and Cr from rock simulate.



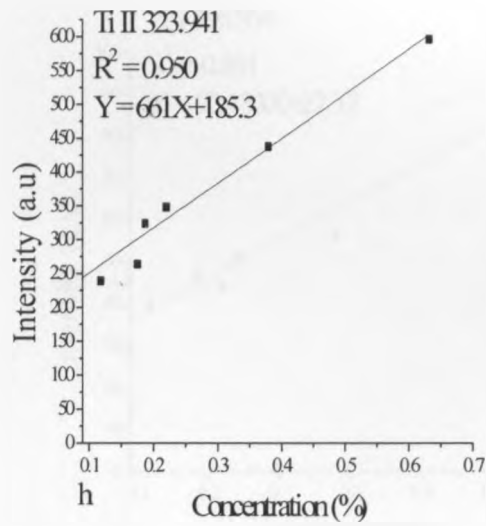
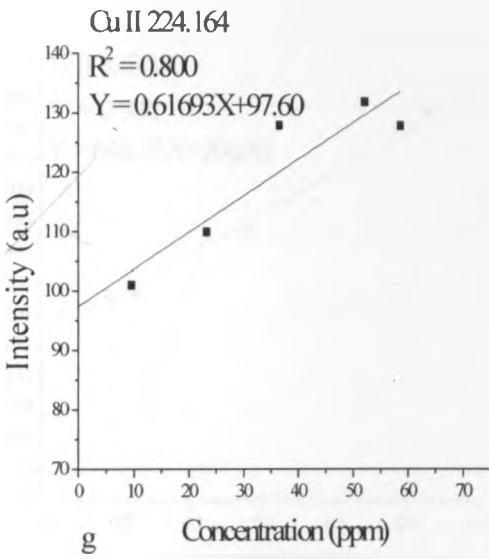
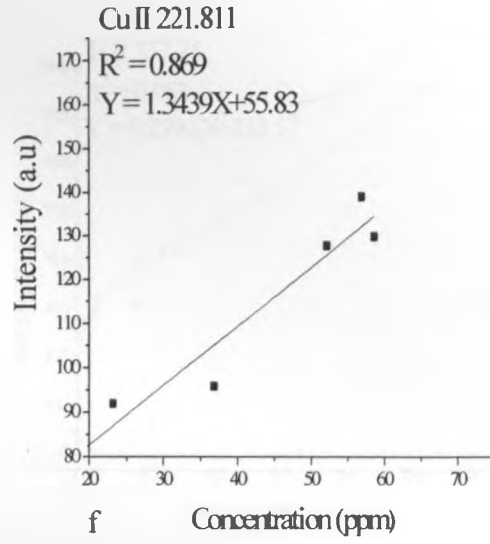
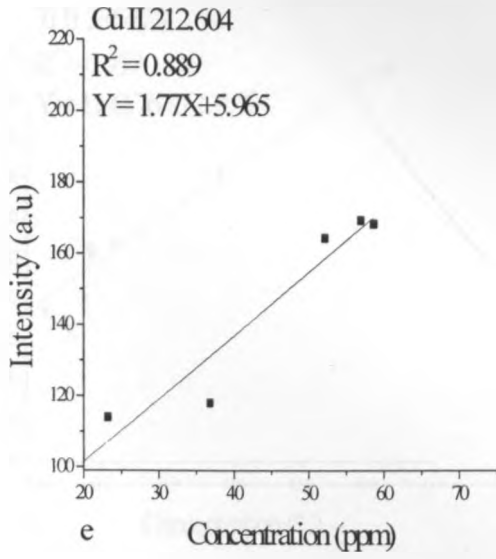


Fig IV (ii): Calibration curves for Cu and Ti lines from rock simulate.

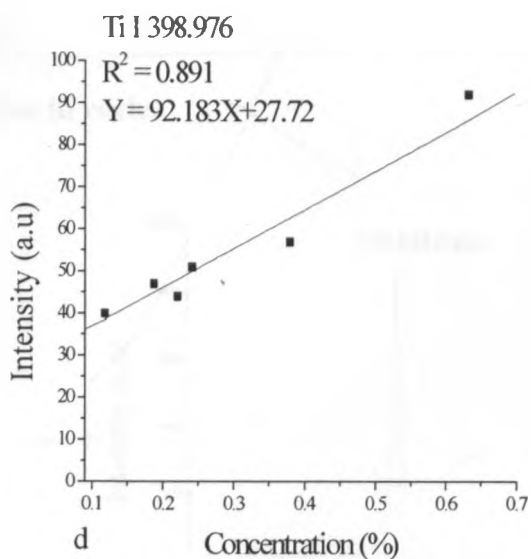
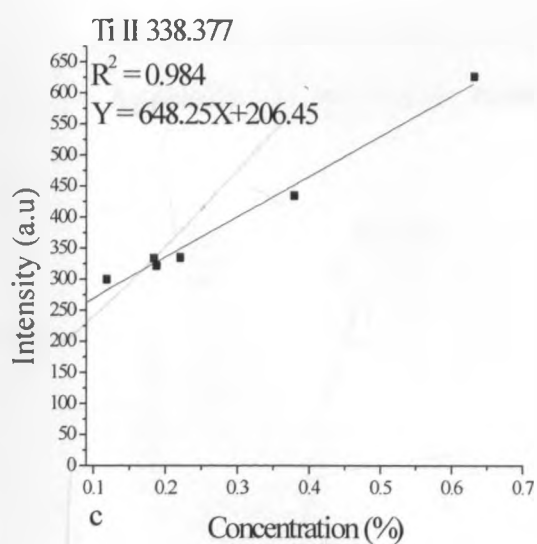
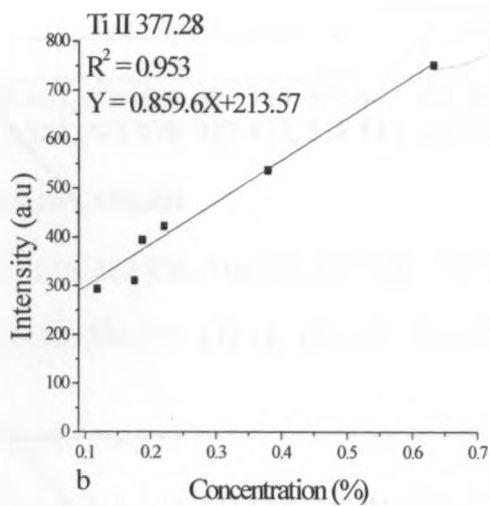
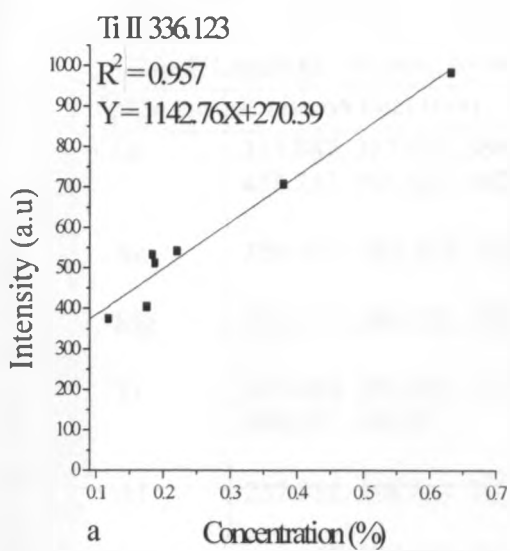


Fig IV (iii): Calibration curves for Ti lines from rock simulate.

Appendix V: Emission lines for elements influencing the clustering of samples in PCA plots

Table I. Loadings resulting from PCA

Element	Emission lines (nm)
Ca	315.887, 317.933, 364.441, 370.603, 373.690, 393.366, 396.847, 422.613, 428.301, 428.936, 430.253, 431.863, 442.514, 443.569, 445.478, 487.813, 518.885, 526.181, 527.027, 534.947
Ba	230.474, 233.527, 315.854, 455.403, 493.401
Mg	279.553, 280.270, 285.213, 383.230, 383.829, 516.733, 517.268, 518.885
Ti	323.653, 325.291, 332.294, 334.188, 336.123, 337.28, 338.377, 453.558, 455.549, 498.173, 499.107, 499.951
Al	237.312, 308.215, 309.271, 394.401, 396.152
Fe	234.350, 238.204, 239.563, 259.940, 263.132, 274.648, 274.932, 275.574, 339.240, 357.010, 358.119, 361.878, 373.486, 374.949, 382.056, 390.648, 421.618, 438.354, 440.475
Si	250.690, 251.611, 252.851, 288.158

Appendix VI: Spectra for molecular lines in rocks

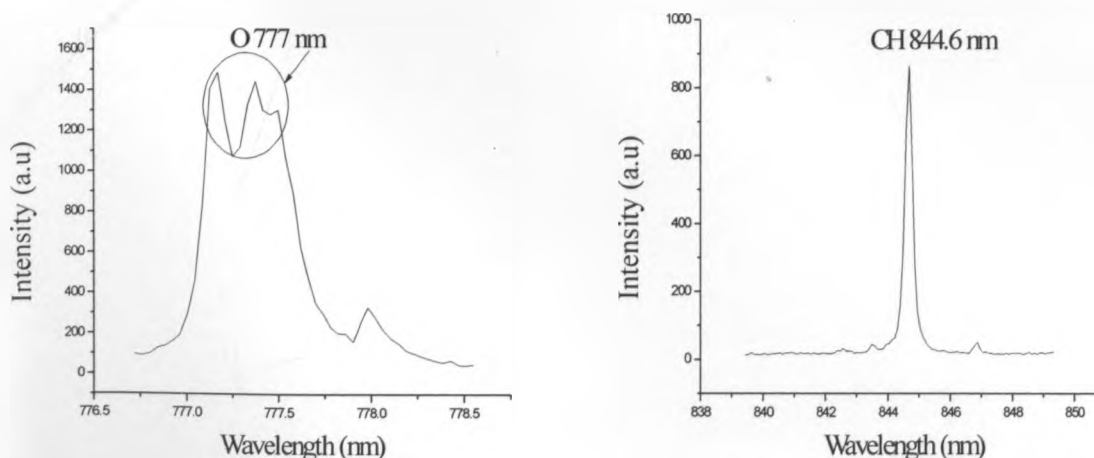


Fig VI. Examples of molecular lines observed in the samples.

Appendix V: Emission lines for elements influencing the clustering of samples in PCA plots

Table I. Loadings resulting from PCA

Element	Emission lines (nm)
Ca	315.887, 317.933, 364.441, 370.603, 373.690, 393.366, 396.847, 422.613, 428.301, 428.936, 430.253, 431.863, 442.514, 443.569, 445.478, 487.813, 518.885, 526.181, 527.027, 534.947
Ba	230.474, 233.527, 315.854, 455.403, 493.401
Mg	279.553, 280.270, 285.213, 383.230, 383.829, 516.733, 517.268, 518.885
Ti	323.653, 325.291, 332.294, 334.188, 336.123, 337.28, 338.377, 453.558, 455.549, 498.173, 499.107, 499.951
Al	237.312, 308.215, 309.271, 394.401, 396.152
Fe	234.350, 238.204, 239.563, 259.940, 263.132, 274.648, 274.932, 275.574, 339.240, 357.010, 358.119, 361.878, 373.486, 374.949, 382.056, 390.648, 421.618, 438.354, 440.475
Si	250.690, 251.611, 252.851, 288.158

Appendix VI: Spectra for molecular lines in rocks

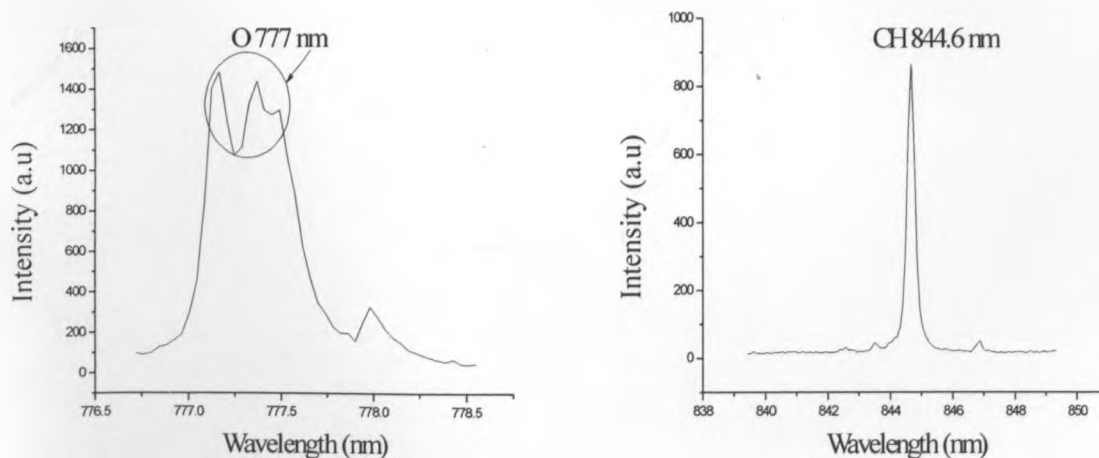


Fig VI. Examples of molecular lines observed in the samples.